Evaluation of Runoff Response to Moving Rainstorms

Jin Liang
Marquette University

EVALUATION OF RUNOFF RESPONSE TO MOVING RAINSTORMS

By

Jin Liang

A Dissertation submitted to the Faculty of the Graduate School,
Marquette University,
in Partial Fulfillment of the Requirements for
the Degree of Doctor of Philosophy

Milwaukee, Wisconsin

December 2010

ABSTRACT
EVALUATION OF RUNOFF RESPONSE TO MOVING RAINSTORMS

JIN LIANG

Marquette University, 2010

The primary hypothesis from the hydrological literature is that downstream moving storms with storm length (L_s) less than watershed length (L_c) magnify the peak discharges. This hypothesis was developed from the kinematic-wave modeling, and was evaluated in a plot between the dimensionless peak discharge and dimensionless storm velocity. Previously unpublished experimental data collected from the Watershed Experimentation System (WES), obtained from the late Professor Ben C. Yen at the University of Illinois at Urbana-Champaign, were used in comparison with the simulation results of the kinematic-wave model. It is found that downstream moving storms with $L_s/L_c < 1$ increase the peak discharges to a limited extent compared to stationary storms, but the kinematic-wave model overstates the increase in the peak flows resulting from downstream moving storms with $L_s/L_c < 1$. This difference between model projections and laboratory data was attributed to backwater effects in the experimental runoff.

To evaluate the importance of the backwater effects, the accuracy of kinematic-wave and dynamic-wave models for the simulation of surface runoff resulting from moving storms was evaluated utilizing the same experimental data. It is found that, the kinematic-wave model cannot deal with the backwater effects resulting from downstream moving storms in the V-shaped watershed in the WES. The kinematic-wave model simulates the upstream moving storms pretty well, whereas it totally overestimates the peak discharges for downstream moving storms.

To confirm the reliability of the nondimensional plots it was necessary to evaluate the kinematic-wave based equations for estimation of the time of concentration. Three methods, i.e., Ben-Zvi's method, the modified Ben-Zvi method, and Izzard's method were applied to determine the time of concentration from the experimental hydrographs of stationary rainstorms reaching the equilibrium state from the WES. The times of concentration determined by these three methods were compared to the mathematical equation proposed by Wong. It is found that a percentage of 89% can be a generally agreeable percentage to evaluate the experimental data from the WES. It is concluded that Wong's equation can predict the time of concentration acceptably well for the simplified watershed with mild overland and channel slopes and long durations.

ACKNOWLEDGEMENTS

Jin Liang

The author would like to thank several individuals for their contributions in preparation of this document. I would like to sincerely express my gratitude to Dr. Charles S. Melching for his constructive guidance and inspiring suggestions as my advisor and mentor throughout my graduate school experience. I also would like to thank the other committee members, Dr. Clifford J. Crandall, Dr. Hector R. Bravo, and Dr. Neal O'Reilly for their valuable suggestions and continuous support for this thesis. I also would like to thank Dr. Kwan Tun Lee for providing his model, and Dr. Morita Masaru for his valuable suggestions.

I would like to thank my dearest mother Guixiang Jin, father Guoan Liang, and sister Qing Liang. I would like to thank my good friends Y. Wang, V.P., U.B., and Nava. Their strong support and sincere encouragement help me all the way to the goal.

TABLE OF CONTENTS

LIST OF TABLES

LIST OF FIGURES

CHAPTER 1 INTRODUCTION

The movement of a rainstorm is one of the most important factors that cause temporal and spatial variability of rainfall. The temporal and spatial variations of rainfall consequently influence the temporal and spatial distributions of surface runoff. The effects of the movement of rainstorms on runoff obviously have both practical and academic significance.

Traditionally, runoff calculations assume simple, static storms ignoring the effects of storm movement, i.e. rainfall is assumed to be a function of time only and is averaged in space and uniformly distributed over the catchment. The rainfall input, which consists of rainfall hyetographs observed at one or more gages, is usually assumed to be uniformly distributed over the catchment without regard to the catchment size or its geographical orientation. The rainfall record from a single rain gauge might not realistically represent the storm's spatial distribution for a watershed. Therefore, the lack of sufficient information about the spatial distribution of short-term rainfall is the greatest source of error in urban runoff simulations (Niemczynowicz, 1988). Unfortunately, one obvious solution to the uncertainty in rainfall spatial distribution, increasing the density of rain gages, is not very realistic because of the time and costs involved.

On the other hand, most hydrological models can accommodate the temporal variability of precipitation, but usually cannot incorporate, without simplification, the spatial variability of precipitation (Richardson and Julien, 1989). When considering the continuously varying intensity of precipitation in space and time, hydrological models typically incorporate simplifying assumptions which apply single parametric values to rainfall intensity in space and

time. The model output, therefore, fails to reflect the effects of temporal and spatial variability in the rainfall input (Ogden and Julien, 1993).

In addition to the application of traditional rain gages, remote sensing of precipitation is widely used to improve rainfall spatial and temporal accuracy. With remote sensors such as an active surface-based weather radar and a passive earth satellites, the precipitation is not captured or directly measured, but obtained from physical, statistical, and empirical relationships between precipitation characteristics and the emitted or reflected radiation from the earth and atmosphere (McFarland, 2008). Discrete temporal and spatial sampling resolutions of remotely sensed input data to a runoff model must be considered as possible sources of error. This error will produce variability in the computed outflow due solely to the temporal and spatial resolution of the input data. It is important to explore the sources of this variability before precipitation data from remote sensors, such as telemetered rain gauges or weather radar, are applied to two-dimensional physically based runoff models (Ogden and Julien, 1993).

The question of whether the dynamic properties of rainfall must be considered when choosing input for runoff modeling can only be answered if the range of the effect is defined in statistical terms. Niemczynowicz (1984b) concluded the error in simulated runoff peak discharge caused by using stationary storms as input will not be very important from a practical point of view. This conclusion was suggested by the magnitude of the occurrence probability for directional bias values. Niemczynowicz (1984b) reported the highest values of directional bias occur for storms with short durations which give low peak flow discharge that is without practical importance. If storm motion has only a minor effect on outflow, stationary rainstorms may be

used in simulations. If the effects of storm motion are large, it is important to specifically model the changes in location of precipitation with time (Ogden et al., 1995).

Using moving storms as rainfall input for runoff simulation has several advantages in comparison with the use of traditional, non-moving rainfall input. The rainfall movement can be a valuable complement to short-term rainfall data. If rainfall movement is considered, not only the catchment parameters and area, but also the geographical orientation of the catchment would be considered to affect the shape of the simulated hydrograph. Areal reduction of rainfall intensity would be achieved without using Area Reduction Factors (ARFs).

1.1 Moving Rainstorms

Rainfall is never uniform nor static. Rainfall is always changing and moving. Rainfall movement is an important part of the rainfall process.

According to the New Oxford American Dictionary, 2nd Edition, the definition of “storm” is a violent disturbance of the atmosphere with strong winds and usually rain, thunder, lightning, or snow. A storm cell is an air mass that contains up and down drafts in convective loops, moves and reacts as a single entity, and functions as the smallest unit of a storm-producing system. According to the classic model formulated by Austin and Houze (1972), the size of rain cells within smaller mesoscale areas (SMSA) varies from about 1 to 10 km^2. Large mesoscale areas (LMSA) contain SMSA, or “clusters of convective cells” within an extension of 50 to 1000 km2. For example, there are four main types of thunderstorms: single cell, multicell cluster, multicell lines (squall lines), and supercell. The type depends on the instability and relative wind

conditions at different layers of the atmosphere ("wind shear"). This term of single cell technically applies to a single thunderstorm with one main updraft. Multicell storms form as clusters of storms but may then evolve into an organized line or lines of storms. Multicell line storms commonly referred to as "squall lines", occur when multicellular storms form in a line rather than clusters. They can be hundreds of miles long and move swiftly.

Rainfall fields consist of complicated cloud structures which develop and decay, come close to or move apart from one another, and travel across the catchment. During passage over the catchment, the rainfall cells develop, grow, decay, and die. The life span of the rainfall structures decreases with their extent, rain intensity within smaller structures is always higher than in the region outside the structure.

The nature of the rainfall process is stochastic. Although stochastic models were established to reproduce structure of the rainfall fields, these models have not been used for practical runoff simulations. However, the rainfall movement, an important part of the rainfall process, can be considered from a deterministic point of view. Experimental evidence proves that there are some prevailing directions of rainfall movement that are typical for a region. The parameters of the rainfall movement for each rainfall event can be derived from multigauge data or calculated from high-altitude wind data.

1.1.1 Parameters Characterizing Storm Movement

Two categories of factors affecting the surface runoff hydrograph include watershed characteristics or hydrometeorologic factors and storm precipitation dynamics. The watershed

characteristics include watershed topography, drainage system pattern, and land use. Storm precipitation characteristics include rainfall amount, intensity and duration, area, distribution, and drop size, as well as velocity and direction of storm movement. The parameters of the rain cell movement include the velocity, direction, duration, and areal coverage. Niemczynowicz and Dahlblom (1984) first developed a computer program to determine the velocity and direction of storm movement and calculated the statistical characteristics of rainfall movement in the city of Lund, Sweden. Niemczynowicz (1984b) combined rainfall movement statistics with the modeled runoff to study the probability distribution of directional bias for differently oriented catchments in Lund.

1.1.1.1 Velocity

Rain storms often move at a speed of 7 ~ 35 km/h (6 ~ 32 ft/s) or 2 ~ 10 times the stream flow velocity, assuming an average stream flow velocity of 3.6 km/h (3 ft/s) (Singh, 1997). The average speed of rain cell movement calculated from 400 rainfall events in Lund, Sweden is 10 m/s (33 ft/s) (Niemczynowicz and Dahlblom, 1984). Hobbs and Locatelli (1978) reported the speed of raincells between 13 and 26 m/s (43 and 85 ft/s) for western California.

Proportions between the time of passage and the time of rain cell development are crucial to describe the rainfall process in a deterministic way. The time of passage of rain cells over the catchment is defined by the physical velocity, V, of rain cell movement and the size of the catchment, L, as follows:

$$T = \frac{L}{V} \tag{1.1}$$

The time of rain cell development is denoted to be T'. For a given total amount of rainfall, when T' is long, the rain cells change slowly, nearly unchanged; when T' is short, the rain cells change quickly.

The lifetime of convective rain cells has been reported to be between 10 and 30 min by Austin and Houze (1972), 15 to 60 min by Felgate and Read (1975), and about 10 to more than 30 min by Hobbs and Locatelli (1978). The lifetime of the rain cell is equal to the duration of the rainfall. If $T' \gg T$, the lifetime of the rain cell is much longer than the time of passage over a given catchment, and the rainfall pattern has no significant changes during the passage. According to some experimental evidence, it is reasonable to expect that the development and decay of the rain cells play a less important role on a small scale relevant to urban catchments than on a large scale relevant to rural basins. Therefore, the one-gage rainfall hyetograph would be representative not only of a point but also of the entire line of rain cell passage over the catchment, assuming that there is no change in the pattern of a rainfall field during its passage over an urban catchment.

If $T' \ll T$, the lifespan of the raincell is shorter than the time of passage, and more than one rain cell may pass over the catchment. The time distribution of rainfall observed in a point gauge is the result of several characteristics of a rainfall field and several processes occurring within this field, such as spatial variation of rain cells, their development and decay, the distance between them, and the direction of their movement.

1.1.1.2 Direction

Storm directions can be distinguished as upstream, downstream, across stream, and angular to the stream. In theory, the storm direction can be any angle to the stream in the watershed.

1.1.1.3 Size

If the size of the rain cells is smaller than the area of the watershed, the watershed is partially covered; if the size of the rain cells is bigger, the watershed is fully covered.

1.1.2 Watershed Characteristics

The effect of storm direction on the stream flow is significantly influenced by the shape and size of the watershed. Tabios et al. (1988) analyzed probabilistically the influence of storm movement in conjunction with watershed shape and size on the stream flow hydrograph using a stochastic space-time rainfall model. Three watershed sizes with areas of 7.77, 1,295 and 2,590 km^2 of two different shapes, one elongated and the other del-shaped (▼), were used. A storm of 10,000 km^2 in effective storm area was used. For the watershed of 7.77 km^2, the storm direction had no effect on peak discharge (Q_p) and the time to peak discharge (T_p). However, for the larger watersheds of 1,295 and 2,590 km^2, the effect of storm direction was pronounced.

1.1.3 Effects of Moving Storms on Runoff

There are three aspects of storm movement for quantifying its influence on the discharge hydrograph: (i) direction (e.g., upstream, downstream, transverse, or angular), (ii) areal coverage

(e.g., full or partial), and (iii) duration (e.g. duration velocity leading to an equilibrium hydrograph or partial equilibrium hydrograph) (Singh, 2002a).

1.1.3.1 Equivalent Storms

Different “equivalent storm” concepts were applied in previous laboratory tests or numerical simulations. This result may be one of the factors that have led to a failure to provide an integrated relationship between the storm movement and the resulting runoff hydrograph (Lee and Huang, 2007).

Yen and Chow (1969) first defined the concept of “equivalent stationary rainstorms” and introduced the concept of “equivalent rainstorms”. The equivalent stationary rainstorm was defined as a rainstorm with the same duration and intensity of rainfall at any point on the watershed as the moving rainstorm but with the rain falling simultaneously over the entire watershed. The equivalent rainstorm was introduced as the storm having different speeds but having the same duration of rainfall at any point in the watershed, and also having the same total volume of rainfall. The equivalent moving storms defined by Yen and Chow (1969) are essentially both equi-volume and equi-intensity.

Richardson and Julien (1989) refined the concept of “equivalent storms” introduced by Yen and Chow (1969) to specify that the volume of water introduced at all points on the watershed and the physical size of the storm must be equal. With this important modification, for equivalent storms moving at different velocities, the rainfall intensity would vary in proportion to the ratio

of the storm speeds. Ogden et al. (1995) also adopted the same concept to incorporate the time to equilibrium in the analysis of storm movement effects on runoff.

Lee and Huang (2007) applied non-linear numerical kinematic-wave models to test a wide range of values for the independent variables without applying the concept of an “equivalent storm.”

1.1.3.2 Equilibrium Discharge

A runoff hydrograph becomes an equilibrium hydrograph when the hydrograph peak is equal to the peak rainfall excess intensity times the watershed area; otherwise the hydrograph remains in partial equilibrium (Singh 2002b).

For storms that reached an equilibrium discharge the experimental rainfall intensity was calculated by the formula $i^* = Q_p/A$, where Q_p was equal to measured peak discharge. If an impervious watershed is subjected to constant rainfall intensity for a duration greater than its time of concentration the product of intensity and area must equal the peak discharge (Xiong and Melching, 2005).

If the length of a storm is large compared with the size of a watershed and the storm speed is relatively slow, then the runoff will reach an equilibrium discharge. In this case, there will not be a substantial effect of storm motion on the peak discharge. Therefore, it is of interest to study whether the storm lengths are shorter than the size of the watershed and whether the storm speeds are different from the mean flow velocity (Lee and Huang, 2007).

Lee and Huang (2007) examined criteria for attainment of the equilibrium discharge from watersheds subjected to moving storms. It was concluded that for storms moving downstream, the runoff can attain equilibrium discharge even though the storm length is shorter than the watershed length and the rainfall duration is less than the runoff equilibrium time for a stationary uniform discharge. The phenomenon of attainment of equilibrium discharge from watersheds subjected to moving storms is contradictory to conventional hydrological design, which assumes the storm duration must equal the time to equilibrium (i.e. time of concentration) to attain the maximum discharge.

1.1.3.3 Peak Discharge

Singh (2002b) concluded that for moving storms covering the plane everywhere for the same duration, in both the equilibrium and the partial equilibrium cases, the peak discharge is independent of the storm direction and storm movement, while for storms covering the plane with spatially varying duration, for the same storm velocity and duration, the peak is greater for the storm moving downstream than for the storm moving upstream. Singh (2002b) also concluded that for the storms of the same duration, the peak discharge is greater for storms moving downstream than that for storms moving upstream.

1.1.3.4 Time to Peak

Foroud et al. (1984) found that for storms moving in the downstream direction, the time to peak was independent of storm velocity if it exceeded the stream flow velocity.

Richardson and Julien (1989) found that the time to equilibrium for block moving storms is inversely proportional to the storm speed (directly proportional to the traverse time of the storm). For storms moving up the plane, the time to equilibrium for the moving storm was the sum of the traverse time of the storm and the stationary storm time to equilibrium. For storms moving down the plane, the moving storm time to equilibrium was equal to the traverse time of the storm, when the storm moved slowly down the plane.

Singh (2002a) found that for moving storms covering the plane everywhere for the same duration: (a) In the equilibrium case the time to peak is affected by the storm velocity and is greater for storms moving upstream than for stationary storms as well as downstream moving storms. (b) In the partial equilibrium case the time to peak is affected by the velocity and is greater for downstream-moving storms than for upstream-moving storms; while stationary storms produce the shortest time to peak. (c) For storms covering the plane with spatially varying duration: For the same storm velocity and duration, the time to peak occurs much later in case of the storm moving upstream than for the storm moving downstream.

1.2 Methods Review

The importance of rainstorm movement on surface runoff has been investigated for more than 40 years. The studies on moving storms have been empirical, numerical, experimental, or analytical. Maksimov (1964) was the first to choose the subject of surface runoff from moving rainstorms. Singh (1997a) presented a survey of investigations dealing with the influence of storm movement.

1.2.1 Empirical Study

Hydrological data analysis has been done to study moving storms. The methods were developed to calculate the dynamic parameters of moving storms (i.e. the storm velocity and direction) using data gathered from dense networks of rain gauges (Shearman, 1977, and Hindi and Kelway, 1977).

Niemczynowicz (1984b) measured the runoff from the storm-water system in Lund at five outlets collecting storm water from about 90% of the total area of the city over a period of 17 months. High-resolution rainfall data were collected through a network of twelve automatic, 1-min rain gauges on a 20 km^2 watershed in Lund, Sweden. Ten intensive events observed between 1979 and 1980 were chosen from about 550 measured rainfall events during three years of measurement as the rainfall input.

1.2.2 Numerical Study

Mathematical rainfall and runoff models have been utilized to study the effect of moving storms on the magnitude and timing of outflow since the advent of the modern computer. Computer models for urban watershed runoff are classified into two categories: hydrologic models and hydraulic models. The hydrologic model can be lumped or distributed, and the hydraulic models typically are based on the kinematic-wave approximation to the full dynamic-wave equations (also known as the de Saint Venant equations). It is noted that the accuracy of these models themselves is an important subject of research for urban stormwater management.

Hydrological models can accommodate the temporal variability of the precipitation, but usually cannot incorporate, without simplification, the spatial variability of precipitation. Results generated from numerical models after these models have been verified by physical models would enhance the study of complex moving storm rainfall-runoff events (Richardson and Julien, 1989).

Marcus (1968) developed a conceptual mathematical model by applying the equations of continuity and momentum for spatially varied unsteady flow to both the overland and channel flows. The discrepancy between the experimental results and those obtained by the approximate dynamic-wave approach model was less than 10%. Another numerical study of moving storms was performed by Surkan (1974) using a simple distributed numerical model. Stephenson (1984) applied a kinematic-wave approximation to simulate runoff hydrographs resulting from moving storms.

Using the Storm Water Management Model (SWMM), Niemczynowicz (1984a) studied the relationship between storm movement parameters and the magnitude of the directional bias on a simple, conceptual catchment storage model based on Manning's equation combined with the continuity equation. Niemczynowicz (1984b) also applied this simulation model on real urbanized catchments in the city of Lund, Sweden. Niemczynowicz (1988) further used the SWMM runoff model to simulate the runoff in Lund by applying the rainfall movement as a complement to limited short-term rainfall data.

Julien et al. (1988) established a finite element runoff model called CASC for spatially varied overland simulation for cascades of planes and for converging and expanding watershed geometries. Richardson and Julien (1989) applied CASC as a one-dimensional finite element overland flow model to simulate and verify the model results for block moving storms over watersheds with simple open book geometries and compared CASC results with laboratory results presented by Yen and Chow (1968). Ogden et al. (1995) utilized the CASC finite element runoff model for one- and two-dimensional physically based runoff simulation to test the suitability of the similarity parameter Vt_e/L_p, where V is the storm speed, t_e is the runoff plane kinematic time to equilibrium, and L_p is the length of the runoff plane, using simple planar and complex watershed topography with moving rainstorms.

Foroud et al. (1984) applied a distributed numerical model based on the time-area concept to examine the effect of moving storms on runoff from a watershed in Quebec. Watts and Calver (1991) studied the effect of storm motion on conceptual catchment response by using a physically based runoff model.

Xiong and Melching (2005) studied the simulation accuracy of typical hydrological and hydraulic routing models, i.e. SWMM and the Dynamic Watershed Simulation Model (DWSM) [a kinematic wave routing model] by testing these models with data from stationary storms obtained from a laboratory experimental system (the Watershed Experimentation System, WES) of Chow and Yen (1974). Xiong and Melching (2005) found that the accuracy of the kinematic-wave routing (DWSM) as indicated by the coefficient of model-fit efficiency is much higher than

that of nonlinear reservoir routing (SWMM), especially for rainstorms with short durations that do not achieve an equilibrium discharge.

Stochastic models were established to reproduce the structure of the rainfall fields, but for practical runoff simulations in urban hydrology these models have not yet been used (Niemczynowicz, 1988).

Lee and Huang (2007) developed non-linear numerical kinematic-wave models to simulate the effect of moving storms on the attainment of equilibrium discharge from an overland plane and from a V-shaped “open book” watershed.

1.2.3 Physical Study

Many studies have utilized experimental techniques based on physical models to investigate moving storm rainfall-runoff processes. The physical laboratory experiments provide some useful visualization, insights, and inspirations for hydrological researchers. They simply simulate the real environment to produce analyzable data that incorporate valuable information, while the complex rainfall and runoff process of moving storms is yet to be accurately numerically modeled. The laboratory experiment results can be used in verification and testing of mathematical computer modeling approaches. However, the construction and operation of a good laboratory watershed is very expensive and complicated. Therefore, only a small number of hydrologists have had access to such watershed apparatus.

The pioneers were Yen and Chow in the 1960s at the University of Illinois at Urbana-Champaign. Yen and Chow (1969) established a laboratory Watershed Experimentation System (WES) to investigate the effect of moving storms on the surface runoff with an impervious surface. The WES system included a 12.2 m by 12.2 m (40 ft by 40 ft) rainfall watershed, 400 raindrop producers forming 100 independent units, water storage and distribution facilities, and control and measurement devices. The watershed was an open-book shape, including a longitudinal channel and two lateral overland planes. The WES experiments were done in three phases from 1965 through 1974, and only the results from Phase 1 were previously published. Yen and Chow (1968, 1969) applied dimensional analysis to the experimental hydrographs to study the influence of moving storms on surface runoff. Through this laboratory study, Marcus (1968) evaluated the importance of the rainstorm movement to the time distribution of surface runoff.

Other early studies were also performed by Amorocho and Orlob (1961), Black (1972), and Townson and Ong (1974). Amorocho and Orlob (1961) reported the limited results of two experiments with the rainstorms moving upstream and downstream and only drew a qualitative conclusion that the movement of the rainstorm affects the characteristics of the runoff hydrographs. Black (1972) utilized a physical laboratory apparatus to investigate the effect of watershed topographical factors (i.e. shape, size, slope, etc.) and storm movement on the outflow hydrographs. Townson and Ong (1974) utilized rainfall simulators to perform a laboratory study of runoff caused by a line storm moving over a conceptual catchment.

Richardson and Julien (1989) utilized Yen and Chow's (1968) laboratory data to validate a one-dimensional application of the CASC finite element overland model that was proposed for simulating the effect of block moving storms over a watershed of simple open book geometry. A total of 9 laterally moving storms and 18 longitudinally moving storms from Yen and Chow's (1968) data set were simulated to verify the one-dimensional numerical model of moving rainstorms. In the process, the numerical model was also calibrated to match the observed data by adjustment of the resistance parameters to obtain refined simulation results. Yen and Chow's hydrographs were corrected for mass balance for all comparisons between simulated and observed results. The agreement results of three typical simulations of storms moving in the three different directions were presented graphically in the paper to simply show the accuracy of the numerical model. However, the accuracy of the simulation results was not further studied statistically and the overall quality of model fit is unknown as are full understanding of the capability and limitations of the model. The lack of adequate proof inevitably undermines the study of the influence of moving storms on the peak discharge and time to peak utilizing the CASC model.

Lee and Huang (2007) also utilized Yen and Chow's (1968, 1969) laboratory data to validate the non-linear numerical kinematic-wave model that was proposed for simulating the effect of moving storms on attainment of the equilibrium discharge from an overland plane and from a V-shaped (open-book) watershed. Only two observed hydrographs one each for downstream and upstream moving storms were selected to validate the numerical model. The comparisons of the observed and computed hydrographs were shown in two graphs, but the model-fit efficiency was not statistically computed, primarily because the original experimental data were not easily

available or readily accessible. Comprehensive verification of the numerical model should be done using a wide range of experimental data. Otherwise, the conclusions of the effects of moving storms on attainment of equilibrium using the kinematic-wave-approximation-based numerical model are questionable.

Although laboratory tests have provided some useful insights for hydrologists, the restriction of the size of the experimental apparatus cannot provide complete knowledge on the subject (Lee and Huang, 2007). Xiong and Melching (2005) pointed out the five limitations of the WES experimental apparatus, compared to the natural rainstorms and urban watershed basins. These include: the short rainfall time duration, the small experimental watershed, the low roughness of the surface of the basin, 100% imperviousness without any initial abstraction, and the simplicity of the watershed basin with a single subarea and a single collecting channel.

1.2.4 Analytical Study

Using the kinematic wave equations, Singh (1998) derived analytical solutions for flow resulting from storms moving up and down a plane. Singh (2002a, b) further derived analytical solutions for flow resulting from a storm moving up or down an infiltrating plane with full and partial areal coverage. Analytic solutions for an overland plane derived by Singh (1998) were used to verify the capability of the numerical model developed by Lee and Huang (2007). An analytical solution is unavailable at present for storms moving on a geometrically complex watershed in which both the overland and channel flow processes are significant (Lee and Huang, 2007).

1.3 Dimensional Analysis

Dimensional analysis can be used to determine basic characteristics of runoff generation in response to moving storms. It is extensively used in this study.

Yen and Chow (1969) first used the dimensional analysis to study the factors affecting surface runoff. The peak discharge was originally expressed in dimensionless form using 13 dimensionless parameters. For each rainstorm tested in their study, some terms in the equation of the dimensionless peak discharge were constants, such as T/iL. Therefore, the dimensionless peak discharge can be defined in the simplified equation as follows:

$$\frac{Q_p}{iA} = f\left(\frac{V}{i}, s_x, \frac{t}{T}\right) \tag{1.2}$$

where Q_p is the peak discharge, A is the area covered by moving storms during the rainfall duration T, s_x is the longitudinal slope of the watershed, V is the velocity of the rainstorm movement, i is the rainfall intensity, t is the discharge starting time, and T is the rainfall duration at a point on the watershed.

Shen et al. (1974) analyzed experimental data for various rainstorm and watershed characteristics by dimensional analysis. For the moving rainstorms tested, the surface runoff can be reduced and expressed in dimensionless form as

$$\frac{Q_p}{iA} = f\left(\frac{ti}{L}, s_x, \frac{Ti}{L}, \frac{VT}{L}\right) \tag{1.3}$$

where L is the length of the watershed. Niemczynowicz (1984a) employed dimensional analysis as per Yen and Chow (1969) and Townson and Ong (1974) to express the relationship between rainfall characteristics and peak discharge for the given catchment as

$$\frac{Q_p}{iA} = f\left(\frac{V}{i}, \frac{Ti}{L}, \frac{t}{T}\right) \tag{1.4}$$

Richardson and Julien (1989) applied three dimensionless parameters q_p/iL, L_s/L, and V_sT_e/L to describe the peak discharge, the length of the storm, and the velocity of the storm, respectively, where q_p is the peak unit discharge, L_s is the length of the rainstorm, and T_e is the time to equilibrium.

Ogden et al. (1995) first identified a dimensionless hydrologic similarity parameter V_sT_e/L which related storm velocity to the influence of storm motion on the hydrograph peak discharge from a one-dimensional runoff plane. L/T_e as a characteristic response velocity was justified by the vertical alignment of the curves, each of which represents equivalent storms of a constant rainfall volume for a specified storm length L_s/L. The effect of storm movement on the peak discharge q_p is studied in the form

$$\frac{q_p}{iL} = f\left(\frac{L_s}{L}, \frac{VT_e}{L}\right) \tag{1.5}$$

Lee and Huang (2007) applied dimensional analysis to obtain the independent variables to be used as control factors in performing a series of numerical tests.

$$\frac{Q_p}{iA} = f\left(\frac{L_s}{L_c}, \frac{VT_e}{L_c}\right) \tag{1.6}$$

where L_c is the channel length in the V-shaped (open book) watershed and T_e is the equilibrium time of the channel flow in the V-shaped catchment or the time of concentration of the channel flow T_{cc}.

1.4 Summary of the Main Findings from Previous Studies

Yen and Chow (1969) found that the equivalent stationary rainstorm produced a higher peak discharge than that of the corresponding moving rainstorm. For a watershed with an impervious surface of simple geometry, the equivalent stationary rainstorms produce the most critical runoff from an engineering viewpoint. The time of occurrence of the peak discharge was earlier for the equivalent stationary storms than for rainstorms moving either upstream or laterally. Under constant intensity with $L_s = L$, the relative discharge Q_p/iA decreases with increasing $|V|/i$. If the storm duration is kept constant, the trend will be reversed, so that increasing $|V|/i$ would increase Q_p/iA.

Richardson and Julien (1989) found that peak discharges were maximized when storms moved down the plane at approximately half the equilibrium flood wave speed $V_s T_e/L$. Storms moving up the watershed produced smaller peak discharges than for equivalent storms moving down the watershed the same speed. As the length of the storm L_s increased (i.e. increased rainfall volume), the maximum peak discharge for equivalent storms increased until the equilibrium discharge was achieved. Increasing the length of the storm further, increased the range of storm velocities which produced equilibrium discharges.

Ogden et al. (1995) found that the effect of storm movement on the peak discharge was greatest when the moving storms travelled a one-dimensional plane in the downstream direction at a dimensionless critical speed of $V_s T_e/L = 0.5$. This finding is valid for all values of the dimensionless storm sizes $L_s/L < 1.0$. The peak discharge is less than the maximum if the storm moves faster or slower than this critical speed. For cases of $L_s/L \geq 1.0$, the maximum peak

discharge is equal to the equilibrium discharge, and in no case could the maximum discharge exceed the equilibrium discharge. For the equivalent rainstorms, the equilibrium discharge can only be attained for storm lengths greater than the length of the overland plane.

Lee and Huang (2007) concluded that for storms moving downstream, the runoff can attain equilibrium discharge even though the storm length is shorter than the watershed length and the rainfall duration is less than the runoff equilibrium time for a stationary uniform discharge. The phenomenon of attainment of equilibrium discharge from watersheds subjected to moving storms is contradictory to conventional hydrological design, which assumes the storm duration must equal the time to equilibrium (i.e. time of concentration) to attain the maximum discharge. Lee and Huang (2007) showed that the dimensionless peak discharge from a moving storm is inversely proportional to the storm speed.

Marcus (1968) reported that agreement between the simulated and experimental results was expected to be better for storms for storms moving downstream than for storms moving upstream for the same rainfall intensity and storm velocity. Marcus (1968) argued that upstream moving storms are associated with smaller discharges, and smaller discharges mean lower depth of flows and therefore higher sensitivity to the effect of raindrop impact. The formulation of the hydrodynamic approach does not account directly for raindrop impact, hence error is expected to be larger when the raindrop impact is more effective.

1.5 Objective of the Research

As previously discussed, many researchers have proposed a variety of methods such as empirical, numerical, experimental, or analytical methods to study the effect of storm movement on the timing and magnitude of runoff. Some researchers verified their numerical models with a very limited amount and variety of the field or laboratory experimental data, and most major hypotheses were developed on the basis of model simulations. They usually developed and applied only one hydraulic model to simulate the moving storms, and their numerical models have never been compared to other models. In addition, the key factors in the hydraulic modeling such as the effect of raindrop impact on the flow resistance and the backwater effect on the drainage of runoff have never been thoroughly examined. Therefore, the runoff response due to moving storms had never been studied with the combination of a great variety of experimental data via statistical analysis, multiple hydraulic models incorporating the variable roughness coefficient and the backwater effect, and dimensional analysis applying the time of concentration as the proper dimensionless parameter.

The primary objective of this research is to evaluate whether downstream moving storms truly magnify the peak discharge for storms with $L_s/L < 1.0$. This evaluation will be done in a non-dimensional comparison of peak discharge and storm movement as has been done in the previous model-based studies. Dimensional analysis has been widely used in many studies to determine the basic characteristics of runoff generation in response to storm movement. The time of concentration, T_e, is a key normalized factor in dimensional analysis. In most previous studies, a thorough examination of the determination of the time of concentration has not been made. The discrepancy between the experimental results and those obtained by the numerical models may

come from the determination of the time of concentration, T_e, or the backwater effect due to the channel capacity limitation. Both of these factors are evaluated in this dissertation.

To identify the importance of the backwater effect the accuracy of the kinematic-wave and dynamic-wave routing models is evaluated by comparing the simulation of surface runoff resulting from upstream and downstream moving storms to a large amount of previously unpublished experimental data collected at the WES. A comprehensive database involving moving storms is developed to build the foundation of this study. The kinematic-wave model for V-shaped (open book) watersheds of Lee and Huang (2007) and dynamic-wave model of Marcus (1968) will be compared to the experimental data in this dissertation. The backwater effect due to the channel capacity limitation is identified in comparison between the results of kinematic-wave and dynamic-wave models. The hypothesis of peak flow magnification by downstream moving storms proposed by other researchers based on model simulation will be tested in comparison with the experimental data.

To evaluate the importance of kinematic-wave based equations for estimation of the time of concentration, comparisons are made to experimental data. Three methods, i.e. Ben-Zvi's method, a modified Ben-Zvi method, and Izzard's method are introduced to determine the time of concentration from the experimental hydrographs. Their results of the methods will be compared to the mathematical equation proposed by Wong (2001), which was used by Lee and Huang (2007) to nondimensionalize the storm velocity. The effect of rainfall intensity on Manning's roughness coefficient n also is evaluated.

CHAPTER 2 EXPERIMENTAL SYSTEM AND EXPERIMENTAL DATA

2.1 Watershed Experimentation System (WES)

The Watershed Experimentation System (WES) was designed and built at the Department of Civil Engineering of the University of Illinois at Urbana-Champion in the 1960s. The WES was developed based on the system engineering concept of integrating the functional components of hydraulic, structural, electronic, pneumatic, and chemical systems (Chow and Yen, 1974). From a functional viewpoint, the WES can also be divided into the components of testing, water recirculation, control, and measurement systems. The testing system included four major parts, which are test basin and substructure, raindrop producers, electronic digital valve assemble (EDVA), and superstructure. The measurement system included sonar depth sensors. The major components in the WES are briefly described in the following sections, and complete details of the WES can be found in the report by Chow and Yen (1974).

2.1.1 Physical and Geometric Characteristics of Test Basin

A schematic of the simplified laboratory watershed is shown in Figure 2.1, and the geometry of the watershed is shown in Figure 2.2. The laboratory test basin is a 40 ft by 40 ft square area with adjustable longitudinal and lateral slopes. A variety of sizes and shapes of the test basin can be configured within the 40 ft by 40 ft square area. The maximum size of the test basin is 40 ft by 40 ft, and a smaller one can be 30 ft by 30 ft. The test basin consists of a longitudinal channel portion and two lateral overland planes. The flow of the test basin consists of overland and channel flows. Both channel and overland flows are considered as one-dimensional flows. The

types of basin surface included the rough side of waterproof tempered masonite boards and smooth aluminum plates. Hence, the surface runoff was simulated in the laboratory test basin with an impervious surface.

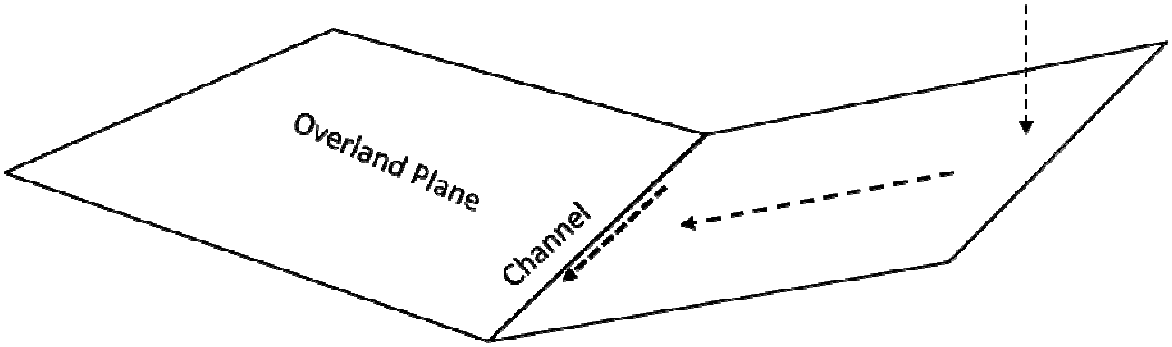

Figure 2.1 A Schematic of the Simplified Laboratory Watershed

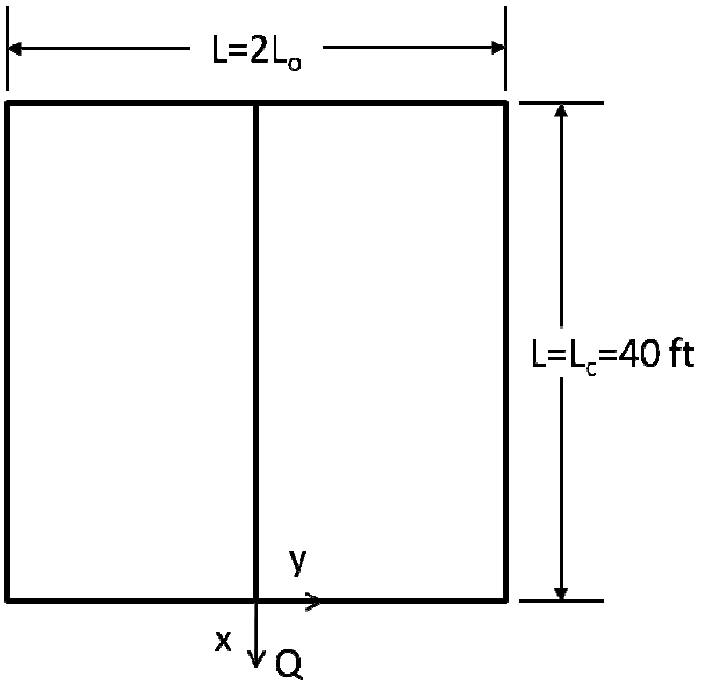

Figure 2.2 Geometry of the Simplified Laboratory Watershed

2.1.2 Raindrop Producers

A picture of a raindrop producer used in the WES is shown in Figure 2.3. The artificial rainfall falling on the laboratory watershed was produced by 400 raindrop producers, each being a 2 ft by 2 ft by 1.75 in. lucite box located approximately 7 ft above the basin surface. Raindrops were randomly produced from 576 polyethylene tubes of 0.023 in. inside diameter (I.D.) and 0.75 in. long inserted into the bottom of each lucite raindrop producer. The equivalent raindrop diameter was 0.14 in., equal to the diameter of a sphere having the same volume as the raindrop. Four raindrop producers form a module covering an area of 16 sq ft and are connected by four 3/8 in. I.D. polyethylene tubes to a common EDVA for water supply, shown in Figure 2.4. Thus, there are 100 hundred modules over the entire basin, each having an EDVA for flow rate control.

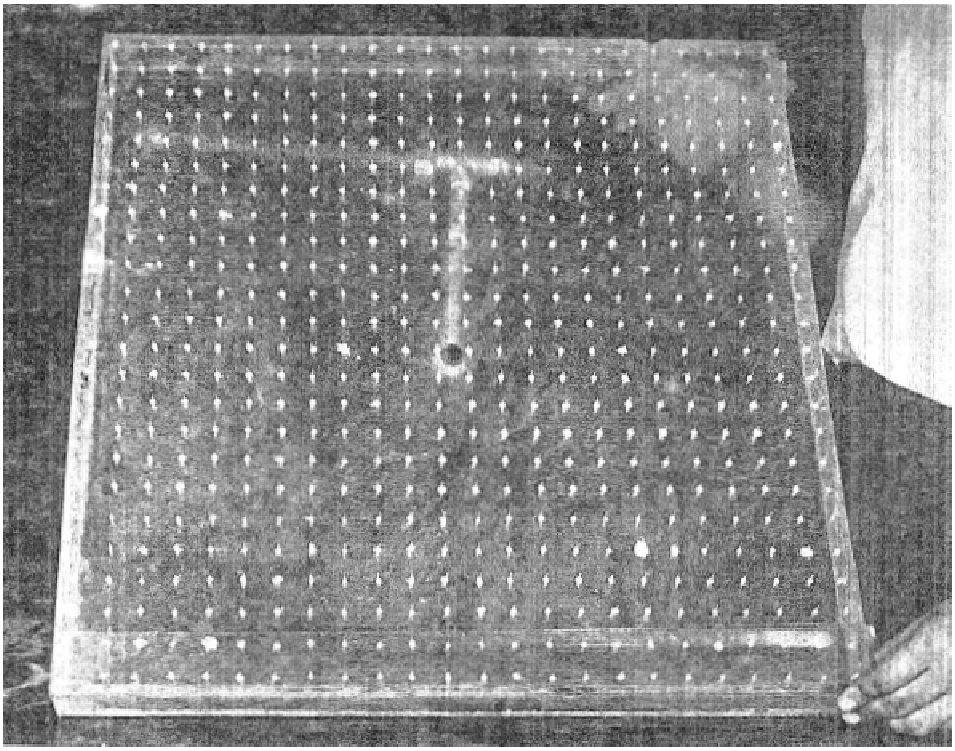

Figure 2.3 A Raindrop Producer in the WES (after Chow and Yen, 1974)

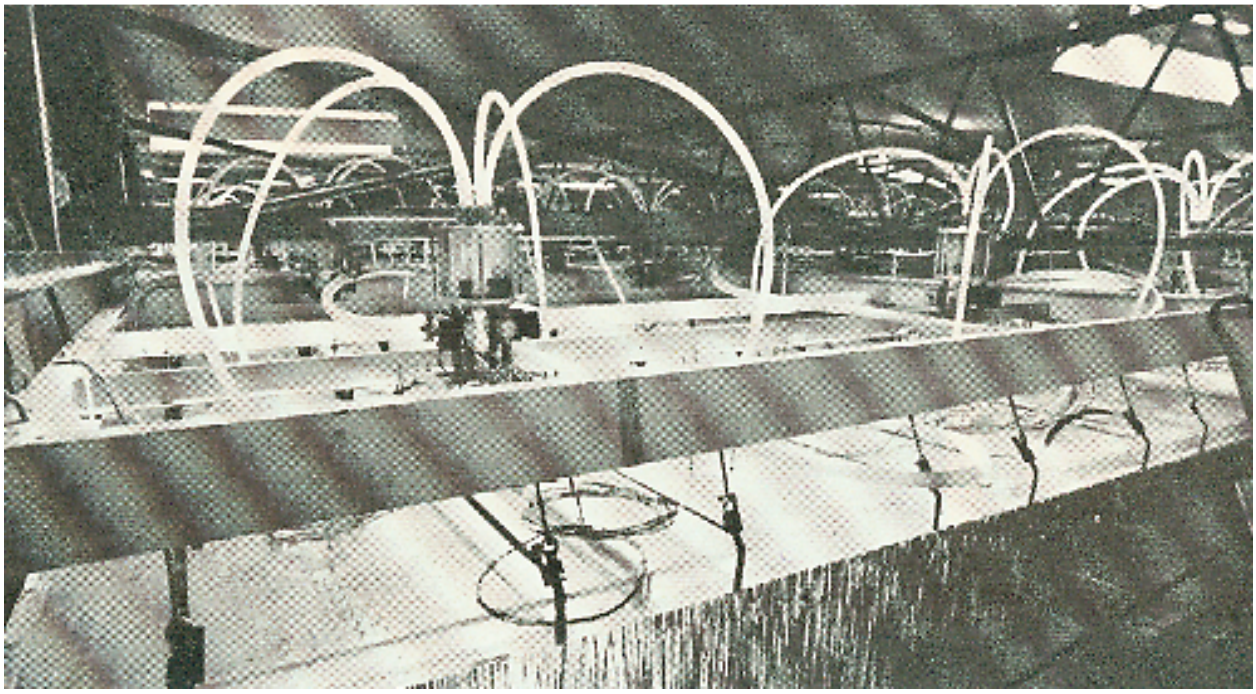

Figure 2.4 Each Electronic Digital Valve Assembly (EDVA) Connected to Each Raindrop Module with Four Polyethylene Tubes

Each EDVA has four solenoid valve-controlled independent flow passages of different discharges to produce 15 different intensities of rainfall nominally ranging from 0.75 to 15 in./hr for desired durations. Since each EDVA can be controlled independently, rainstorms of varying temporal and areal distributions, particularly moving rainstorms can be generated and tested in the WES.

The EDVA has two 4.75 in. I.D. cylinders 2.1 in. and 4.1 in. long, respectively. The short cylinder is connected to the water supply distribution network by a 3/4 in. I.D. polyethylene tube and the long cylinder is connected to four raindrop producers by four 42 in. long 3/8 in. I.D. polyethylene tubes. The two cylinders are connected by four solenoid valves. The solenoid

valve is operated by electric magnetic force so that there are only two positions for flow, namely, fully open or completely closed. The flow rate through these four solenoid valves within each module is at the ratio of 1:2:4:8. Each of the solenoid valves can be commanded independently either by manual control or by the electric pulses transmitted from a PDS 1020 digital computer through an electronic digital-analog interface console.

Therefore, by programming the desired operating rainstorm patterns on watersheds of different sizes or shapes within the size of 40 ft square, the temporal and spatial distribution of the rainfall, with the limitation of 4-ft stepwise (or block) variation in the longitudinal and/or lateral directions, can be achieved by proper control of the solenoid valves. The constancy of the flow rate through the solenoid valves is ensured by a constant pressure difference of 12 psi between the upstream and downstream ends of the valves which is maintained by a pneumatic control system.

2.1.3 Measurement System

Four types of measurement devices were used in the WES to measure the flow rate delivered into the raindrop producers and the discharge from the basin. The former is measured by Potter Flowmeters and an elbow meter, and the latter by the sonars and the Constant-Discharge Floating –Siphon Stage-Recorder System (CDFS).

The two sonars are located at 2 ft from either side of the central line of the storage tank, shown in Figure 2.5. They measure the depth of the water in the tank at an interval of 5 seconds. The sonars are sensitive enough to detect depths to an accuracy of approximately 1/30 in. The water

depth also can be recorded continuously by the CDFS. The purpose of using these dual measurement systems was to provide a means of double checking the experimental measurements and a means to perform experiments when the electronic components, particularly the computer, are not functioning properly (Chow and Yen, 1974).

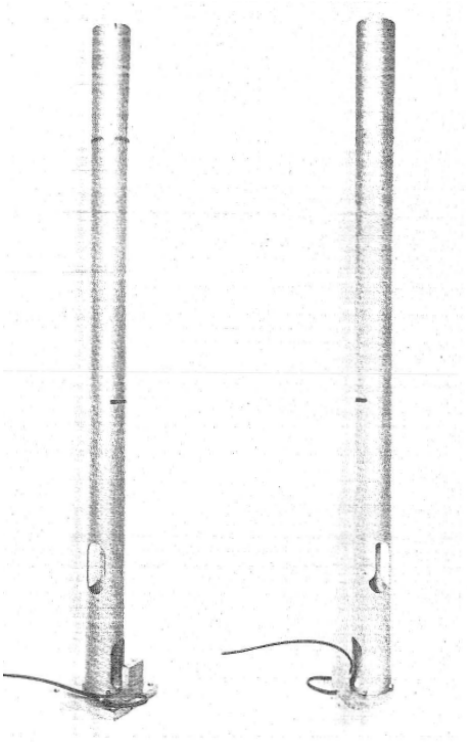

Figure 2.5 Sonar Depth Sensors (after Chow and Yen, 1974)

2.1.4 Capabilities and Limitations of the WES

The most significant feature of the WES is its capability to produce rainfalls with different temporal and areal distributions. The velocity of the movement can be uniform or nonuniform, and is equal to 4/t where t is the time interval to progress from one module to the next. The moving rainstorm can be of constant rainfall intensity as investigated by Marcus (1968), Yen and

Chow (1969), and Shen et al. (1974) or with intensities of linear or nonlinear variations (Chow and Yen, 1974).

The experimental data provided by the WES is extremely useful in the verification of various mathematical watershed hydrodynamic models and to provide information in developing a practical method to predict prototype watershed runoff; such as was done by Chow and Ben-Zvi (1973).

Xiong and Melching (2005) analyzed the five limitations of the WES. The biggest limitation is that the roughness coefficient of the smooth aluminum plates as the basin surface is much lower than those of channels or overland surfaces in the real world. Other major limitations of experimental data relative to the real world include a small and simple geometric watershed without any infiltration, and very short rainfall duration.

2.1.5 Improvement of WES

The WES had been under continuous improvement and modification since experiments began for watershed runoff for stationary and moving rainstorms. After 5 years of continuous service of the WES, it was observed that during the experiments, a uniform distribution of rainfall intensity on some portions of the watershed area was difficult to maintain. The major sources of trouble were the weakening of the power supply to the solenoid valves of the EDVA, which control the rainfall intensity, and the clogging of capillary tubings of some raindrop producers. The clogging problem was solved by cleaning the 230,400 capillary tubings one by one with needles. It also was found at the early stage that the power supply unit to the solenoid valves of the EDVA was

underdesigned, and although a corrective measure was made temporarily to fix the problem, after five years of operation, a new power supply unit was added to the WES. The CDFS also was developed to improve the experimental measurement accuracy as a double check (Chow and Yen, 1973).

2.1.6 Experimental Program of the WES

Beginning in 1965 several thousand experiments on surface runoff were performed in the WES. In the last of three research grants from 1969 to 1973, a comprehensive systematic experimental program was undertaken to collect data from the WES for future analysis. Although the experimental accuracy had been greatly improved since 1970, it was difficult to maintain the high experimental accuracy required for a reliable verification of the mathematical models, since the electronic and mechanical components deteriorate quickly with time, and the cost of maintenance and repair efforts were great (Chow and Yen, 1973). Therefore, all necessary experiments were performed in the shortest time possible.

2.2 The Experimental Data

The WES data basically consisted of input and output data. Input data included the characteristics of the rainstorm and the properties of the watershed. Output data are the measured hydrographs which are temporal distributions of the surface runoff. The characteristics of the rainstorms include rainfall intensity and duration, as well as velocity and direction of storm movement. The properties of the watershed include dimensions of the watershed topography, and the longitudinal and lateral slopes.

Two major types of experimental rainfall were well studied with the WES; namely, uniform stationary storms and moving storms including moving upstream or downstream. Nonuniform stationary storms and laterally moving storms were also studied to some extent (e.g., Shen et al., 1974). Only the results from Phase 1 of the moving rainstorm experiments were previously published (Yen and Chow, 1968). The previously unpublished data from Phases 2 and 3 of this study were obtained by Professor Charles S. Melching at Marquette University from Professor Ben C. Yen and compiled for this study. The tests in Phases 2 and 3 are studied only if the rainfall and geometric parameters (dimensions of the watershed, longitudinal and lateral slopes, storm intensity, storm length, storm duration, and storm velocity) and the measured hydrographs are available for the tests.

From Phases 2 and 3, a total number of 61 experimental stationary storms reaching the equilibrium discharge are available, and a total number of 114 experimental moving storms are available, 32 of which have the storm length equal to the length of the watershed. These data are the focus of the analyses done in this dissertation.

2.2.1 Previous Moving Storms Studies with the WES by Yen and Chow and Their Students

Previous moving storms studies with data from the WES were done by Yen and Chow (1969) and their students (Marcus, 1968, Ben-Zvi, 1970, Shen et al., 1974) are summarized to help reveal the motivation of the experimental investigations in Phases 2 and 3. That is, what's new in the data from Phases 2 and 3 compared to Phase 1 data may be determined from the summaries in Tables 2.1 and 2.2. It can be seen that, the experiments on both stationary and moving

rainstorms from Phases 2 and 3 were characterized by higher rainfall intensities and a greater variety of lengths of rainfall, compared to the experiments from Phase 1.

In the final years of the WES all effort was directed toward collecting more experimental results while the system was still functioning well. Unfortunately, the Phase 2 and 3 data never were analyzed by any of the original project investigators for some historic reasons. The experimental results in the form of computer print-outs silently sat in boxes in the basement of the Hydrosystems Laboratory at the University of Illinois from 1975 to 2000. Therefore, it is of interest and significance to mine the useful information out of the WES Phase 2 and 3 data. Since the Phase 1 data has been analyzed, the Phase 2 and 3 data are reviewed and summarized in comparison with the Phase 1 data.

Analysis of the 101 moving rainstorm experiments done in Phase 1 of the WES study (Yen and Chow, 1968) has formed the basis of many of the studies of the effects of storm movement on flood generation.

Shen et al. (1974) conducted experiments for 3 different intensities and 7 different durations of rainfall on a 40 ft by 40 ft watershed with 1% basin slope for 3 different speeds of storms moving towards upstream and downstream. The characteristics of the experimental moving storms measured by Shen et al. (1974) are listed in Table 2.3. The data from Phases 2 and 3 are as listed in Table 2.4 and 2.5.

Ben-Zvi (1970) conducted experiments with stationary rainstorms, and proposed an exponential relationship between Q_p/iA and T/t_p, where t_p is the time of occurrence of peak discharge.

Marcus (1968) conducted experiments with moving rainstorms, and showed the significance of the parameter V/i in affecting the dimensionless hydrographs of Q/Q_p and t/t_p, where Q is the surface runoff and t is the time. Yen and Chow (1968) reanalyzed Marcus's experimental data based on dimensional analysis to demonstrate the importance of the movement of rainstorms on the time distribution of the surface runoff, and found that the relative peak discharge, Q_p/iA, decreased with increasing $|V|/i$.

The moving rainstorms tested by Marcus (1968) had uniform intensities moving at constant velocities across the watershed, and the rainfall duration at any point in the watershed was equal to the length of time required for the rainstorm front to travel across the watershed. Consequently, Marcus's as well as Yen and Chow's conclusions are valid only for moving rainstorms with this particular pattern of storm length equal to watershed length tested (Shen et al., 1974).

Table 2.1 Ranges of Watershed and Storm Characteristics for Previously Evaluated WES Experiments on Moving Rainstorms in Comparison with those for the Experiments in Phases 2 and 3

	Watershed characteristics				Moving rainstorm characteristics			
	Size (ft^2)	L_x (ft)×L_y (ft)	S_x[1]% + S_y[2]%	Surface	i_e[3] (in./hr)	T (min)	V_x[4] (ft/s)	V_y[5] (ft/s)
Harbaugh (1966)	1024		1.0/1.75+1	Masonite				
Rao (1968)	1024/1600		0.5/1.5/3+1	Masonite				
Marcus (1968)	1024	32×32	0.5/1/1.75/2.9+1	Masonite	3.5/ 6.5	L/|V|	0.1/0.2/ 0.133/0.4	0.1/0.2/ 0.133/0.4
Yen and Chow (1968)	1024	32×32	0.5/1/1.75/2.9+1	Masonite	3.5/6.7	L/|V|	0.1/0.2/ 0.133/0.4	0.1/0.2/ 0.133/0.4
Ben-Zvi (1970)	160~1600		0.5/1.5/3+1	Masonite Aluminum				
Shen (1974)		40×40/24/16/8, 20/8×40	1+1	Aluminum	4.3~13	30/60/100/120/ 200/240/400	0.1/0.2/0.4	0.1~0.4
Phase 2	200~600	40×40/32/24/16/8, 20/8/4×40	1+0.5/1/3/5, 0.5/2/3+1	Aluminum	6/10/15	30/60/100/120/ 200/240/400	0.044/0.022/ 0.1/0.2/0.4	0.1~0.4
Phase 3	200~1600	40×40	1+0.5/1/5, 0.5/1/2/3+1	Aluminum	6/10/15	30/60/100/120/ 200/240/400	0.1/0.2/0.4	0.1~0.4

[1] S_x is the watershed longitudinal slope.
[2] S_y is the watershed lateral slope.
[3] The rainfall intensities of moving storms in Phases 2 and 3 are nominal intensities, whereas those in Marcus (1968), Yen and Chow (1968), and Shen et al. (1974) are actual intensities.
[4] V_x is the velocity component of the rainstorm moving along the x direction.
[5] V_y is the velocity component of the rainstorm moving along the y direction.

Table 2.2 Ranges of Watershed and Storm Characteristics for Previously Evaluated WES Experiments on Stationary Rainstorms in Comparison with Those for the Experiments in Phases 2 and 3

	Watershed characteristics				Stationary rainstorm characteristics	
	Size (ft^2)	L_x (ft) × L_y (ft)	S_x[1]% + S_y[2]%	Surface	i_e[3] (in./hr)	T (min)
Harbaugh (1966)	1024		1.0/1.75+1	Masonite		
Rao (1968)	1024/1600		0.5/1.5/3+1	Masonite		
Marcus (1968)	1024	32×32	0.5/1/1.75/2.9+1	Masonite	3.5~6.5	T=L/|V|
Ben-Zvi (1970)	160~1600		0.5/1.5/3+1	Masonite Aluminum		
Shen (1974)		40×40/32/24/16/8, 20/ 8/4×40	0.5/1/3+1	Aluminum	4.4~13.2	30/60/120/ 240
Phase 2	200~1600	40×40/32/24/16/8, 20/8/4×40	1+0.5/1/3/5, 0.5/2/3+1	Aluminum	6/8/10/15	30/60/120/ 180/ 240
Phase 3		40×40/32/24/16/8, 20/8/4×40	1+0.5/1/3/5, 0.5/2/3+1	Aluminum	6/8/10/15	30/60/120/ 180/ 240

[1] S_x is the watershed longitudinal slope.
[2] S_y is the watershed lateral slope.
[3] The rainfall intensities of moving storms in Phases 2 and 3 are nominal intensities, whereas those in Marcus (1968), Yen and Chow (1968), and Shen et al. (1974) are actual intensities.

Table 2.3 Nominal Intensities of Moving Rainstorms of Different Durations and Movement Velocities on a 40 ft by 40 ft Watershed with $S_x = S_y = 1\%$ (after Shen et al., 1974)

		Duration																					
		30			60			100			120			200			240			400		
0.4	Downstream	5	9	12	4	8	12	5	8	12	5	8	12						11			
	Upstream	5	9	12	4	8	12	5	9	12	5	8	12						11			
	Lateral												12									
0.2	Downstream			13	5	9	13				5	9	12	5	8	12	5	8	12			
	Upstream			13	5		13				5	8	12	5	8	12	5	8	12			
	Lateral												12									
0.1	Downstream						12				5	9	12				5	8	12	5	8	11
	Upstream						13				5	9	12				4	8	12	5	8	11
	Lateral												12									

Table 2.4 Nominal Intensities of Moving Rainstorms of Different Durations and Movement Velocities on a 40 ft by 40 ft Watershed with $S_x = S_y = 1\%$ in Phase 2

		Duration																					
		30			60			100			120			200			240			400			
0.4	Downstream	6	10	15	6	10	15		10				15				6	10	15				
	Upstream	6	10	15	6	10	15	6	10	15	6	10	15				6	10	15				
	Lateral																						
0.2	Downstream			15			15					10	15	6	10	15	6	10	15				
	Upstream			15			15					10	15	6	10	15	6	10	15				
	Lateral																						
0.1	Downstream						15						15				6	10	15	6	10	15	
	Upstream						15						15				6	10	15	6	10	15	
	Lateral																						

Table 2.5 Nominal Intensities of Moving Rainstorms of Different Durations and Movement Velocities on a 40 ft by 40 ft Watershed with $S_x = S_y = 1\%$ in Phase 3

		Duration																					
		30			60			100			120			200			240			400			
0.4	Downstream	6	10	15	6	10	15	6	10	15	6	10	15				6	10	15				
	Upstream	6	10	15	6	10	15	6	10	15	6	10	15				6	10	15				
	Lateral																						
0.2	Downstream			15		10	15						15	6	10	15	6	10	15				
	Upstream			15		10	15						15	6	10	15	6	10	15				
	Lateral																						
0.1	Downstream						15					10					6	10	15	6	10	15	
	Upstream						15					10	15				6	10	15	6	10	15	
	Lateral																						

2.2.2 Calculated Intensity from Equilibrium Discharge

In general the exact rainfall intensity in the experiments was unknown because of the nature of the experiments and the experimentation system. For stationary storms that reached an equilibrium discharge the experimental rainfall intensity was calculated by the formula $i = Q_p/A$ where Q_p was equal to measured peak discharge. If an impervious watershed is subjected to constant rainfall intensity for a duration greater than its time of concentration the product of intensity and area must equal the peak discharge.

All of the computed rainfall intensities from observed plateau (equilibrium discharge) hydrographs are lower than the nominal values for the WES. The average values of rainfall intensities were calculated for each nominal intensity, respectively, and the results are listed in the Table 2.6. The tests include results from experiments on test watersheds smaller than 40 ft by 40 ft. The values of calibrated rainfall intensities in Phase 1 are obtained from the calibration curve constructed by Chow and Yen (1974) on October 20, 1967.

Table 2.6 Comparison of Nominal Intensities and Average Computed Values

$I_{nominal}$ (in./hr)	$I_{calibrated}$ (in./hr) in Phase 1	Avg. I_{com} (in./hr) in Phase 2	Avg. I_{com} (in./hr) in Phase 3
6	5.5	4.5916	4.2296
8	7.3	6.9307	6.7931
10	9.1	8.1784	7.8181
15	13.7	11.2092	10.8900

The calibrated rainfall intensities in Phase 1 range from 91% to 92% of the nominal values. The computed rainfall intensities in Phase 2 range from 74% to 86% of the nominal values, and in Phase 3 from 68% to 87%. The calibrated rainfall intensities are just a percentage of the nominal

values, because the EDVA cannot produce the intended nominal rainfall intensities in Phase 1 even at the beginning of the WES experiments. It makes sense that the average computed rainfall intensities for Phases 2 and 3 are much smaller when compared to the nominal values and the calibrated values in Phase 1. This discrepancy primarily results from the wear and tear on the equipment, primarily clogging of the raindrop tubes, and different rates of the wear and tear on the raindrop producer modules, but human errors in recording also may be factors (Xiong and Melching, 2005).

Experiments on stationary and moving rainstorms were done in the WES through Phases 1, 2, and 3. Since the simulated watershed is relatively small, compared to the area of watersheds in reality, only the experimental data from the maximum area (40 ft by 40 ft) of the watershed were considered in this dissertation.

CHAPTER 3 SIMULATION OF SURFACE RUNOFF

3.1 Saint-Venant Equations

Distributed flow routing models can be used to describe the transformation of storm rainfall into runoff over a watershed to produce a flow hydrograph at the watershed outlet. The basic equations are well known as the de Saint-Venant equations (also known as the dynamic-wave equations), which consist of continuity and momentum equations for unsteady flow. The de Saint-Venant equations, first developed by Barre de Saint-Venant in 1871, are the governing equations for one-dimensional, unsteady open channel flow.

A variety of simplified forms of the de Saint-Venant equations have been proposed and used in hydraulic engineering and hydrology, each defining a one-dimensional distributed routing model. The momentum equation in the dynamic-wave model consists of the terms for the physical processes that govern the flow momentum. These terms are: the local acceleration term, the convective acceleration term, the pressure force term, the gravity force term, and the friction force term. Alternative distributed flow routing models are produced by using the full continuity equation while eliminating some terms of the momentum equation. The simplest distributed model is the kinematic wave model, which neglects the local acceleration, convective acceleration, and pressure terms in the momentum equation; that is, it assumes $S_0 = S_f$ and the friction and gravity forces balance each other. The non-inertia model neglects the local and convective acceleration terms but incorporates the pressure term.

Dynamic wave routing was first used by Stoker (1953) and by Isaacson et al. (1954) in their pioneering investigation of flood routing for the Ohio River. In the early 1970s, the U.S. National Weather Service (NWS) Hydrologic Research Laboratory began to develop a dynamic wave routing model based upon the implicit finite-difference solution of the de Saint-Venant equations. The model known as DWOPER (Dynamic Wave Operational Model) has been implemented on a variety of rivers with backwater effects and mild bottom slopes (Chow et al., 1988).

Fread (1984) developed a comprehensive dynamic wave model (FLDWAV) for one-dimensional unsteady flows in a single or branched waterway. This model is a synthesis of two widely used models, DWOPER (Fread, 1978) and DAMBRK (Fread, 1980). The model is an implicit (four-point, nonlinear) finite-difference solution of the de Saint-Venant equations. Its special features include allowing the roughness coefficient to vary with discharge or water surface elevation, and distance along channel (Singh, 1996).

Kinematic-wave modeling has been considered as a fast and accurate way of solving a wide range of water resources problems in the past thirty years. The kinematic-wave technique is applied to overland and channel flow routing in some famous hydraulic softwares, such as HEC-RAS, DUFLOW, and MIKE 11.

Marcus (1968) also developed a dynamic-wave model for open-book watersheds by applying the equations of continuity and momentum for spatially varied unsteady flow to both the overland and channel flows. A total of 14 moving storms were simulated on an IBM 7094 computer, of

which 6 were moving downstream, 5 were moving upstream, and 3 were moving laterally. The cases were moving storms with intensities of 3.5 or 6.5 in./hr on a basin with a 1% channel slope and a 1% overland slope. Six moving storms were chosen for demonstration, since they represented different values of rainfall intensity and storm velocity. One storm moving downstream showed the best agreement between the computed and experimental values, while one storm moving upstream showed the poorest agreement.

Marcus (1968) used a finite-difference approach to approximate the partial derivatives with equivalent difference quotients. Three forms of differences are commonly considered: forward, backward, and central differences. The error in finite difference approximation can be first order, second order, or higher, which can be derived from Taylor's theorem. Both forward (downwind) and backward (upwind) finite differences are first-order approximations, while the central difference is a second-order approximation. Therefore, the central finite difference approximation is more accurate than the first- or second- order finite difference approximations. Forward, backward, or central finite differences can yield both explicit and implicit schemes.

3.2 Dynamic-Wave Model

3.2.1 Dynamic-Wave Equations

The continuity equation for a one-dimensional spatially varied unsteady flow with the effective rainfall inflow is

$$y\frac{\partial v}{\partial x} + v\frac{\partial y}{\partial x} + \frac{\partial y}{\partial t} = i_e \tag{3.1}$$

where v is the velocity along the x direction, averaged over the depth of flow, y, and i_e is effective rainfall intensity, which equals the rainfall intensity for the WES, that acts as the lateral inflow per unit time per unit length in the x direction for the overland flow plane.

The momentum equation is

$$\frac{\partial v}{\partial t} + v\frac{\partial v}{\partial x} + g\frac{\partial y}{\partial x} = g(S_0 - S_f) \tag{3.2}$$

where S_0 is the slope of the channel bottom and S_f is the total flow frictional resistance gradient.

For a V-shaped catchment, essentially the same equations are then applied to the channel flow portion, for which the computed flow uses a lateral inflow composed of both the overland portion and the rain falling directly on the channel. Thus, the continuity equation becomes

$$q_l = vy \tag{3.3}$$

$$y\frac{\partial v}{\partial x} + v\frac{\partial y}{\partial x} + \frac{\partial y}{\partial t} = \frac{q_l}{T} + i_e \tag{3.4}$$

where T is the width of the overland land flow strip considered in the modeling.

The value of S_f at a point can be expressed approximately as

$$S_f = \frac{v^2 n^2}{y^{4/3}} \tag{3.5}$$

where

$$n = 0.017y^{-0.166} \tag{3.6}$$

for a masonite surface of 1% slope. In Section 3.4, detailed information is given on Equation (3.6).

In the Marcus (1968) dynamic-wave model, the equations were first applied to the overland flow portion, for which the rainfall is the only lateral inflow. The same equations were then applied to the channel flow portion, for which the computed flow used the lateral inflow composed of both the overland flow portion and the rainfall on the channel.

3.2.2 Explicit Finite Difference Approximations

In the explicit schemes the set of finite difference algebraic equations are manipulated so that unknown parameters are expressed explicitly as functions of known quantities, allowing them to be solved directly. Depending on the number and position of the grid points used in expressing the finite difference to approximate the derivatives, there are many different explicit schemes. They include the Lax-Wendroff scheme, diffusive scheme, MacCormack scheme, leap-frog schemes, and other staggered schemes.

The simplest explicit scheme consists of a forward difference scheme for the time derivative and a central difference scheme for the spatial derivative using known terms on time line. The two governing equations were rewritten in finite difference forms so that values of velocity and depth for each succeeding time and spatial interval can be calculated based on the previously calculated values.

The finite difference approximation for the terms in Equations (3.1) and (3.2) is

$$\frac{\partial\, y_i^k}{\partial x} = \frac{y_{i+1}^k - y_{i-1}^k}{2\Delta x} \tag{3.7}$$

$$\frac{\partial\, y_i^{k+1}}{\partial t} = \frac{y_i^{k+1} - y_i^k}{\Delta t} \tag{3.8}$$

$$\frac{\partial\, v_i^k}{\partial x} = \frac{v_{i+1}^k - v_{i-1}^k}{2\Delta x} \tag{3.9}$$

$$\frac{\partial\, v_i^{k+1}}{\partial t} = \frac{v_i^{k+1} - v_i^k}{\Delta t} \tag{3.10}$$

Substituting these terms into Equations (3.1) and (3.2) yields two equations as a basis for the numerical computations.

$$y_i^{k+1} = y_i^k + \Delta t\left(\frac{y_{i-1}^k v_{i-1}^k - y_{i+1}^k v_{i+1}^k}{2\Delta x}\right) \tag{3.11}$$

$$\frac{y_i^{k+1} - y_i^k}{\Delta t} + \frac{v_{i+1}^k - v_{i-1}^k}{2\Delta x} + g\frac{y_{i+1}^k - y_{i-1}^k}{2\Delta x} = g\left(S_0 - S_f\right) \tag{3.12}$$

where Δt and Δx are time and space steps, i and k are time and space indices.

3.2.3 Initial and Boundary Conditions

3.2.3.1 Initial Conditions

The initial values at every node along the x-axis must be known. One of the most difficult initial conditions is that represented by a dry channel, for which $v = 0$ and $y = 0$. This condition imposes a singularity problem on the first computational step advanced by Δt. A number of schemes have been proposed to overcome such a difficulty. Chen and Chow (1968) suggested the use of a slow steady uniform flow as the initial condition for which $y = rt$ and v was computed by a uniform flow formula. Following the basic concept of this suggestion, Karliotis

and Chow (1970) determined the initial depth of flow y_i from laboratory observations. They further postulated that the flow would not commence until the amount of initial depth had been built up to break the surface tension force. Accordingly, the assumed initial conditions in this study can be stated as

$$t = 0 \tag{3.13}$$

The initial condition is the flow condition in the laboratory watershed when computation starts, $t = 0$, i.e., either the discharge $Q(x, 0)$, or the velocity $V(x, 0)$, paired with the depth $y(x, 0)$. For the WES system, theoretically, this initial condition is dry bed with zero depth, zero velocity, and zero discharge. However, this zero initial condition imposes a singularity in the numerical computation. To avoid this singularity problem either a small depth or a small discharge is assumed so that the computation can start. $y(x, t_0) = y_i$ and $v(x, t_i) = v_i$ where $v_i = 0$ for a dry surface channel and corresponds to a uniform flow velocity when a small base flow is present. The initial depth of flow $h_0$is related to t_0, the initial time of flow, by $y_0 = rt_0$. All the quantities used in the foregoing equations are dimensional. The appropriate initial depth depends on many factors such as surface tension, viscosity of water, raindrop impact, ground surface slope, and roughness. Assumptions must be made to estimate the y_0 value under the combined influence of these factors. Marcus (1968) considered that there is no flow initially at the time $t = 0$, therefore, $y_0 = 0$.

3.2.3.2 Boundary Conditions

Upstream boundary condition

Proper upstream boundary conditions may consist of specifying the flow depth, velocity, or the relationship between them such as a stage-discharge rating. A flow regulation structure can also furnish such information. In this laboratory model, the fixed watershed divide uniquely defines a no-flow condition at the upstream station. Therefore, the condition at the upstream station is prescribed as

$$V_{upstream} = 0 \tag{3.14}$$

For this assumption, the flow will always start with a subcritical flow state (Hsie and Chow, 1974).

Downstream boundary condition

The downstream boundary condition may be a discharge hydrograph or a restriction on the flow such as the critical depth. However, often times when such knowledge is unavailable, a normal flow condition is specified. In modeling the laboratory watershed runoff, a free overfall can be prescribed as the downstream boundary condition for both overland and channel flows since the water discharges into the respective receiving channel and tank in the form of a nappe. Thus, the flow depth at the downstream station is given by a critical depth, D_c as

$$D_c = F_r^2 V_c^2 \tag{3.15}$$

where F_r is the Froude number, and V_c is the critical velocity.

The interaction between overland flow and channel flow can be simulated in the dynamic-wave model. The effect of flow depth in the channel on the lateral inflow is preserved by retaining the pressure term $\frac{\partial y}{\partial x}$, as shown from writing the spatial derivative of the depth in Eq. (3.16) below.

$$\frac{\Delta y}{\Delta x} = \frac{y_{downstream} - y_{upstream}}{\Delta x} \tag{3.16}$$

3.3 Kinematic-Wave Model

In this study, the non-linear numerical kinematic-wave model developed by Lee and Huang (2007) for moving storms on a V-shaped (open book) watershed was utilized to simulate the experimental storms in Phases 2 and 3 of the WES experiments.

In a kinematic wave, the gravity and friction forces are balanced and pressure forces and acceleration effects are ignored. The kinematic wave approximation is useful for applications where the channel slopes are steep and backwater effects are negligible. The kinematic wave model is helpful in describing downstream wave propagation when the channel slope is greater than about 1% and there are no waves propagating upstream due to disturbances such as tides, tributary inflows, or reservoir operations. A dynamic wave routing model is required when backwater effects from downstream disturbances are not negligible (Chow et al., 1988).

The kinematic-wave method was first proposed by Lighthill and Whitham (1955) as the simplest distributed hydraulic routing model. It has subsequently been used in many rainfall-runoff simulation models. Singh (1996, 1997b) compiled extensive books on the kinematic-wave method applications in surface water and environmental hydrology.

3.3.1 Kinematic-Wave Equations

Kinematic-wave theory can be applied for overland flow and channel routing, for cases where the local acceleration, convective acceleration, and the pressure terms in the momentum equation can be neglected; the bed slope, S_0, is assumed to equal the friction slope, S_f.

$$S_0 = S_f \tag{3.17}$$

For an overland plane model, the flow depth can be expressed as

$$y = \alpha^{-1/\beta} q^{1/\beta} \tag{3.18}$$

where y is the flow depth and q is the unit discharge rate. Using Manning's equation to compute S_f the constant β is 5/3, and the constant α can be estimated as $S_0^{0.5}/n$, and n is the Manning roughness coefficient. This depth-discharge relation has been reported to be a better form of the the kinematic wave equation for numerical computations (Li et at., 1975).

For channel flow in the watershed, the channel cross-sectional area, A_c, can be expressed in terms of the channel flow rate as

$$A_c = \alpha_c^{-1/\beta_c} Q^{1/\beta_c} \tag{3.19}$$

where α_c and β_c are constants.

The momentum equation is

$$S_c = S_f \tag{3.20}$$

where S_c is the channel slope.

3.3.2 Implicit Finite Difference Approximations

In the implicit finite difference schemes, the spatial partial derivatives are replaced in terms of the values at the unknown time level. The unknown variables in the algebraic equations for the entire system have to be solved simultaneously in these methods. Several implicit finite difference schemes have been used for unsteady open channel flows. The weighted four point scheme, or Preissmann scheme has been extensively used since the early 1960s. The system of equations is a set of nonlinear algebraic equations. It can be solved by the Newton-Raphson method, or double sweep method (Cunge et al., 1980).

The implicit scheme of the finite difference approximation can be used to solve kinematic wave equations for both overland and channel flows. For overland flow, the kinematic wave equation can be expressed as

$$\frac{\partial}{\partial t}\left(\alpha^{-1/\beta} q^{1/\beta}\right) + \frac{\partial q}{\partial x} = i_e \tag{3.21}$$

Equation (3.20) can be expanded by the finite-difference method in an implicit form. In Equation (3.21), the unknown discharge q_{i+1}^{k+1} is on the left-hand side, and all the known values are on the right-hand side. This implicit scheme leads to a nonlinear scheme. Therefore, the Newton and Rhaphson method will be required to solve the equations.

$$\begin{aligned} &\frac{\Delta t}{\Delta x} q_{i+1}^{k+1} + \alpha^{-1/\beta}\left(q_{i+1}^{k+1}\right)^{1/\beta} \\ &= \frac{\Delta t}{\Delta x} q_{i}^{k+1} + \alpha^{-1/\beta}\left(q_{i+1}^{k}\right)^{1/\beta} \\ &+ \Delta t\left[\frac{(i_e)_{i+1}^{k+1} + (i_e)_{i+1}^{k}}{2}\right] \end{aligned} \tag{3.22}$$

The known right-hand side at each finite-difference grid point is

$$C = \frac{\Delta t}{\Delta x} q_i^{k+1} + \alpha^{-1/\beta} \left(q_{i+1}^k\right)^{1/\beta} + \Delta t \left[\frac{(i_e)_{i+1}^{k+1} + (i_e)_{i+1}^k}{2}\right] \tag{3.23}$$

Hence, the residual error is defined as

$$f\left(q_{i+1}^{k+1}\right) = \frac{\Delta t}{\Delta x} q_{i+1}^{k+1} + \alpha^{-1/\beta} \left(q_{i+1}^{k+1}\right)^{1/\beta} - C \tag{3.24}$$

For the channel flow in a V-shaped catchment, the procedure is similar to that for an overland plane, resulting in Equations (3.24) and (3.25).

$$f\left(Q_{i+1}^{k+1}\right) = \frac{\Delta t}{\Delta x} Q_{i+1}^{k+1} + \alpha_c^{-1/\beta_c} \left(Q_{i+1}^{k+1}\right)^{1/\beta_c} - C \tag{3.25}$$

$$C = \frac{\Delta t}{\Delta x} Q_i^{k+1} + \alpha_c^{-1/\beta_c} \left(Q_{i+1}^k\right)^{1/\beta_c} + 2\Delta t q_{i+1}^{k+1} \tag{3.26}$$

The initial estimate for q_{i+1}^{k+1} or Q_i^{k+1} is important for the convergence of the iterative scheme. One approach is to use the solution from the linear scheme which also uses an implicit scheme, as the first approximation to the nonlinear scheme. Li et al. (1975) performed a stability analysis indicating that the scheme using Equation (3.21) is unconditionally stable. They also showed that a wide range of values of $\Delta t/\Delta x$ could be used without introducing large errors in the shape of the discharge hydrograph (Chow et al., 1988).

3.3.3 Initial and Boundary Conditions

The kinematic wave model does not require a downstream boundary condition to obtain a solution. The initial condition is needed to start the numerical computation. There is no flow initially at the time $t = 0$, therefore $y = 0$. For simplicity, it is assumed that $y = 0$ at the upstream boundary throughout the process.

3.4 Evaluation of Flow Resistance

It is difficult to determine the resistance to unsteady spatially varied flow under rainfall conditions. First, a fixed Manning's n is used. A value of 0.014 was proposed by Xiong and Melching (2005) on the basis of which value from the appropriate range of n for aluminum plates from the literature yielded the best simulation results. Second, a variable Manning's n is used to approximate the overall flow resistance as affected by raindrop impact.

Harbaugh (1966) and Marcus (1968) proposed a variable Manning's n as a function of depth of flow on a 1% slope surface as

$$n = ay^b \tag{3.27}$$

where a is a coefficient which accounts for the fact that the flow is non-uniform and unsteady and also accounts for the raindrop impact. The value of a is equal to 0.017 as proposed by Marcus (1968), and b is equal to -0.166 obtained by Harbaugh (1966) for the laboratory watershed in the WES. In the algorithm, n_{x1} and n_{x2} are expressed as

$$(n_{x1})_i^k = 0.5\left(a\left(y_{i-1}^k\right)^b + a\left(y_i^k\right)^b\right) \tag{3.28}$$

$$(n_{x2})_i^k = 0.5\left(a\left(y_i^k\right)^b + a\left(y_{i+1}^k\right)^b\right) \tag{3.29}$$

In this dissertation research, n_{x1} and n_{x2} are set always greater than 0.009 the same as for the dynamic-wave model based on Marcus (1968).

CHAPTER 4 ANALYSIS OF COMPARISON OF KINEMATIC-WAVE AND DYNAMIC-WAVE MODELS

4.1 Testing of the theory that Downstream Moving Storms Magnify Peak Discharge

4.1.1 Relationship Between Dimensionless Peak Discharge and Dimensionless Storm Velocity

Lee and Huang (2007) performed a series of numerical simulations using their kinematic-wave model to analyze the effect of moving storms on attainment of equilibrium discharge for a V-shaped (open book) watershed. The characteristics of the watershed and moving storms are listed in Table 4.1. A family of relation curves among the dimensionless peak discharge $Q_p/(i_eA)$, storm length to watershed length ratio L_s/L, and dimensionless storm velocity V_sT_e/L was obtained for different storm velocities and storm lengths with a constant rainfall intensity, as shown in Figure 4.1. According to Lee and Huang (2007), the term V_sT_e/L was used to represent the ratio of the storm velocity to the mean channel flow velocity in the V-shaped watershed. However, V_sT_{cc}/L is the right term to incorporate the mean channel flow, since $T_e = T_{co} + T_{cc}$ (see Chapter 5). T_{cc} is calculated with Wong's (2001) equation, and T_{co} is calculated with Henderson and Wooding's equation (1964), see details in Section 5.2. It should be noted that Richardson and Julien (1989) and Ogden et al. (1995) did similar analyses and obtained similar results for overland planes.

Table 4.1 Watershed and Rainfall Characteristics Used by Lee and Huang (2007)

$L \times W$ (ft × ft)	S_c	S_o	n_c	n_o	i_e (in./hr)	L_s/L
30 × 5	4%	4%	0.04	0.04	3.5	0.2, 0.4, 0.6, 0.8, 1.0

In order to compare to the experimental data in Phases 2 and 3, Lee and Huang's (2007) kinematic-wave model was used to perform a series of simulations for various ratios of the storm length and watershed or channel length. There are six different values of L_s/L, i.e. 0.15, 0.3, 0.6, 1.0, 1.2, and 2.4. Only the simulation for L_s/L =1.0 was also performed by Lee and Huang (2007). The other characteristics of the watershed and moving storms remained the same as shown in Table 4.1. The characteristics of the watershed and moving storms don't affect the shape of the curves, since the dimensionless parameters obtained from dimensional analysis are used in the construction of the curves. The simulated and observed peak discharges were extracted from the corresponding simulated and observed hydrographs. The time of concentration for channel flow, T_{cc}, is calculated by using Wong's (2001) equation, discussed in Section 5.2.

The experimental data from 30 moving storms described in Section 4.3.1 are used to compared Lee and Huang's (2007) curve for $L_s/L = 1$ in Figure 4.2. Figure 4.2 shows good agreement between simulated and observed results for upstream moving storms. However, it seems that the kinematic-wave model cannot simulate the downstream moving storms very well. The most likely reason is that the kinematic-wave model cannot deal with the backwater effects in the experiment. The overland flow reaching the channel in the WES is high especially for the downstream moving storms, and the channel does not have enough capacity to deliver the high flow, so the backwater occurs. A dynamic-wave model incorporates the backwater effect and is evaluated in Section 4.5.

The experimental data from the 82 other moving storms described in Section 4.3.2 are used to verify the curves for $L_s/L_c \neq 1$, as shown in Figures 4.3 to 4.7. In all cases, the kinematic-wave model can simulate the upstream moving storms quite well. However, the discrepancy between the simulated and observed results of the downstream moving storms is very distinct. Figures 4.4 to 4.6 are good examples to represent the disagreement between the simulated and observed results of downstream moving storms. For moving storms with $L_s/L_c < 1$, the equilibrium discharge cannot be attained, and the maximum discharge is a portion of the equilibrium discharge, as shown in Figures 4.4 and 4.5. In this case, the maximum peak discharge occurs when the dimensionless storm velocity is approximately 0.1 ~ 0.2, which is much smaller compared to that from the kinematic-wave model simulation. For moving storms with $L_s/L_c \geq 1$, the equilibrium discharge can be attained, and the maximum discharge is equal to the equilibrium discharge, as shown in Figures 4.6 and 4.7. However, in this case, the range of the velocities of the moving storms attaining the equilibrium discharge is quite narrower than the simulated result of the kinematic-wave model. Furthermore, there is no discernable effect of storm motion on peak discharge, when a storm is large compared to the watershed length, $L_s \gg L_c$, and the storm velocity is relatively slow such that $L/V_s > T_{cc}$.

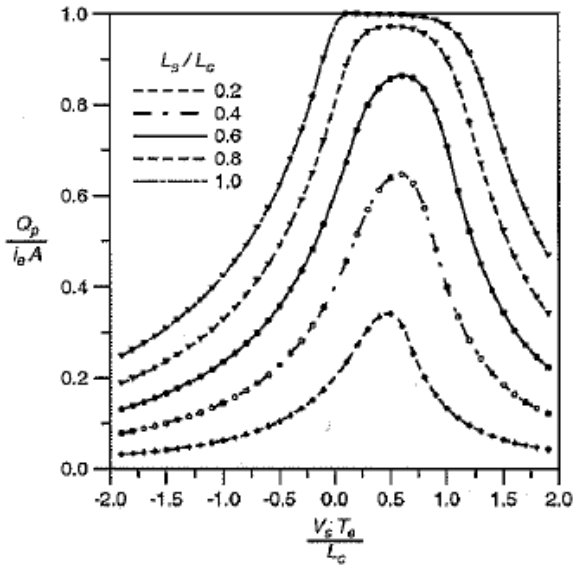

Figure 4.1 Figure 12 from Lee and Huang (2007) (Note L_c = L)

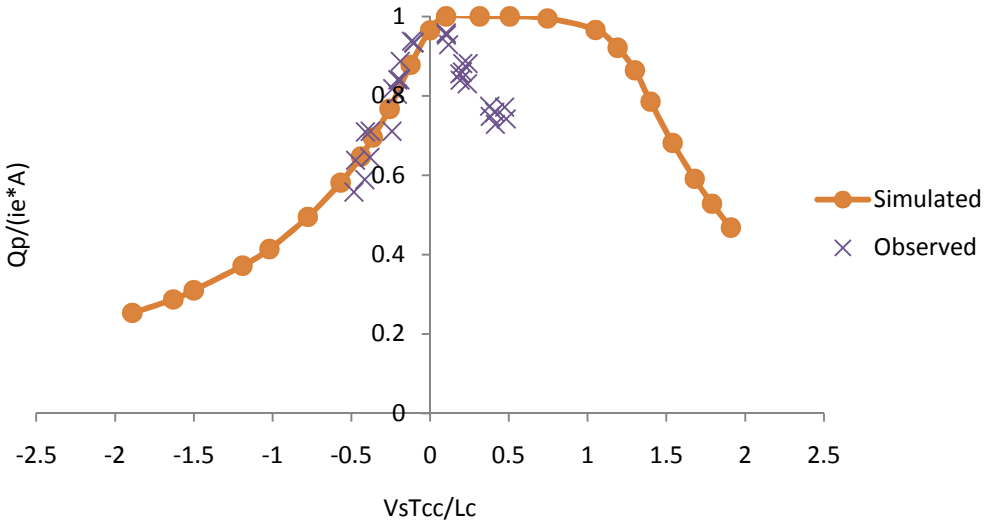

Figure 4.2 Relationship Between $Q_p/(i_eA)$ and V_sT_{cc}/L_c as Simulated Using Lee and Huang's (2007) Kinematic-Wave Model and as measured in the WES experiments for Moving Storms with $L_s/L_c = 1$ in Phases 2 and 3

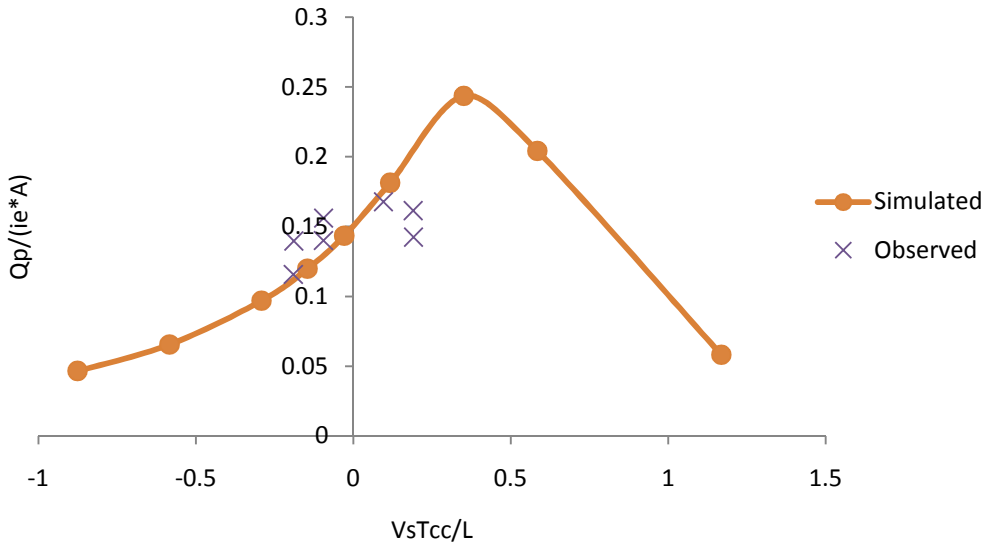

Figure 4.3 Relationship Between $Q_p/(i_eA)$ and V_sT_{cc}/L_c as Simulated Using Lee and Huang's (2007) Kinematic-Wave Model and as measured in the WES experiments for Moving Storms with $L_s/L_c = 0.15$ in Phases 2 and 3

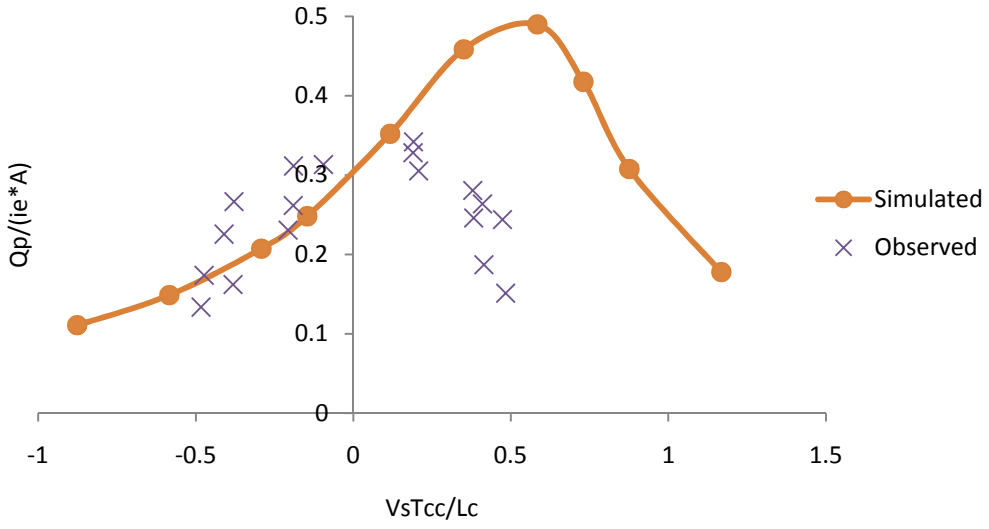

Figure 4.4 Relationship Between $Q_p/(i_eA)$ and V_sT_{cc}/L_c as Simulated Using Lee and Huang's (2007) Kinematic-Wave Model and as measured in the WES experiments for Moving Storms with $L_s/L_c = 0.3$ in Phases 2 and 3

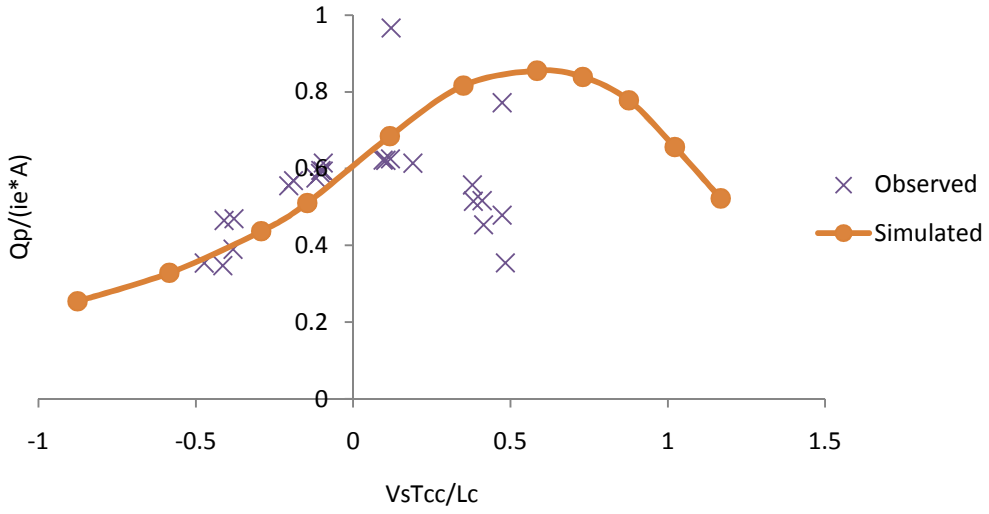

Figure 4.5 Relationship Between $Q_p/(i_eA)$ and V_sT_{cc}/L_c as Simulated Using Lee and Huang's (2007) Kinematic-Wave Model and as measured in the WES experiments for Moving Storms with $L_s/L_c = 0.6$ in Phases 2 and 3

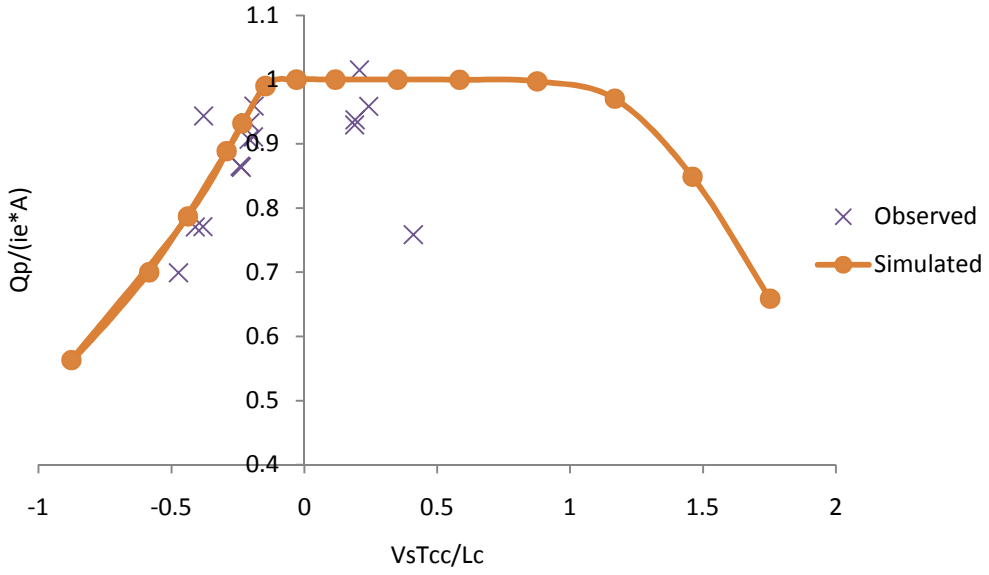

Figure 4.6 Relationship Between $Q_p/(i_eA)$ and V_sT_{cc}/L_c as Simulated Using Lee and Huang's (2007) Kinematic-Wave Model and as measured in the WES experiments for Moving Storms with $L_s/L_c = 1.2$ in Phases 2 and 3

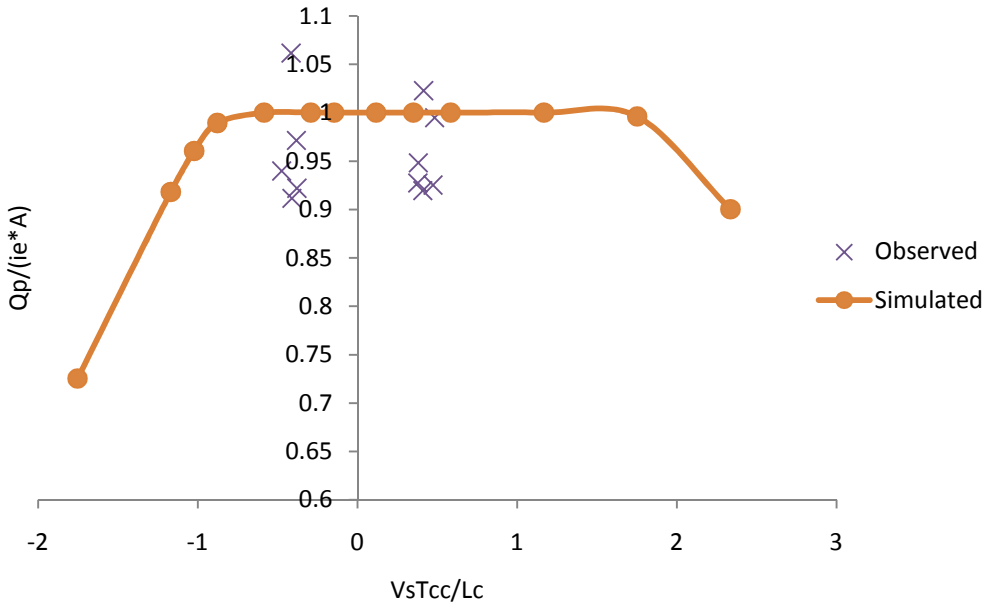

Figure 4.7 Relationship Between $Q_p/(i_eA)$ and V_sT_{cc}/L_c as Simulated Using Lee and Huang's (2007) Kinematic-Wave Model and as measured in the WES experiments for Moving Storms with $L_s/L_c = 2.4$ in Phases 2 and 3

4.1.2 Comparison of the Relationship Between Dimensionless Peak Discharge and Dimensionless Storm Velocity as Simulated by Kinematic-Wave and Dynamic-Wave Models

In Lee and Huang's (2007) kinematic-wave model, a fixed Manning's roughness coefficient n, i.e. 0.014 was used to evaluate the resistance to overland and channel flows, while in Marcus's (1968) dynamic-wave model, a variable Manning's n was applied to approximate the flow resistance varying with depth. Therefore, in order to examine the effect of the variable Manning's n on the performance of Lee and Huang's (2007) kinematic-wave model, Lee and Huang's (2007) kinematic-wave model was modified to incorporate the variable Manning's roughness coefficient. The influence of the variable Manning's n on the performance of the kinematic-wave model can be investigated. The difference of the performance between kinematic-wave and dynamic-wave models both applying the variable Manning's n can be considered resulting from the difference of the hydraulic theories between the kinematic-wave and dynamic-wave techniques.

Marcus's (1968) dynamic-wave model and the modified Lee and Huang's (2007) kinematic-wave model were used to perform the same series of numerical simulations as in the previous section to evaluate the influence of storm movement on the peak discharge. The results of the numerical simulations from these two models and Lee and Huang's (2007) kinematic-wave model are compared to the experimental data from 114 moving storms described in Sections 4.3.1 and 4.3.2, as shown in Figures 4.8 to 4.12.

According to Figure 4.8, there is an overall good agreement between the simulated results of the dynamic-wave model and the experimental data. The dynamic-wave model can reproduce the

upstream moving storms as well as downstream moving storms. The modified kinematic-wave model can simulate the downstream moving storms pretty well, while the simulation results for the upstream moving storms are consistently below the experimental data points.

The same conclusions can be drawn according to Figures 4.9 to 4.12. The dynamic-wave model has the best simulation results for both downstream and upstream moving storms compared to the experimental data. The modified kinematic-wave model tends to undersimulate both downstream and upstream moving storms. The kinematic-wave model simulates the upstream moving storm pretty well, while it totally oversimulates the downstream moving storm.

In Section 4.3, the ability of the kinematic-wave model to simulate experimental moving storms is evaluated. In Section 4.4, the ability of the dynamic-wave model to simulate experimental moving storms is evaluated. Finally, in Chapter 5, the accuracy of Wong's (2001) time of concentration equation, which was used to nondimensionalize the measured data, is evaluated.

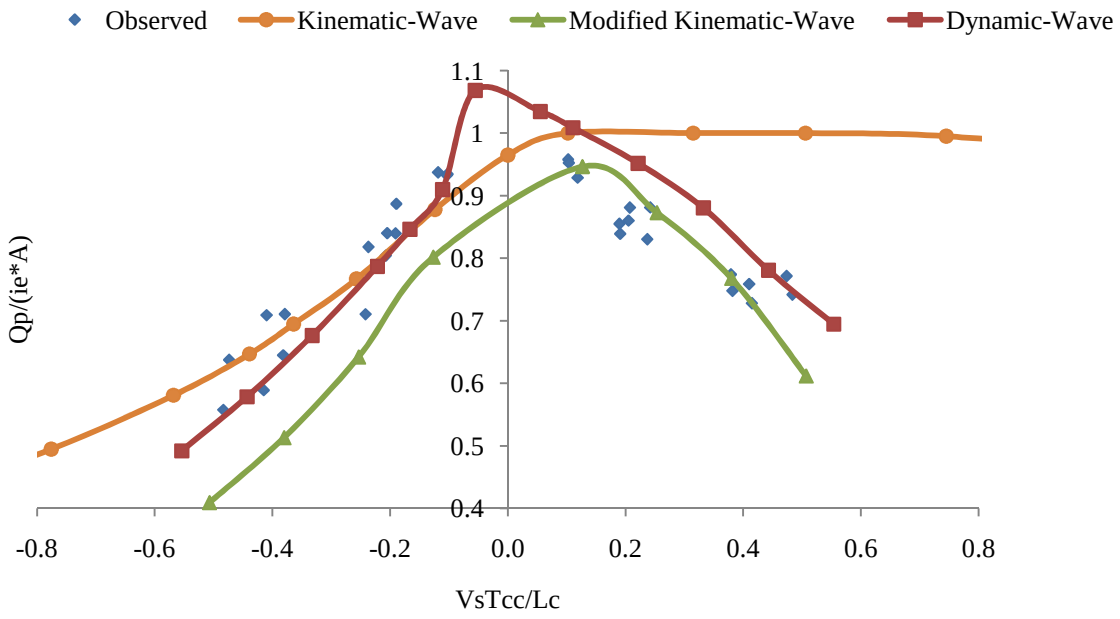

Figure 4.8 Relationship Between $Q_p/(i_eA)$ and V_sT_{cc}/L_c as Simulated Using Lee and Huang's (2007) Kinematic-Wave Model, the Modified Kinematic-Wave Model, and Marcus's (1968) Dynamic-Wave Model as measured in the WES experiments for Moving Storms with $L_s/L_c = 1$ in Phases 2 and 3

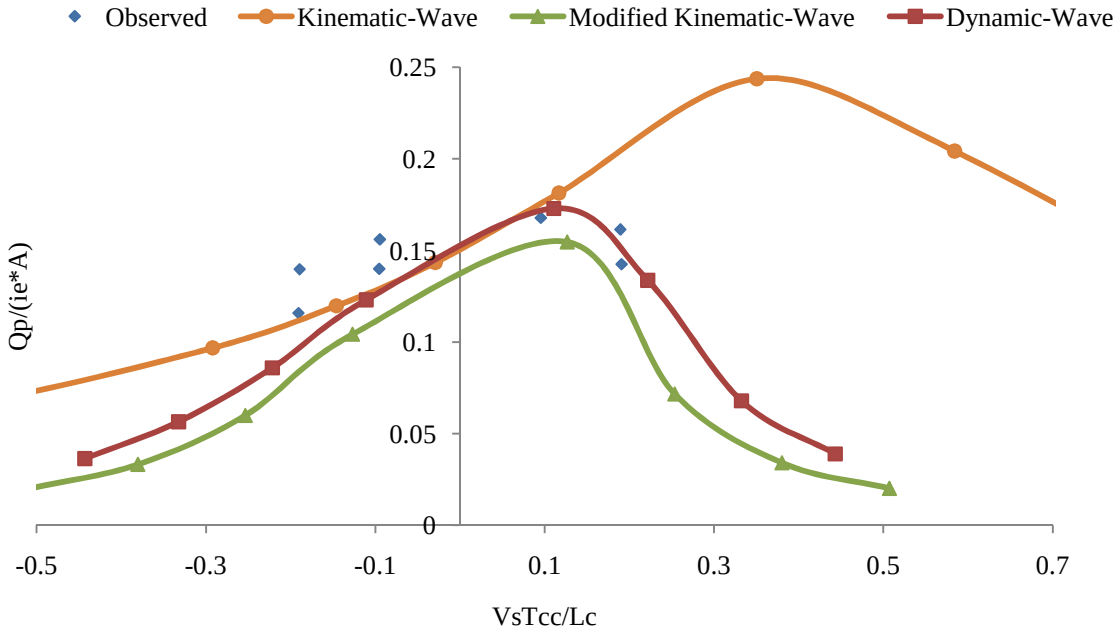

Figure 4.9 Relationship Between $Q_p/(i_eA)$ and V_sT_{cc}/L_c as Simulated Using Lee and Huang's (2007) Kinematic-Wave Model, the Modified Kinematic-Wave Model, and Marcus's (1968) Dynamic-Wave Model as measured in the WES experiments for Moving Storms with $L_s/L_c = 0.15$ in Phases 2 and 3

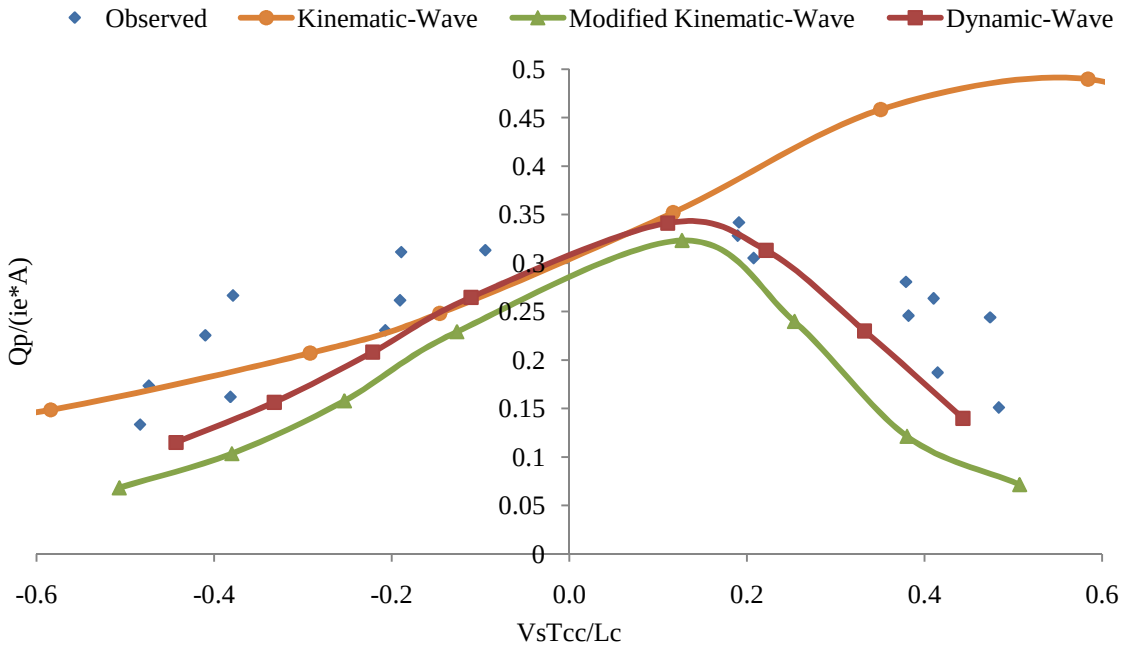

Figure 4.10 Relationship Between $Q_p/(i_eA)$ and V_sT_{cc}/L_c as Simulated Using Lee and Huang's (2007) Kinematic-Wave Model, the Modified Kinematic-Wave Model, and Marcus's (1968) Dynamic-Wave Model as measured in the WES experiments for Moving Storms with $L_s/L_c = 0.3$ in Phases 2 and 3

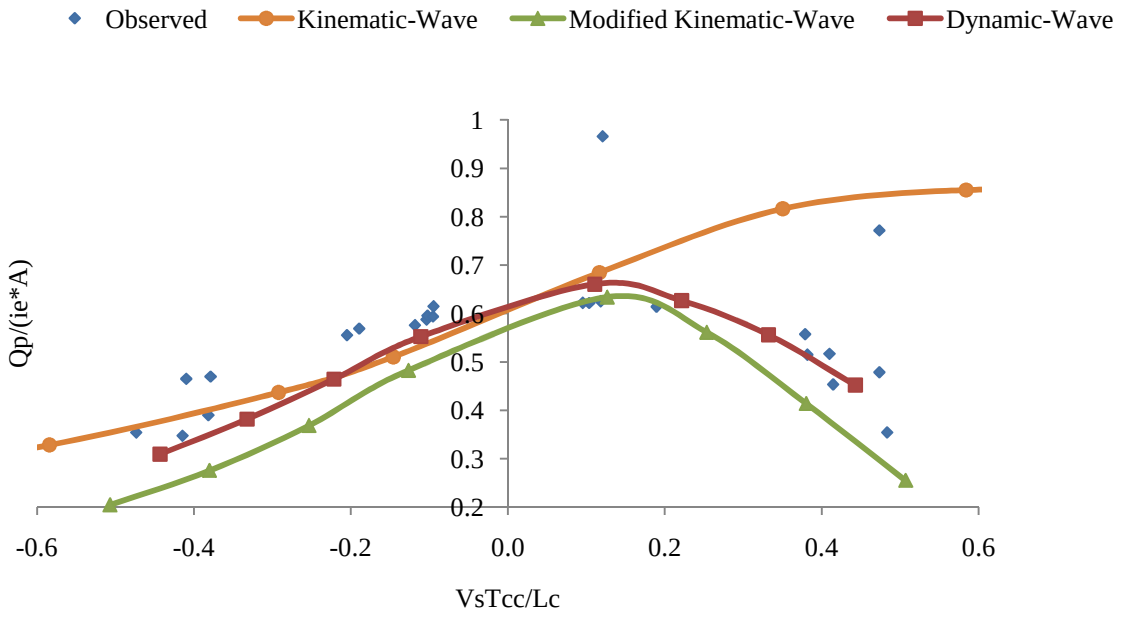

Figure 4.11 Relationship Between $Q_p/(i_eA)$ and V_sT_{cc}/L_c as Simulated Using Lee and Huang's (2007) Kinematic-Wave Model, the Modified Kinematic-Wave Model, and Marcus's (1968) Dynamic-Wave Model as measured in the WES experiments for Moving Storms with $L_s/L_c = 0.6$ in Phases 2 and 3

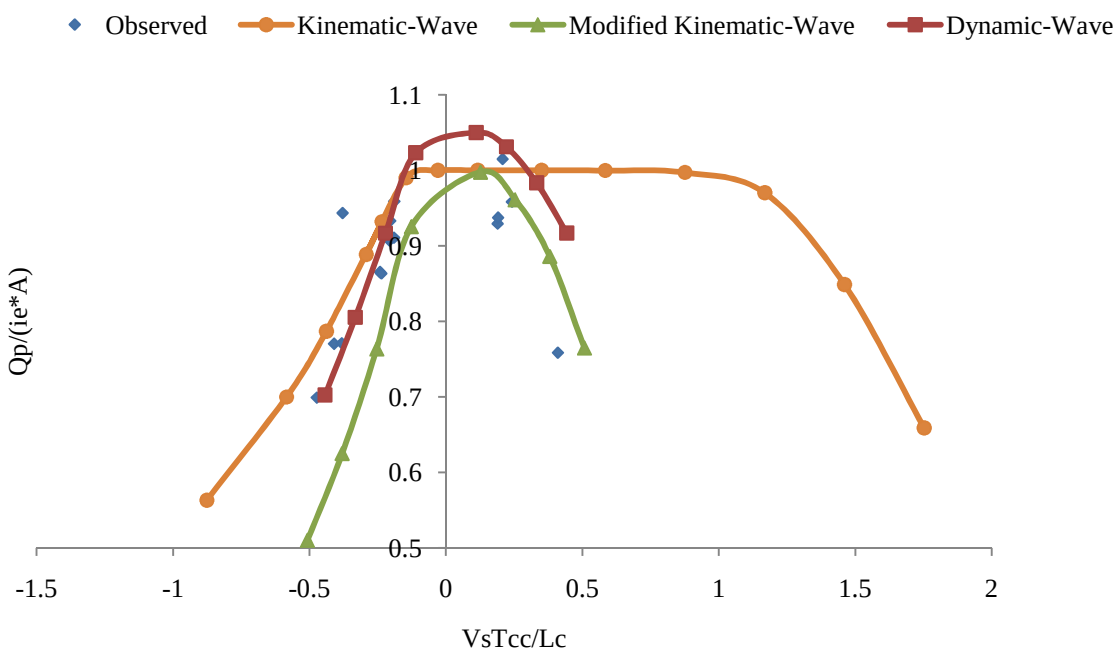

Figure 4.12 Relationship Between $Q_p/(i_eA)$ and V_sT_{cc}/L_c as Simulated Using Lee and Huang's (2007) Kinematic-Wave Model, the Modified Kinematic-Wave Model, and Marcus's (1968) Dynamic-Wave Model as measured in the WES experiments for Moving Storms $L_s/L_c = 1.2$ in Phases 2 and 3

4.2 Statistical Evaluation of the Modeling Results

The performance of hydrologic and hydraulic modeling is commonly evaluated through comparisons of simulated and observed flows. A number of criteria can be used by hydrologists to provide quantitative assessment of the goodness-of-fit of model simulations to observations. There are several frequently used goodness of fit criteria to assess the predictive ability of a model, such as Nash-Sutcliffe coefficient of model-fit efficiency, coefficient of determination, and index of agreement. The selection of a specific model-fit criterion can be a challenge for even the most experienced hydrologist since each criterion may place emphasis on different systematic and/or dynamic types of simulated and/or observed behaviors, and none of the criteria can perform ideally (Kraus et al., 2005).

The Nash-Sutcliffe coefficient of model-fit efficiency is one of the most widely used model-fit criteria and it was introduced by Nash and Sutcliffe (1970). The coefficient of model-fit efficiency, E, is calculated as:

$$E = \frac{\sum_{i=1}^{N}\left(Q_{O_i} - Q_O\right)^2 - \sum_{i=1}^{N}\left(Q_{O_i} - Q_{S_i}\right)^2}{\sum_{i=1}^{N}\left(Q_{O_i} - Q_O\right)^2} = 1 - \frac{\sum_{i=1}^{N}\left(Q_{O_i} - Q_{S_i}\right)^2}{\sum_{i=1}^{N}\left(Q_{O_i} - Q_O\right)^2} \tag{4.1}$$

where Q_{O_i} = observed runoff at time t_i; Q_{S_i} = simulated runoff at time t_i; Q_O = average observed runoff over the entire experiment computed at a fixed time step, Δt, and N = the number of hydrograph ordinates considered. The Nash-Sutcliffe efficiency ranges from $-\infty$ to 1. An efficiency of 1 means perfect agreement between modeled and observed values. An efficiency less than zero indicates that the mean value of the observed variable would have been a better

predictor than the model. Essentially, the closer the model efficiency is to 1, the more accurate the model is. Beran (1999) and Hall (2001) concluded that a coefficient of efficiency of 0.95 or more is required to ensure good model performance. James and Burges (1982) suggested that an excellent quality of fit is achieved, if the coefficient of model-fit efficiency exceeds 0.97.

According to the definition of the Nash-Sutcliffe efficiency, E, as given in Eq. (4.1) it incorporates the squared differences between the observed and simulated values. Therefore, this model-fit criterion is very sensitive to the peak and high flows of the hydrograph, at the expense of improvements during low flow conditions (Kraus et al., 2005). This characteristic is important in the real engineering world, since the peak flows are of primary concern in engineering planning and design. However, this fact also results in the largest disadvantage of the Nash-Sutcliffe efficiency. It will lead to an overestimation of the model performance during peak flows and an underestimation during low flow conditions (Kraus et al., 2005).

The Nash-Sutcliffe efficiency also is not very sensitive to systematic model over- or under-prediction (poor water balance) especially during low flow periods (Kraus et al., 2005). Since the Nash-Sutcliffe criterion is more focused on the reproduction of the dynamics (i.e. timing, rising limb, and falling limb) compared to the volume of the hydrograph, additional measures such as absolute and relative volume errors or the root mean square error are necessary to quantify volume errors for a thorough model evaluation. It is recommended by Krause et al. (2005) that for sound scientific model calibration and validation a combination of different model-fit criteria will be complemented by the assessment of absolute or relative volume errors.

Therefore, the coefficient of model-fit efficiency, E, was calculated for each experimental test to study the accuracy of the simulation results. The percentage difference of the simulated and observed mass of runoff for all experimental tests also is calculated by the following equation:

$$\Delta M\% = \frac{M_s - M_o}{M_o} \times 100\% \tag{4.2}$$

where M_s is the simulated mass of runoff, and M_o is the observed mass of runoff.

4.3 Analysis of the Results of Kinematic-Wave Modeling

The hydrographs for the total of 114 experimental moving storms were simulated using Lee and Huang's (2007) V-shaped (open book) watershed kinematic-wave model. The 114 moving storms are divided into two groups for study. The first group consists of 32 moving storms with storm length equal to watershed length, and the second group has the other 82 moving storms with storm length not equal to watershed length.

In Lee and Huang's (2007) kinematic-wave model, the computational time interval is 1 or 2 seconds. The computational grid numbers of overland and channel flow are 51 and 101, respectively. The value of Manning's roughness coefficient n for smooth aluminum planes in the WES was determined to be 0.014 by trial and error but constrained by information in the literature (Xiong and Melching, 2005). The fixed Manning's n value of 0.014 was used in all the simulations, since the overland and channel part of the watershed was the smooth side of an aluminum plane.

4.3.1 Analysis of the Results for 32 Moving Storms with Storm Length Equal to Watershed Length

The geometric characteristics of the watersheds and the properties of the moving storms for the 32 experimental runs are listed in Table 4.2. The specific experimental condition for an individual test is listed in Table 4.3. As shown in Table 4.3, the 32 moving storms consist of 16 sets of upstream and downstream moving storms. In each set, the upstream moving storm and its corresponding downstream moving storm have the same rainfall intensity, duration, and the opposite velocities, i.e. the same speed but in opposite directions.

Table 4.2 Experimental Conditions for 32 Storms with the Storm Length Equal to the Watershed Length in Phases 2 and 3

$L \times W$ (ft × ft)	L_s (ft)	S_x	S_y	$I_{nominal}$ (in./hr)	V_x (ft/s)	V_y (ft/s)	T_d (s)
40 × 40	40	1%	1%	6, 10, 15	±0.1, ±0.2, ±0.4	0	100, 200, 400

It is noted that all of the 32 moving storms have a storm length, L_s, equal to the watershed length, L, i.e. $L = L_s$. The duration of the moving storm, T_d, satisfies the relation between storm length and storm velocity defined by:

$$T_d = L_s/|V_x| \tag{4.3}$$

The width of the moving storms, W_s, is equal to the width of the watershed W, i.e. 40 ft. Since $L = L_s$, we also have $T_d = L/|V_x|$.

Table 4.3 Comparison of Kinematic-Wave Simulated and Observed Runoff for 32 Laboratory Storms with Storm Length Equal to Watershed Length

Test No.	T_d (s)	V_x (ft/s)	i_e (in./hr)	E	ΔM%
1116	100	-0.4	4.2296	0.6096	0.043%
723			4.5916	0.9612	5.817%
1075			7.8181	0.9336	1.303%
721			8.1784	0.9827	4.162%
1054			10.8900	0.9689	3.636%
718			11.2092	0.9799	4.486%
1117		0.4	4.2296	0.7361	-10.331%
716			4.5916	0.8397	6.345%
1080			7.8181	0.4098	3.116%
722			8.1784	0.8309	8.593%
1053			10.8900	0.8395	4.972%
717ab			11.2092	0.8589	4.015%
1137	200	-0.2	4.2296	0.9568	5.992%
715ab			4.5916	0.9765	4.003%
1074			7.8181	0.9797	-0.609%
727			8.1784	0.9884	4.188%
1050			10.8900	0.9897	0.722%
725			11.2092	0.9792	4.411%
1133		0.2	4.2296	0.9549	-0.806%
728			4.5916	0.8878	10.592%
1072			7.8181	0.9555	0.481%
726			8.1784	0.9188	5.693%
1052			10.8900	0.8576	3.336%
724			11.2092	0.9357	7.928%
662ab	400	-0.1	4.5916	0.9606	4.660%
1143			7.8181	0.9842	-0.257%
667abc			8.1784	0.9654	3.804%
1147			10.8900	0.9525	13.937%
661		0.1	4.5916	0.9583	-2.914%
1144			7.8181	0.9878	-0.813%
668abc			8.1784	0.9620	7.468%
1151			10.8900	0.9430	13.368%

The comparison results, E and $\Delta M\%$, of simulated and observed runoff for the 32 moving storms are listed in Table 4.3. According to Table 4.3, the average coefficient of model-fit efficiency for all 32 tests is 0.9077. Among the total of 32 tests, the coefficients of 23 tests are over 0.90, 19 of which are over 0.95, and 9 of which are over 0.97. The coefficients of the other 9 tests are lower than 0.90, 1 of which are lower than 0.50, and 6 of which are between 0.8 and 0.9, as shown in Figure 4.13. On average, the simulation results from Phase 2 are much better than those from Phase 3. The average coefficient of model-fit efficiency for the 16 tests in Phase 2 is 0.9366, while it is only 0.8787 for the 16 tests in Phase 3. According to Table 4.4, for the same nominal rainfall intensities, the coefficients of model-fit efficiency for the tests in Phase 2 are much higher than those in Phase 3.

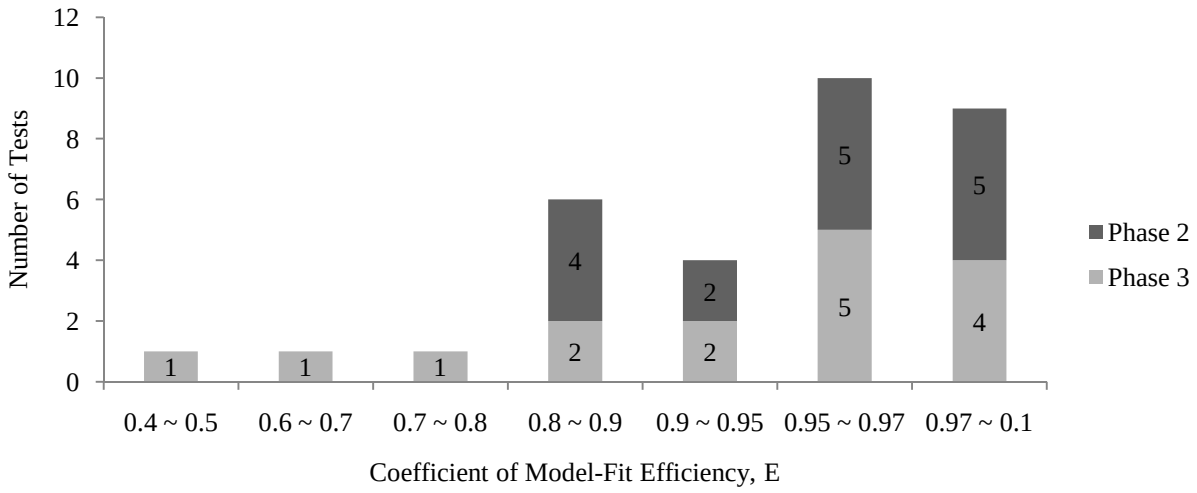

Figure 4.13 Distribution of Coefficient of Model-Fit Efficiency, E, for 32 Test Storms with Storm Length Equal to Watershed Length

Table 4.4 Coefficients of Model-Fit Efficiency for Various Rainfall Intensities in Phases 2 and 3

	ie, in./hr	E	No. of Tests
Phase 2	4.5916	0.9307	6
Phase 2	8.1784	0.9414	6
Phase 2	11.2092	0.9384	4
Phase 3	4.2296	0.8144	4
Phase 3	7.8181	0.8751	6
Phase 3	10.8900	0.9252	6

The longer the duration of the moving storms, the higher is the value of the coefficient of model-fit efficiency. As listed in Table 4.5, the values of the coefficients for the different durations of moving storms are 0.8292 for 100 s, 0.9484 for 200 s, and 0.9642 for 400 s, respectively. When only considering the tests from Phase 2 or Phase 3, the same trend of the values of the coefficients in terms of the rainfall duration can be observed.

Table 4.5 Coefficients of Model-Fit Efficiency for Various Storms Durations in Phases 2 and 3

	Duration (s)		
	100	200	400
Phases 2 and 3	0.8292	0.9484	0.9642
Phase 2	0.9089	0.9477	0.9616
Phase 3	0.7496	0.9490	0.9669

As seen in Figures 4.14 to 4.16, for each set of upstream and downstream moving storms, the simulation result for the upstream moving storm is better than that of the corresponding downstream moving storm. On average, the simulations for the upstream moving storms are better than those for the downstream moving storms. The average coefficient for all the upstream moving storms is 0.9480, while it is 0.8673 for all the downstream moving storms. According to Table 4.6, the average value of the coefficients for the upstream moving storms is higher than

that for the downstream moving storms with the same speed. This conclusion can also be drawn when considering experimental tests in Phases 2 or 3.

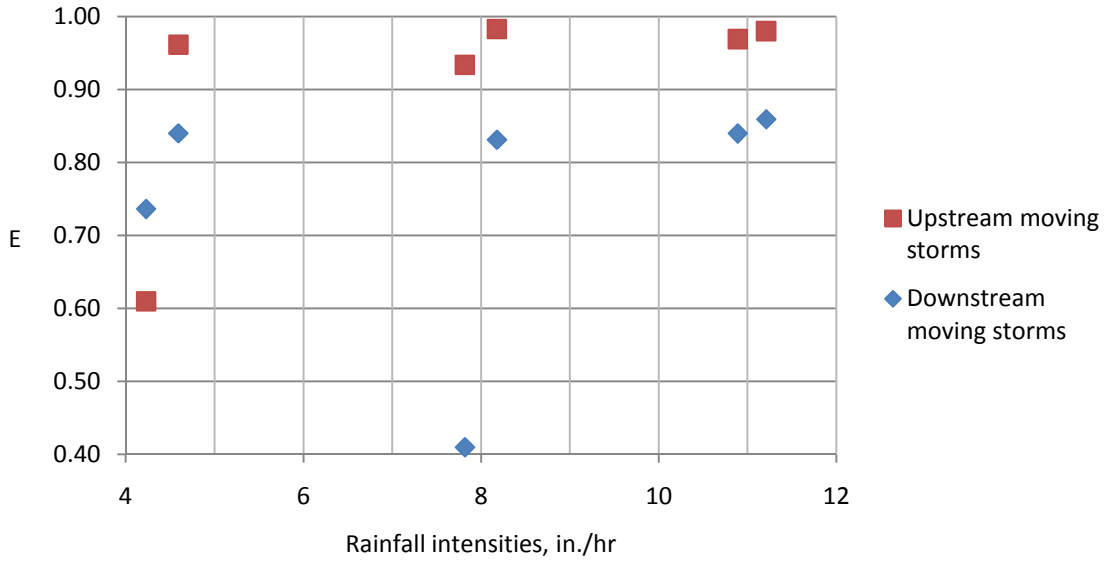

Figure 4.14 Coefficients of Model-Fit Efficiency for Six Sets of Upstream and Downstream Moving Storms with T_d = 100 s, and $|V_s|$ = 0.4 ft/s

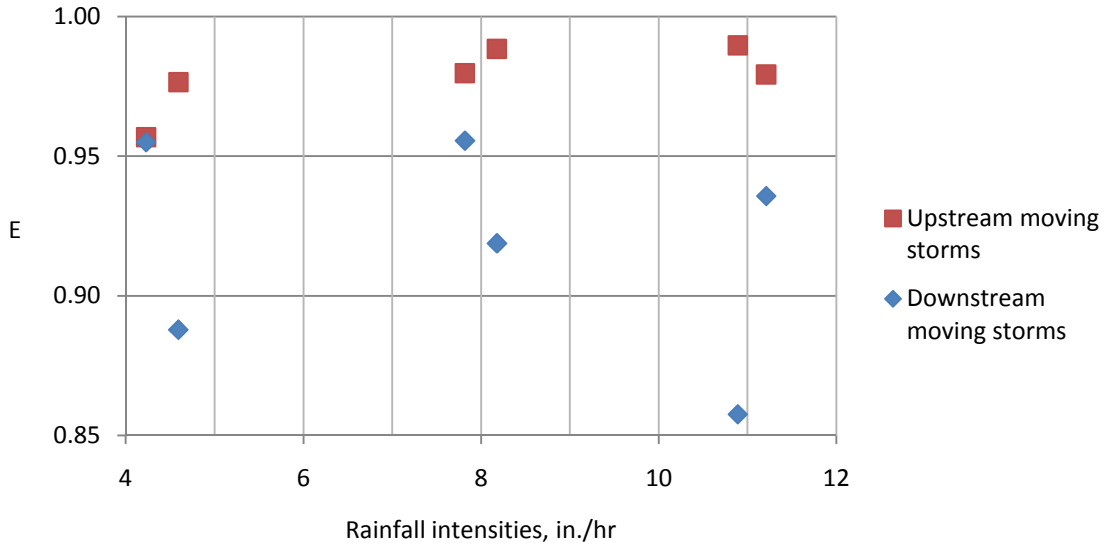

Figure 4.15 Coefficients of Model-Fit Efficiency for Six Sets of Upstream and Downstream Moving Storms with T_d = 200 s, and $|V_s|$ = 0.2 ft/s

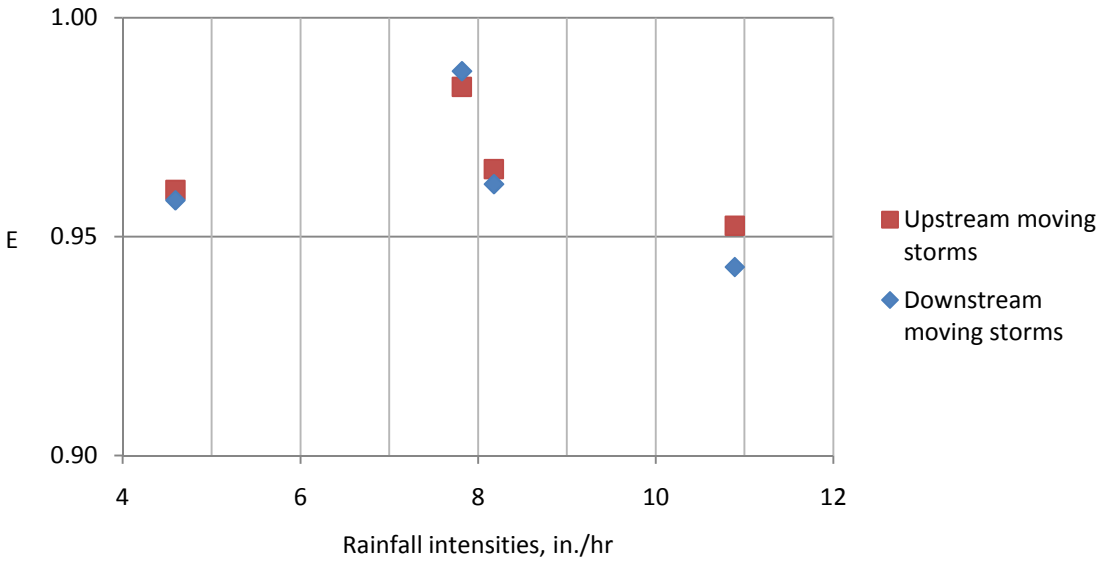

Figure 4.16 Coefficients of Model-Fit Efficiency for Three Sets of Upstream and Downstream Moving Storms with T_d = 400 s, and $|V_s|$ = 0.1 ft/s

Table 4.6 Coefficients of Model-Fit Efficiency for Various Storm Velocities in Phases 2 and 3

	Velocity (ft/s)					
	-0.4	-0.2	-0.1	0.1	0.2	0.4.
Phases 2&3	0.9060	0.9784	0.9657	0.9628	0.9184	0.7525
Phase 2	0.9746	0.9814	0.9630	0.9601	0.9141	0.8432
Phase 3	0.8373	0.9754	0.9683	0.9654	0.9227	0.6618

The simulation results are subject to three types of error: volume error, bias, and timing error. Timing error is the primary error that occurs in the model simulation results. Due to timing errors, the simulated flows are displaced by certain amounts of time, relative to the observed flows. The displacement of the simulated hydrograph is visually apparent compared to the observed hydrographs, as shown in Figures 4.17 to 4.19. This phenomenon is more evident for upstream moving storms, shown in Figures 4.17 and 4.18. It can be seen that, if the simulated hydrograph is moved some time steps to the right (i.e. later), the simulated and observed

hydrographs will have a better agreement. Therefore, in order to better investigate the bias error of the simulation results, the simulated hydrographs were moved several time steps if necessary.

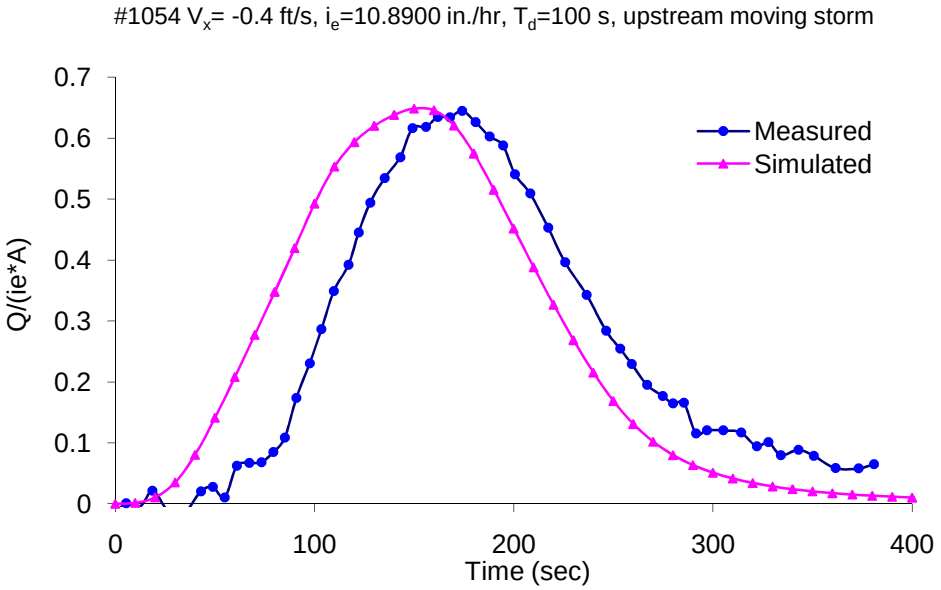

Figure 4.17 Comparison of Measured and Simulated Hydrographs for Test 1054

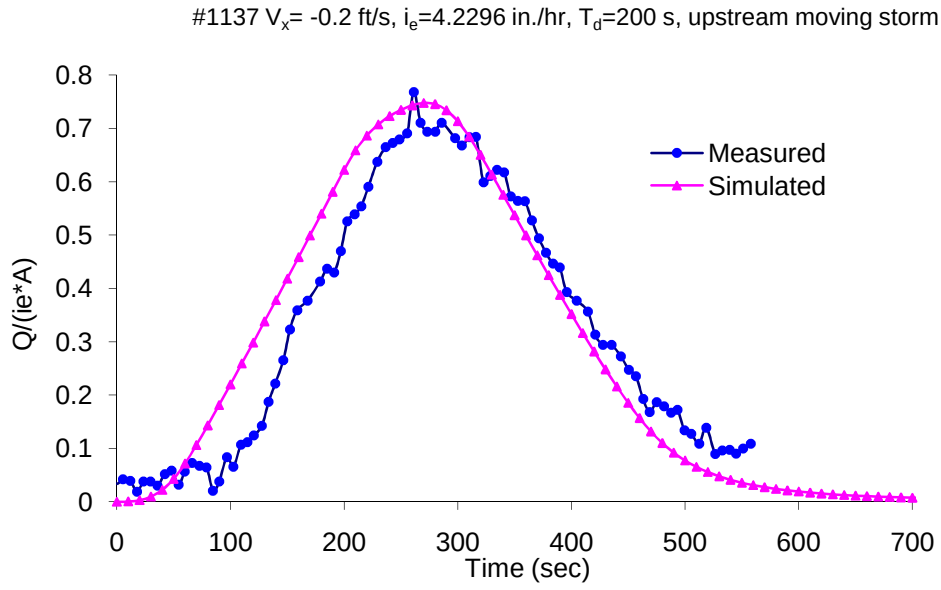

Figure 4.18 Comparison of Measured and Simulated Hydrographs for Test 1137

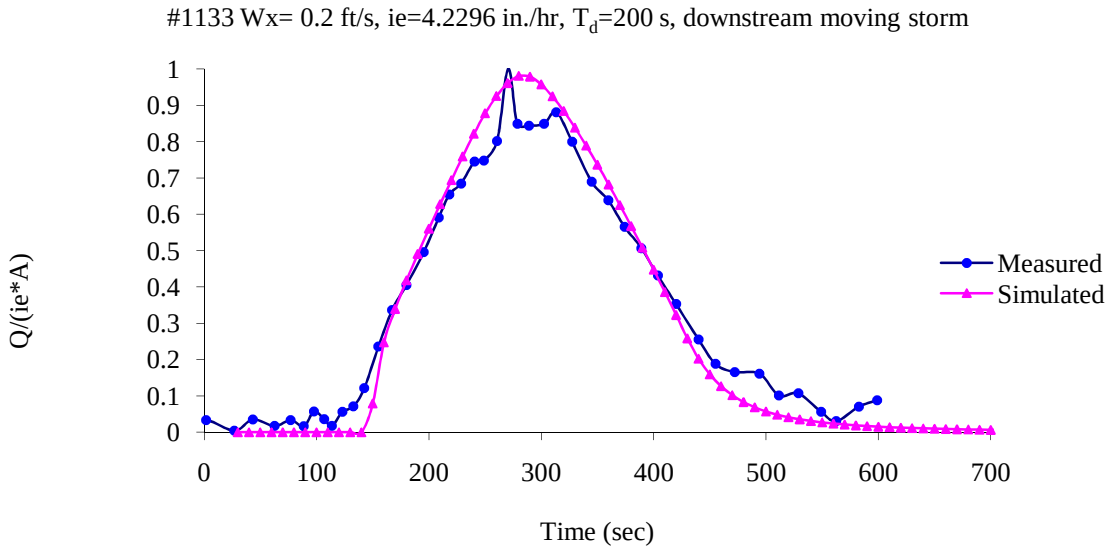

Figure 4.19 Comparison of Measured and Simulated Hydrographs for Test 1133

4.3.2 Analysis of the Results for 82 Moving Storms with Storm Length Not Equal to Watershed Length

The observed hydrographs of 82 moving storms from experimental Phases 2 and 3 were also simulated using Lee and Huang's (1997) V-shaped (open book) watershed kinematic-wave model. The geometric characteristics of the watersheds and the properties of the moving storms for the 82 experimental runs are listed in Table 4.7. The specific experimental condition for an individual test is listed in Table 4.8. As shown in Table 4.8, the 82 moving storms consist of 38 complete sets of upstream and corresponding downstream moving storms. The remaining 6 single upstream or downstream moving storms are missing their corresponding downstream or upstream counterparts.

Table 4.7 Experimental Conditions for 82 Storms with the Storm Length not Equal to the Watershed Length in Phases 2 and 3

$L \times W$ (ft × ft)	$L_s = V_x \times T_d$ (ft)	W_s (ft)	S_x	S_y	$I_{nominal}$ (in./hr)	V_x (fps)	V_y (fps)	T_d (s)
40 × 40	6, 12, 24, 48, 96	40	1%	1%	6, 10, 15	±0.1, ±0.2, ±0.4	0	30, 60, 120, 240

Table 4.8 Comparison of Simulated and Observed Runoff for 82 Moving Storms for which the Storm Length Does Not Equal the Watershed Length

Test No.	T_d (s)	V_x (fps)	i_e (in./hr)	E	ΔM
1132[1]	30	-0.4	4.2296	-2.5252	-12.264%
714ab			4.5916	0.3884	-18.999%
[2]			7.8181		
712ab			8.1784	0.7996	-13.202%
1039			10.8900	0.8249	-1.628%
702ab			11.2092	0.8361	-18.387%
	60		4.2296		
743ab			4.5916	0.9142	13.652%
1089			7.8181	0.8873	7.342%
742ab			8.1784	0.9490	1.806%
1176			10.8900	0.9333	2.579%
681			11.2092	0.9202	0.173%
745ab	120		4.5916	0.9554	13.076%
739ab			8.1784	0.9764	9.689%
1061			10.8900	0.9731	3.505%
737			11.2092	0.9682	10.146%
	240		4.2296		
758ab			4.5916	0.9638	6.660%
1088			7.8181	0.9920	-0.599%
749ab			8.1784	0.9712	8.739%
1067			10.8900	0.9812	7.256%
756ab			11.2092	0.9469	10.465%

Test No.	V_x (ft/s)	E	ΔM
1131	0.4	-2.2458	13.833%
713ab		0.5245	-10.463%
1178		-0.3732	2.630%
711ab		0.6361	-0.982%
1038		0.1092	14.247%
710ab		0.7703	-0.310%
1114		-0.6868	5.187%
744ab		0.7408	10.841%
1090		0.5693	13.229%
741		0.7627	3.851%
1175		0.6749	7.966%
680		0.8216	-1.253%
746ab		0.9051	0.819%
738ab		0.8400	12.004%
1129		0.9135	7.774%
757ab		0.8857	9.683%
1087		0.9672	4.036%
747		0.8711	12.310%
1070		0.9295	6.809%
755ab		0.8865	10.094%

[1] A set of two tests of upstream and corresponding downstream moving storms is listed in the same row for comparison.
[2] Blank means the experimental data are not available.

Test No.	T_d (s)	V_x (ft/s)	i_e (in./hr)	E	ΔM
1077	30	-0.2	10.8900	0.6803	-9.103%
708ab			11.2092	0.8365	-3.940%
1172	60		7.8181	0.8983	0.213%
1171			10.8900	0.9282	-3.695%
692			11.2092	0.9128	-14.073%
687	120		8.1784	0.9690	2.748%
678abc			11.2092	0.9667	-0.853%
1139	240		4.2296	0.9874	-1.853%
736ab			4.5916	0.9625	11.760%
1064			7.8181	0.9931	-1.684%
733ab			8.1784	0.9899	5.159%
1060			10.8900	0.9860	1.997%
731ab			11.2092	0.9708	5.604%

Test No.	V_x (ft/s)	E	ΔM
1076	0.2	0.3658	-2.184%
709ab		0.7438	-5.183%
1173		0.7834	8.846%
1035		0.8375	-9.685%
691		0.8556	-2.474%
686		0.6942	-3.028%
679ab		0.9200	0.074%
1140		0.9525	-1.830%
735ab		0.8908	11.796%
1179		0.9818	-1.966%
732ab		0.9536	3.668%
1058		0.9693	-1.382%
730ab		0.9592	7.434%

1078	60	-0.1	10.8900	0.8936	-3.176%
707			11.2092	0.8439	-4.536%
701ab	120		11.2092	0.9455	-2.971%
	240		4.2296		
698abc			4.5916	0.9370	0.111%
1113			7.8181	0.9698	-1.806%
695			8.1784	0.9771	-1.365%
1066			10.8900	0.9413	-2.329%
683			11.2092	0.9744	0.051%

1079	0.1	0.8640	0.550%
706		0.7828	-0.367%
700ab		0.9572	-6.472%
1127		0.47562	0.4935
697		0.9549	-1.759%
1111		0.9739	0.025%
694		0.9609	2.086%
1065		0.9455	-0.970%
685		0.9739	0.231%

The key characteristic of these 82 moving storms is that their storm lengths do not equal the watershed length, i.e. $L \neq L_s$. Therefore, their rainfall durations satisfy $T_d = L_s/|V_x|$ but $T_d \neq L/|V_x|$. The 82 moving storms studied in this section are characterized by $T_d \neq L/|V_x|$, while the 32 moving storms analyzed in Section 4.3.1, satisfy $T_d = L/|V_x|$.

According to Eq. (4.3), if the duration of the moving storm is known to be T_d, the length of the storm is $L_s = V_x \times T_d$. The lengths of the moving storms in Phases 2 and 3 of the WES experiments are listed in Table 4.9. The various ratios of L_s to L (i.e. 40 ft) for moving storms are also obtained. The 82 moving storms have the values of L_s/L of 0.15, 0.3, 0.6, 1.2, and 2.4, while the 32 moving storms analyzed in Section 4.3.1 have the value of 1. The comparison results of simulated and observed runoff for the 82 moving storms are listed in Table 4.8.

Table 4.9 Various Ratios of Storm Length (L_s) to Watershed Length (L) for Moving Storms in Experimental Phases 2 and 3

T_d (s)	V_s (ft/s)	L_s (ft)	L_s/L
30	0.2	6	0.15
30	0.4	12	0.3
60	0.1	6	0.15
60	0.2	12	0.3
60	0.4	24	0.6
100	0.4	40	1
120	0.1	12	0.3
120	0.2	24	0.6
120	0.4	48	1.2
200	0.2	40	1
240	0.1	24	0.6
240	0.2	48	1.2
240	0.4	96	2.4
400	0.1	40	1

According to Table 4.8, the average coefficient of model-fit efficiency for all the tests is 0.7504. The coefficients of 45 tests are over 0.90, 30 of which are over 0.95, and 15 of which are over 0.97. The coefficients of the other 37 tests are lower than 0.90, 8 of which are lower than 0.50, and 16 of which are between 0.8 and 0.9, as shown in Figure 4.20. It can be also seen that on average, the simulation results from Phase 2 are much better than those from Phase 3. The average coefficient for the tests in Phase 2 is 0.8759, while it is only 0.5820 in Phase 3. It should be noted that the mass differences between the simulated and observed results are pretty big some experiments such as Tests 714ab, 702ab, 746ab, and 1172. It is solely due to the experimental data which are not accurate at all.

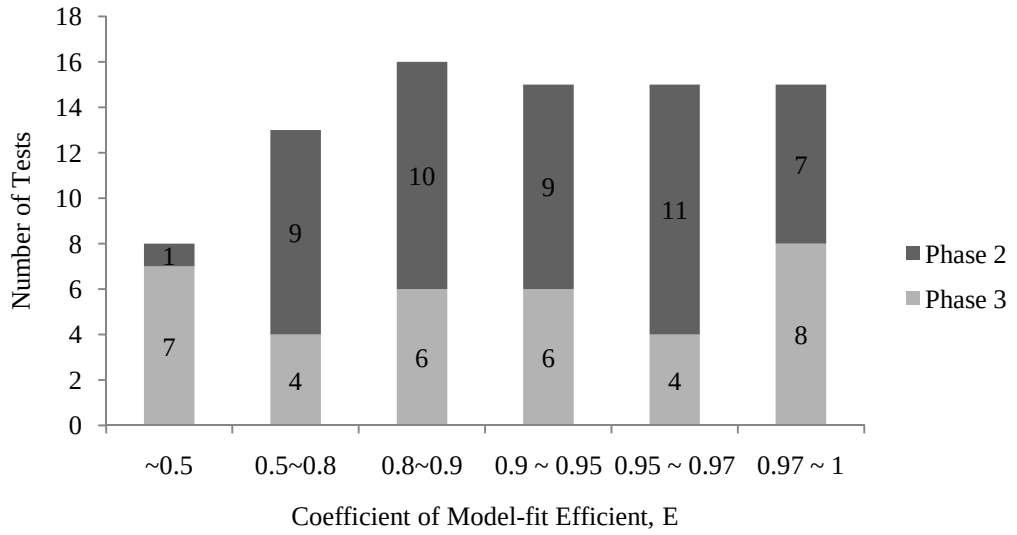

Figure 4.20 Distribution of Coefficient of Model-Fit Efficiency, E, for 82 Test Storms with Storm Length Not Equal to Watershed Length

As shown in Table 4.10, for storms moving upstream or downstream, the greater the movement speed, the lower is the value of the coefficient of model-fit efficiency. The coefficients of model-fit efficiency for all the rainstorms with velocity of -0.1 fps are 0.9353, much higher than those

for rainstorms with other velocities. This conclusion can be also drawn when considering experimental tests in Phases 2 or 3.

The values of the coefficients for the different durations of moving storms are listed in Table 4.11. The overall trend is that the longer the duration of the moving storms, the higher is the value of the coefficient of model-fit efficiency. When considering the tests in Phase 2 or 3, this trend is more obviously observed.

As seen in Figures 4.21 and 4.22, for 10 sets of upstream and downstream moving storms, the simulation result of the upstream moving storm is better than that of the corresponding downstream moving storm. On average, the simulations for the upstream moving storms are better than those for the downstream moving storms. The average coefficient of model-fit efficiency for all the upstream moving storms is 0.8305, while it is 0.6742 for all the downstream moving storms.

According to Table 4.12, the average value of the coefficients of model-fit efficiency for the upstream moving storms are higher than those for the downstream moving storms with the same speed. This conclusion can be also drawn when considering experimental tests in Phases 2 or 3. For the various durations of the moving storms in Phases 2 and 3, the simulation results for the upstream moving storms are also better than those for the downstream moving storms, as shown in Table 4.12. For the various durations of the moving storms in Phase 2 or 3, the same trend is observed in detail, as shown in Table 4.14. For the various intensities of the moving storms, the

simulation results for the upstream moving storms are better than those for the downstream moving storms, as shown in Table 4.15.

Table 4.10 Coefficients of Model-Fit Efficiency for Various Storm Velocities in Phases 2 and 3

	Velocity (ft/s)					
	-0.4	-0.2	-0.1	0.1	0.2	0.4
Phases 2 and 3	0.7187	0.9293	0.9353	0.8785	0.8390	0.4751
Phase 2	0.8825	0.9440	0.9356	0.9260	0.8596	0.7859
Phase 3	0.4381	0.9122	0.9349	0.8192	0.8150	0.0953

Table 4.11 Coefficients of Model-Fit Efficiency for Various Storms Durations in Phases 2 and 3

	Duration (s)			
	30	60	120	240
Phases 2 and 3	0.6919	0.8504	0.9180	0.9461
Phase 2	-0.4520	0.6894	0.9731	0.9361
Phase 3	0.1581	0.7660	0.9226	0.9414

Table 4.12 Coefficients of Model-Fit Efficiency for Various Storm Directions

	Upstream	Downstream
Phase 2	0.9115	0.8388
Phase 3	0.6707	0.4750

Table 4.13 Coefficients of Model-Fit Efficiency for Various Storm Durations in Terms of Directions of Movement

	Duration (s)			
	30	60	120	240
Upstream	0.2630	0.9081	0.9649	0.9715
Downstream	0.0663	0.6369	0.8633	0.9146

Table 4.14 Coefficients of Model-Fit Efficiency for Various Storm Durations in Terms of Directions of Movement in Phases 2 and 3

	Duration (s)	Upstream	Downstream	No. Up	No. Down
Phase 2	30	0.7152	0.6687	4	4
Phase 2	60	0.9080	0.7927	5	5
Phase 2	120	0.9635	0.8633	6	5
Phase 2	240	0.9659	0.9263	9	9
Phase 3	30	-0.3400	-0.5360	3	4
Phase 3	60	0.9081	0.5071	5	6
Phase 3	120	0.9731	-	1	0
Phase 3	240	0.9787	0.9030	7	9

Table 4.15 Coefficients of Model-Fit Efficiency for Various Rainfall Intensities in Terms of Directions of Movement in Phases 2 and 3

	i_e (in./hr)	Upstream	Downstream	No. of tests
Phase 2	4.5916	0.8535	0.8170	12
Phase 2	8.1784	0.9475	0.8170	14
Phase 2	11.2092	0.9202	0.8671	21
Phase 3	4.2296	-0.7689	-0.1146	7
Phase 3	7.8181	0.9481	0.6504	11
Phase 3	10.8900	0.9047	0.7120	17

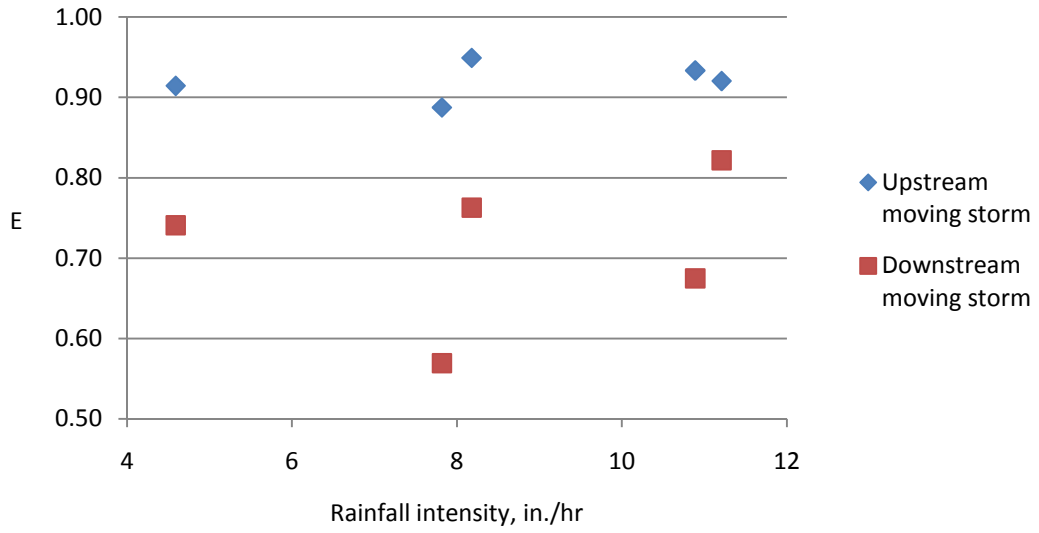

Figure 4.21 Coefficients of Model-Fit Efficiency for Five Sets of Upstream and Downstream Moving Storms with T_d = 60 s, and $|V_s|$ = 0.4 ft/s

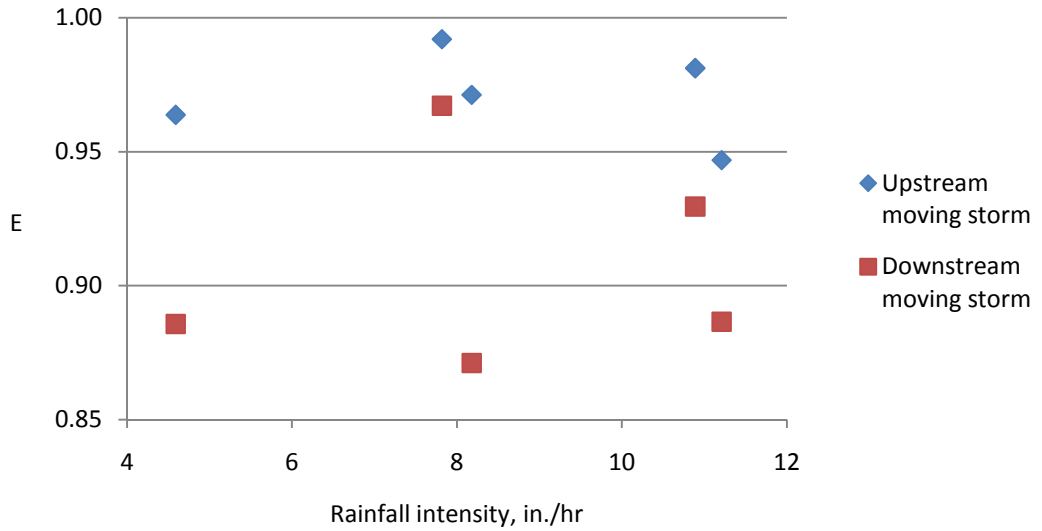

Figure 4.22 Coefficients of Model-Fit Efficiency for Five Sets of Upstream and Downstream Moving Storms with T_d = 240 s, and $|V_s|$ = 0.4 ft/s

4.4 Analysis of the Results of Dynamic-Wave Modeling

In the previous section, Lee and Huang's (2007) kinematic-wave model didn't yield satisfactory simulation results for the downstream moving storms, compared to the upstream moving storms. Therefore, it is of special interest to simulate the downstream moving storms using the dynamic-wave model. In this section, Marcus's (1968) dynamic-wave model is used to simulate a total 58 downstream moving storms from the experimental Phases 2 and 3. The 58 downstream moving storms consist of 16 downstream moving storms among 32 moving storms with storm length equal to watershed length, and 42 downstream moving storms among the 82 moving storms with storm length not equal to watershed length.

In Marcus's (1968) dynamic-wave model, the computational time interval is 0.01 s. The computational grid numbers of overland and channel flow are 51 and 101, respectively. The overland length (L_o) is 20 ft, and the channel effectively is 2 ft wide. A variable Manning's n is

used to approximate the resistance to the overland and channel flows in the experimental watershed (see Section 3.4).

4.4.1 Analysis of the Results for 16 Downstream Moving Storms with Storm Length Equal to Watershed Length

A summary of the coefficient of model-fit efficiency for the 16 downstream moving storms in Phases 2 and 3 is listed in Table 4.16. The percentage difference of the simulated and observed mass of runoff for all tests also is calculated and included in Table 4.16.

Table 4.16 Comparison of Dynamic-Wave Simulated and Observed Runoff for 16 Downstream Moving Laboratory Storms with Storm Length Equal to Watershed Length

Test No.	T_d (s)	V_x (ft/s)	i_e (in./hr)	E	ΔM
1117	100	0.4	4.2296	0.9034	-15.247%
716	100		4.5916	0.9651	-2.924%
1080	100		7.8181	0.9457	1.608%
722	100		8.1784	0.9502	4.883%
1053	100		10.8900	0.9392	6.847%
717ab	100		11.2092	0.9467	1.880%
1133	200	0.2	4.2296	0.9624	-0.725%
728	200		4.5916	0.9183	10.216%
1072	200		7.8181	0.9721	2.582%
726	200		8.1784	0.9297	6.729%
1052	200		10.8900	0.9524	5.965%
724	200		11.2092	0.9354	10.110%
661	400	0.1	4.5916	0.9390	11.554%
1144	400		7.8181	0.9822	3.758%
668abc	400		8.1784	0.9571	10.974%
1151	400		10.8900	0.8930	19.607%

According to Table 4.16, the average coefficient of model-fit efficiency for the 16 downstream moving storms using dynamic-wave modeling is 0.9432. The coefficients of 16 tests using the dynamic-wave model are over 0.90, 7 of which are over 0.95, and 2 of which are over 0.97, as

shown in Figure 4.23. The average coefficient of model-fit efficiency for the tests in Phase 2 is 0.9427, while it is 0.9438 in Phase 3. The average values of the coefficients for the different durations of moving storms are 0.9417 for 100 s, 0.9450 for 200 s, and 0.9428 for 400 s, respectively.

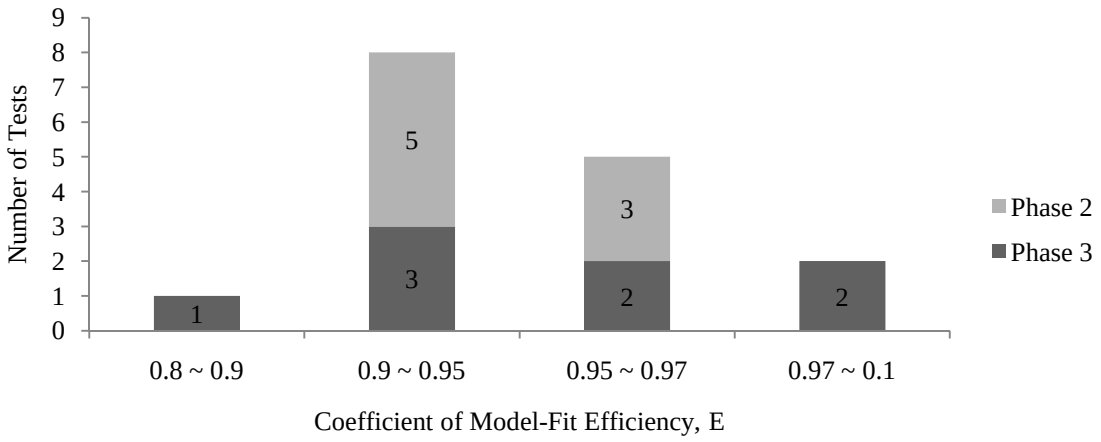

Figure 4.23 Distribution of Coefficient of Model-Fit Efficiency, E, for 16 Downstream Moving Test Storms with Storm Length Equal to Watershed Length

4.4.2 Analysis of the Results for 42 Downstream Moving Storms with Storm Length Not Equal to Watershed Length

Thirty-five of the seventy-five moving storms with storm length not equal to watershed length are downstream moving storms characterized by $T_d \neq L/|V_x|$, while the 16 moving storms analyzed in Section 4.4.1, have $T_d = L/|V_x|$. The comparison results of simulated and observed runoff for the 42 downstream moving storms are listed in Table 4.17. It should be noted that the mass differences between the simulated and observed results are pretty big for several experiments such as Tests 713ab, 711ab, and 1131. The comparison of measured and simulated hydrographs for Test 711ab is shown in **Error! Reference source not found.Error! Reference source not found.**.

Table 4.17 Comparison of Dynamic-Wave Simulated and Observed Runoff for 42 Laboratory Storms with Storm Length Not Equal to Watershed Length

Test No.	T_d (s)	V_x (ft/s)	i_e (in./hr)	E	ΔM
1076	30	0.2	10.8900	0.8203	-7.897%
709ab		0.2	11.2092	0.9119	-13.022%
1131		0.4	4.2296	0.4805	-46.127%
713ab		0.4	4.5916	0.1975	-67.122%
1178		0.4	7.8181	0.8906	-10.795%
711ab		0.4	8.1784	0.7692	-27.478%
1038		0.4	10.8900	0.9786	0.393%
710ab		0.4	11.2092	0.9198	-10.421%
1079	60	0.1	10.8900	0.8475	-3.717%
706		0.1	11.2092	0.7721	-1.264%
1173		0.2	7.8181	0.9395	5.695%
1035		0.2	10.8900	0.9484	-11.443%
691		0.2	11.2092	0.9627	-2.705%
1114		0.4	4.2296	0.8348	-7.116%
744ab		0.4	4.5916	0.9103	0.207%
1090		0.4	7.8181	0.9097	7.894%
741		0.4	8.1784	0.9668	-0.204%
1175		0.4	10.8900	0.9672	4.859%
680		0.4	11.2092	0.9712	-2.079%
700ab	120	0.1	11.2092	0.9005	-4.162%
686		0.2	8.1784	0.9533	-0.219%
679ab		0.2	11.2092	0.9726	1.871%
746ab		0.4	4.5916	0.9252	-3.111%
738ab		0.4	8.1784	0.9317	9.826%
1127	240	0.1	4.2296	0.3740	-3.503%
697		0.1	4.5916	0.9414	-1.076%
1111		0.1	7.8181	0.9736	-0.078%
694		0.1	8.1784	0.9554	5.205%
1065		0.1	10.8900	0.9419	-2.964%
685		0.1	11.2092	0.9512	5.059%
1140		0.2	4.2296	0.9497	-0.939%
735ab		0.2	4.5916	0.8984	13.597%
1179		0.2	7.8181	0.9858	1.364%
732ab		0.2	8.1784	0.8506	4.865%
1058		0.2	10.8900	0.9747	2.034%
730ab		0.2	11.2092	0.9309	10.655%
1129		0.4	4.2296	0.9536	7.647%
757ab		0.4	4.5916	0.8967	8.574%
1087		0.4	7.8181	0.9596	6.004%
747		0.4	8.1784	0.8795	13.003%
1070		0.4	10.8900	0.9443	9.964%
755ab		0.4	11.2092	0.8927	12.591%

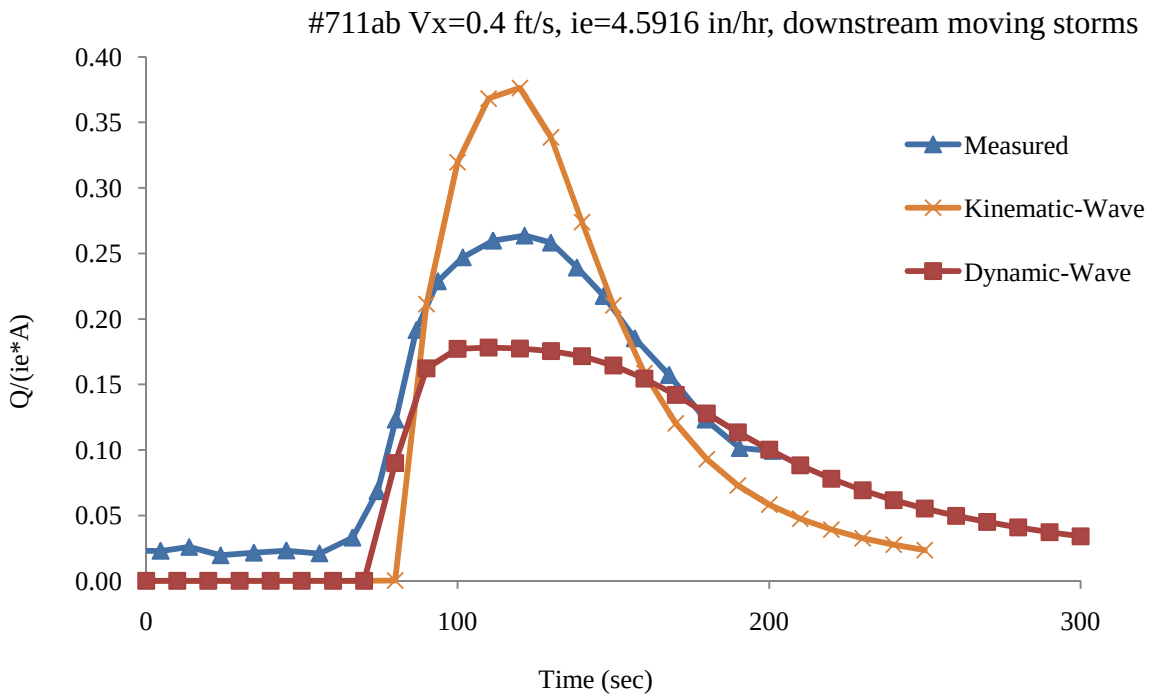

Figure 4.24 Comparison of Measured and Simulated Hydrographs for Test 711ab

According to Table 4.17, the average coefficient of model-fit efficiency for all the tests is 0.8794. The coefficients of 28 tests are over 0.90, 14 of which are over 0.95, and 6 of which are over 0.97. The coefficients of the other 14 tests are lower than 0.90, and 9 of which are between 0.8 and 0.9, as shown in Figure 4.25. It can be also seen that on average, the simulation results from Phase 2 are better than those from Phase 3. The average coefficient for the tests in Phase 2 is 0.8809, while it is 0.8776 for the tests in Phase 3. As shown in Table 4.18, it didn't turn out that the slower the speed of the moving storms, the higher is the value of the coefficient of model-fit efficiency. The coefficients of model-fit efficiency for all the rainstorms with velocity of 0.2 fps are 0.9307, much higher than those for rainstorms with other velocities.

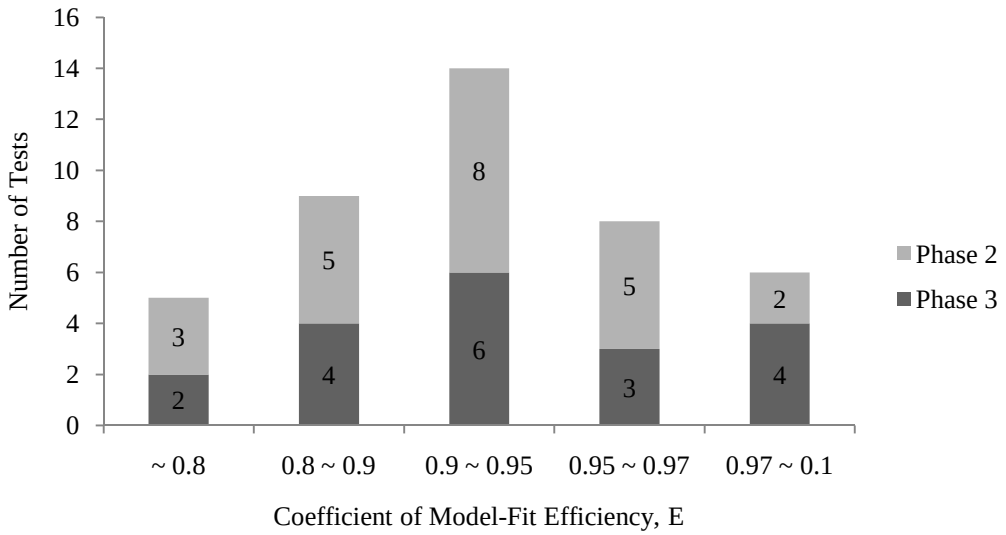

Figure 4.25 Distribution of the Coefficient of Model-Fit Efficiency, E, for 42 Downstream Moving Test Storms with Storm Length Not Equal to Watershed Length

Table 4.18 Coefficients of Model-Fit Efficiency for Various Rainstorm Velocities for Downstream Moving Tests

Rainstorm velocity (ft/s)	Average E
0.1	0.8508
0.2	0.9307
0.4	0.8590

According to Table 4.19, when the duration of the moving storms is short such as 30 s, the coefficient of model-fit efficiency is small, and the simulation result is poor. The overall trend is that the longer the duration of the moving storms, the higher is the value of the coefficient of model-fit efficiency. When considering the tests in Phase 2 or 3, this trend is observed.

Table 4.19 Coefficients of Model-Fit Efficiency for Various Storm Durations In Phases 2 and 3

	Duration (s)			
	30	60	120	240
Phase 2	0.6996	0.9166	0.9367	0.9108
Phase 3	0.7925	0.9078	-	0.8953
Phases 2&3	0.7460	0.9118	0.9367	0.9030

4.5 Comparison of the Simulation Results by Kinematic-Wave and Dynamic-Wave Modeling

4.5.1 Comparison of the Results for 16 Downstream Moving Storms with Storm Length Equal to Watershed Length

Marcus's (1968) dynamic-wave model works pretty well for all of the 16 downstream moving storms with storm length equal to watershed length, compared to Lee and Huang's (2007) kinematic-wave model. Table 4.20 shows the comparison of the simulation results by kinematic-wave and dynamic-wave models for the 16 downstream moving storms with storm length equal to watershed length. According to Table 4.20, the average coefficient of model-fit efficiency for the 16 downstream moving storms using dynamic-wave modeling is 0.9432, while the average is 0.8673 using kinematic-wave modeling. The distributions of the coefficients of the 8 tests in Phase 2 and the 8 tests in Phase 3 are shown in Figures 4.26 and 4.27, respectively. As seen in Figure 4.28, for the downstream moving storms with an intensity of about 8 in./hr, the simulation results are improved a lot by using the dynamic-wave model.

Table 4.20 Comparison of the Simulation Results from Kinematic-Wave and Dynamic-Wave Models for 16 Downstream Moving Storms with Storm Length Equal to Watershed Length

Test No.	T_d (s)	V_x (ft/s)	i_e (in./hr)	Kinematic-Wave		Dynamic-Wave	
				E	ΔM	E	ΔM
1117	100	0.4	4.2296	0.7361	-10.331%	0.9034	-15.247%
716	100		4.5916	0.8397	6.345%	0.9651	-2.924%
1080	100		7.8181	0.4098	3.116%	0.9457	1.608%
722	100		8.1784	0.8309	8.593%	0.9502	4.883%
1053	100		10.8900	0.8395	4.972%	0.9392	6.847%
717ab	100		11.2092	0.8589	4.015%	0.9467	1.880%
1133	200	0.2	4.2296	0.9549	-0.806%	0.9624	-0.725%
728	200		4.5916	0.8878	10.592%	0.9183	10.216%
1072	200		7.8181	0.9555	0.481%	0.9721	2.582%
726	200		8.1784	0.9188	5.693%	0.9297	6.729%
1052	200		10.8900	0.8576	3.336%	0.9524	5.965%
724	200		11.2092	0.9357	7.928%	0.9354	10.110%
661	400	0.1	4.5916	0.9583	-2.914%	0.9390	11.554%
1144	400		7.8181	0.9878	-0.813%	0.9822	3.758%
668abc	400		8.1784	0.9620	7.468%	0.9571	10.974%
1151	400		10.8900	0.9430	13.368%	0.8930	19.607%

Table 4.21 Comparison of the Simulations Results from Kinematic-Wave and Dynamic-wave Models for 16 Downstream Moving Storms with Storm Length Equal to Watershed Length in Phases 2 and 3

	Kinematic-Wave	Dynamic-Wave
Phases 2 & 3	0.8673	0.9432
Phase 2	0.8990	0.9427
Phase 3	0.8355	0.9438

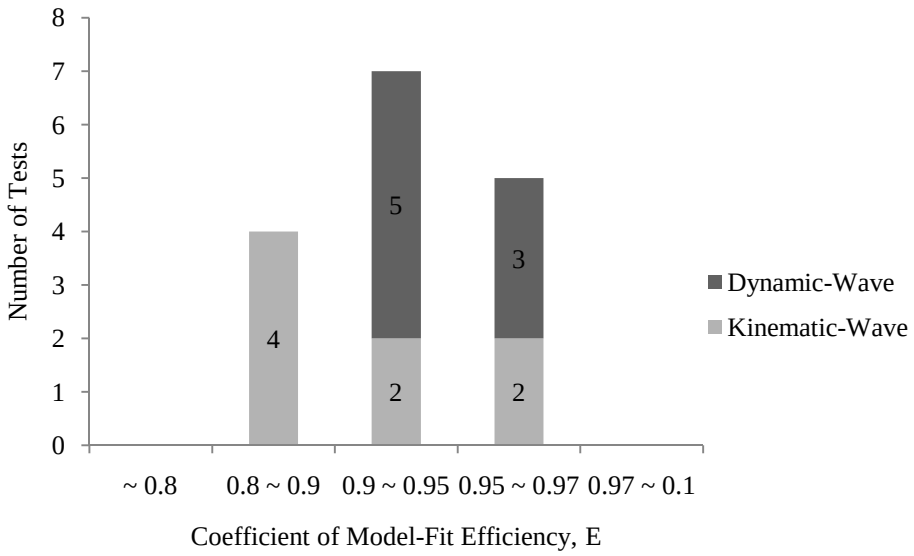

Figure 4.26 Comparison of Distributions of the Coefficient of Model-Fit Efficiency, E, for 8 Downstream Moving Storms with Storm Length Equal to Watershed Length in Phase 2

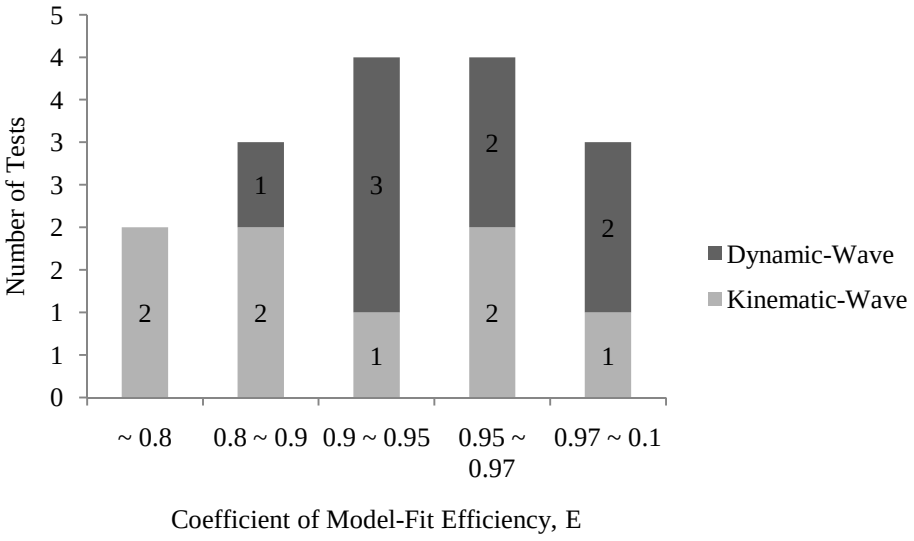

Figure 4.27 Comparison of Distributions of the Coefficient of Model-Fit Efficiency, E, for 8 Downstream Moving Storms with Storm Length Equal to Watershed Length in Phase 3

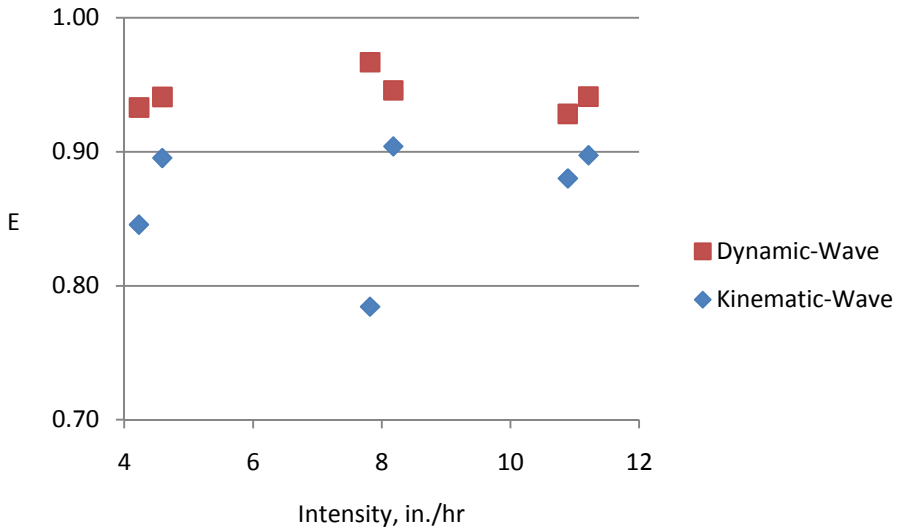

Figure 4.28 Comparison of the Coefficient of Model-Fit Efficiency, E, for 12 Downstream Moving Storms with Storm Length Equal to Watershed Length

4.5.2 Comparison of the Results for 42 Downstream Moving Storms with Storm Length Not Equal to Watershed Length

Marcus's (1968) dynamic-wave model works better for the 42 downstream moving storms with storm length not equal to watershed length, compared to Lee and Huang's (2007) kinematic-wave model. According to Table 4.22, the average coefficient of model-fit efficiency for the 42 downstream moving storms using dynamic-wave modeling is 0.8794, while the average is 0.6789 using kinematic-wave modeling. It can also be seen that the simulation results of 19 tests in Phase 3 are much better when using the dynamic-wave model compared to the kinematic-wave model. The comparison of distributions of the coefficients of 23 tests in Phase 2 and 19 tests in Phase 3 are shown in Figures 4.29 and 4.30, respectively. Table 4.23 shows the comparison of the simulation results from the kinematic-wave and dynamic-wave models for the 42 downstream moving storms.

Table 4.22 Comparison of the Simulations Results from Kinematic-Wave and Dynamic-Wave Models for 42 Downstream Moving Storms with Storm Length Not Equal to Watershed Length in Phases 2 and 3

	Kinematic-Wave	Dynamic-Wave
Phases 2 & 3	0.6789	0.8794
Phase 2	0.8473	0.8809
Phase 3	0.4750	0.8776

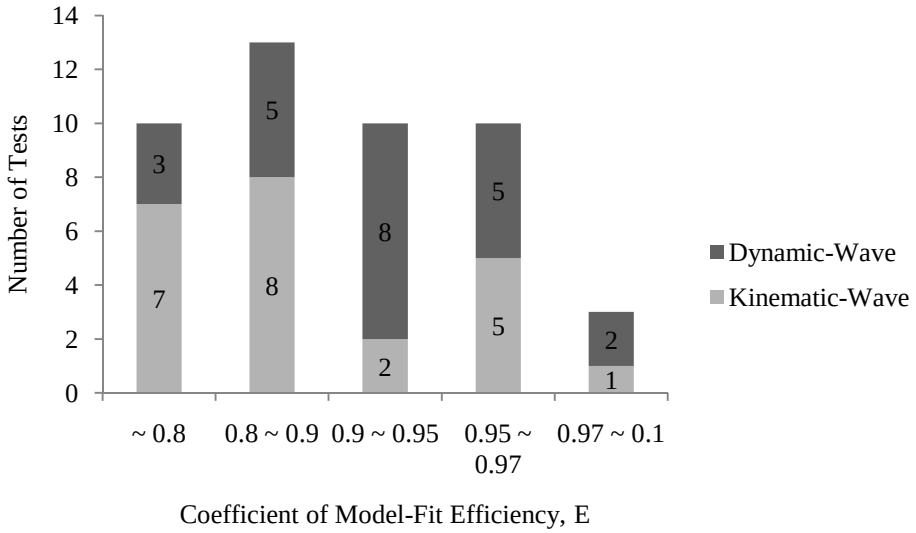

Figure 4.29 Comparison of Distributions of Coefficient of Model-Fit Efficiency, E, for 23 Test Storms with Storm Length Not Equal to Watershed Length in Phase 2

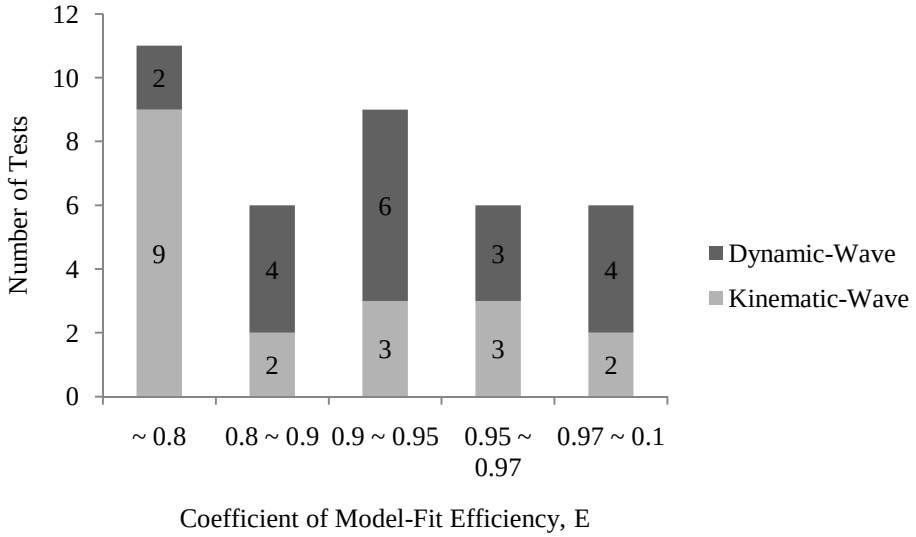

Figure 4.30 Comparison of Distributions of Coefficient of Model-Fit Efficiency, E, for 19 Test Storms with Storm Length Not Equal to Watershed Length in Phase 3

Table 4.23 Comparison of the Simulation Results from Kinematic-Wave and Dynamic-Wave Models for 42 Downstream Moving Storms with Storm Length Not Equal to Watershed Length

Test No.	T_d (s)	V_x, (ft/s)	i_e (in./hr)	Kinematic-Wave		Dynamic-Wave	
				E	ΔM	E	ΔM
1076	30	0.2	10.8900	0.3658	-2.184%	0.8203	-7.897%
709ab	30	0.2	11.2092	0.7438	-5.183%	0.9119	-13.022%
1131	30	0.4	4.2296	-2.2458	13.833%	0.4805	-46.127%
713ab	30	0.4	4.5916	0.5245	-10.463%	0.1975	-67.122%
1178	30	0.4	7.8181	-0.3732	2.630%	0.8906	-10.795%
711ab	30	0.4	8.1784	0.6361	-0.982%	0.7692	-27.478%
1038	30	0.4	10.8900	0.1092	14.247%	0.9786	0.393%
710ab	30	0.4	11.2092	0.7703	-0.310%	0.9198	-10.421%
1079	60	0.1	10.8900	0.8640	0.550%	0.8475	-3.717%
706	60	0.1	11.2092	0.7828	-0.367%	0.7721	-1.264%
1173	60	0.2	7.8181	0.7834	8.846%	0.9395	5.695%
1035	60	0.2	10.8900	0.8375	-9.685%	0.9484	-11.443%
691	60	0.2	11.2092	0.8556	-2.474%	0.9627	-2.705%
1114	60	0.4	4.2296	-0.6868	5.187%	0.8348	-7.116%
744ab	60	0.4	4.5916	0.7408	10.841%	0.9103	0.207%
1090	60	0.4	7.8181	0.5693	13.229%	0.9097	7.894%
741	60	0.4	8.1784	0.7627	3.851%	0.9668	-0.204%
1175	60	0.4	10.8900	0.6749	7.966%	0.9672	4.859%
680	60	0.4	11.2092	0.8216	-1.253%	0.9712	-2.079%
700ab	120	0.1	11.2092	0.9572	-6.472%	0.9005	-4.162%
686	120	0.2	8.1784	0.8903	-2.829%	0.9533	-0.219%
679ab	120	0.2	11.2092	0.9200	0.074%	0.9726	1.871%
746ab	120	0.4	4.5916	0.9051	0.819%	0.9252	-3.111%
738ab	120	0.4	8.1784	0.8400	12.004%	0.9317	9.826%
1127	240	0.1	4.2296	0.4935	2.140%	0.3740	-3.503%
697	240	0.1	4.5916	0.9549	-1.759%	0.9414	-1.076%
1111	240	0.1	7.8181	0.9739	0.025%	0.9736	-0.078%
694	240	0.1	8.1784	0.9609	2.086%	0.9554	5.205%
1065	240	0.1	10.8900	0.9455	-0.970%	0.9419	-2.964%
685	240	0.1	11.2092	0.9739	0.231%	0.9512	5.059%
1140	240	0.2	4.2296	0.9525	-1.830%	0.9497	-0.939%
735ab	240	0.2	4.5916	0.8908	11.796%	0.8984	13.597%
1179	240	0.2	7.8181	0.9818	-1.966%	0.9858	1.364%
732ab	240	0.2	8.1784	0.9536	3.668%	0.8506	4.865%
1058	240	0.2	10.8900	0.9693	-1.382%	0.9747	2.034%

4.6 Summary of Comparison of Kinematic-Wave and Dynamic-Wave Models

The nondimensional plot comparisons in Section 4.1 indicates that kinematic-wave model results overstate the increase in peak flow resulting from downstream movement because they do not consider the backwater effect resulting from the limitations of channel capacity. This conclusion is supported by the comparisons of the simulations results of the kinematic-wave and dynamic-wave models.

The simulation results of the kinematic-wave and dynamic-wave models are statistically evaluated using Nash-Sutcliffe coefficient of model-fit efficiency. The dynamic-wave model yields better simulation results for downstream moving storms than the kinematic-wave model, since for downstream moving storms the average coefficient of the simulations results of the dynamic-wave is higher than the kinematic-wave model. This model-fit criterion is very sensitive to the peak and high flows of the hydrographs, therefore, the accuracy of the dynamic-wave model to simulate the peak and high flows is higher than the kinematic-wave model.

CHAPTER 5 DETERMINATION OF THE TIME OF CONCENTRATION

The time of concentration of surface runoff in a watershed is one of the most significant parameters in hydrologic design. For example, in the Rational Method for storm drainage design, the design rainfall intensity is determined based on rainfall duration equal to the time of concentration. The time of concentration is also widely used in dimensional analysis in theoretical studies. Richardson and Julien (1989) applied the time of concentration in a dimensionless parameter to study the effect of moving rainstorms on runoff from a single overland plane. Ogden et al. (1995) applied the time of concentration to identify a dimensionless storm speed similarity parameter which relates storm speed to the influence of storm motion on the hydrograph peak discharge from a one-dimensional runoff plane.

In these earlier studies, the time of concentration t_c is used to normalize the moving storm velocity in the dimensionless parameter $V_s T_e / L$, and the dimensionless storm velocity is widely applied in dimensionless plots to analyze the influence of storm movement on peak discharge. The validity of the earlier results is based on a valid value of the time of concentration. Therefore, it is necessary to examine the determination of time of concentration t_c and its influence on the earlier results. In this chapter, determination of the time of concentration is evaluated by comparing the experimental data from stationary rainstorms in experimental Phases 2 and 3 to the equation proposed by Wong (2001).

There are a number of definitions of the time of concentration for a watershed. Shen et al. (1974) reviewed the four most popular definitions of the time of concentration, t_c. They are as follows:

1. The time required for the surface runoff from the “hydraulically” farmost point of the drainage basin to reach its outlet (Chow, 1964);
2. The time required for the surface runoff to reach an equilibrium state (Eagleson, 1970);
3. The time required for the water in the channel at the gauging station to rise from the low to the maximum stage, i.e., equivalent to the time of occurrence of peak discharge (Rasmer, 1927);
4. The time required for the flow to reach a percentage of the maximum or equilibrium discharge for the purpose of simplicity in data utilization, such as the methods proposed by Izzard (1946) and Ben-Zvi (1970).

Shen et al. (1974) argued that Ben-Zvi (1970) attempted to clearly define the equilibrium state, but had yet to reach a generally agreeable percentage of the peak discharge, and the percentage was easily subject to personal judgment. Shen et al. (1974) also concluded that the effects of watershed and rainstorm characteristics on the time of concentration, t_c, depend on the definition adopted for t_c. Shen et al. (1974) suggested that the time from the commencement of rainfall excess to the occurrence of the peak discharge for rainstorms with sufficiently long duration should be taken as the time of concentration. Therefore, in this study, the methods proposed by Izzard (1946) and Ben-Zvi (1970) are applied to experimentally determine the time of concentration for a V-shaped watershed.

5.1 Methods Review

As previously discussed, there are several different techniques to determine the time of concentration from the experimental hydrographs of stationary rainstorms. The selected hydrographs of stationary rainstorms in experimental Phases 2 and 3 are characterized by a rising limb, a plateau, i.e. a steady equilibrium stage, and a recession limb. The corresponding stationary rainstorms have sufficiently long duration to reach the equilibrium plateau. However, in real-world laboratory experiments such as in the WES, the ideal hydrographs featuring a perfect plateau with constant discharges cannot be obtained, mainly due to the limitations of the experimental system, such as lack of stability of rainfall production and accuracy of discharge measurement. Therefore, the use of the imperfect experimental hydrographs leads to a somewhat arbitrary procedure to determine the time of concentration. In this section, three procedures or methods, i.e. Ben-Zvi's method, a modified Ben-Zvi method, and Izzard's method are introduced to determine the time of concentration from the experimental hydrographs.

5.1.1 Ben-Zvi's Method

Ben-Zvi (1970) proposed a technique dealing for the determination of the time of concentration from the experimental hydrographs from the WES. Ben-Zvi's (1970) experiments conducted on the aluminum surface in the WES were performed with stationary rainstorms having different intensities and durations of rainfall. In this chapter, the technique proposed by Ben-Zvi (1970) is described and named as Ben-Zvi's method.

5.1.1.1 Description of Ben-Zvi's Method

The time of concentration, t_c, is determined as the time from the commencement of the rainfall until the time of occurrence of the last measured discharge whose common logarithm is at least 0.05 logarithmic cycles below a straight line which is fitted to the peak outflow hydrograph for a case where the runoff achieves a near constant peak discharge measured from the 5th (mentioned in the text of Ben-Zvi (1970) or 4th from Figure 5.1 below) to 8th minute of the rainfall duration (Ben-Zvi, 1970). The technique for the determination of the time of concentration is schematically shown in Figure 5.1.

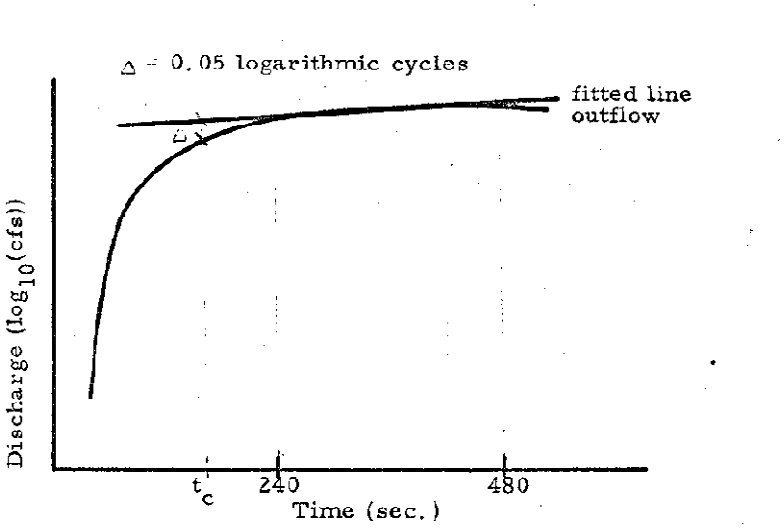

Figure 5.1 Ben-Zvi's Technique for Determination of Time of Concentration (after Ben-Zvi, 1970)

In order to reduce the effect of the measurement error on the visualized trend of the gradual rise of the discharge, the hydrographs of the 8-minute duration experiments were plotted on semi logarithmic paper as shown in Figure 5.1. Strictly speaking, the logarithms of discharges of the 8-minute duration experiments were plotted on regular paper, rather than the discharges plotted

on a semi-logarithmic paper. Although both ways of plotting have the same visual effect, the former has an advantage for related computation.

5.1.1.2 Mathematical form of Ben-Zvi's Method

According to the description of Ben-Zvi's method, major equations used in Ben-Zvi's method are:

$$t_c = t_2 - t_1 \tag{5.1}$$

$$t_1 = 0 \; and \; t_c = t_2 \tag{5.2}$$

where t_c the time of concentration in seconds, t_1 is is the beginning time of rainfall in seconds, which in the experimental system is recorded as zero, and t_2 is the time of occurrence of the last measured discharge whose common logarithm is at least 0.05 logarithmic cycles below the straight line.

The time, t_2, satisfies the following equations:

$$\log \mathrm{Q}_{\mathrm{line}}(t_2) - \log \mathrm{Q}\,(t_2) \geq \Delta = 0.05 \tag{5.3}$$

$$\mathrm{Q}_{\mathrm{line}} = \mathrm{mt} + \mathrm{b} \tag{5.4}$$

$$\mathrm{Q} = \mathrm{f(t)} \tag{5.5}$$

where $\mathrm{Q}_{\mathrm{line}} = \mathrm{mt} + \mathrm{b}$ is the best fit straight line for the chosen part of hydrograph, and $Q = \mathrm{f(t)}$ is the discharge (Q) hydrograph as a function of time, t. Equation (5.3) can be transformed into the following form:

$$\frac{\mathrm{Q}(t_2)}{\mathrm{Q}_{\mathrm{line}}(t_2)} \leq 0.89 \tag{5.6}$$

5.1.1.3 Specific steps for Ben-Zvi's Method

Specific steps for Ben-Zvi's method as follows:

1) Take the logarithm with base 10 of the discharge data points measured from the time period between $T/2$ and T of the rainfall duration.
2) Construct a best fit straight line from the logarithms of these selected discharge data points.
3) Find the earliest measured discharge data point whose common logarithm is at most 0.05 logarithmic cycles below the best fit straight line.

$$\log \mathrm{Q}_{\mathrm{line}}(t_2) - \log \mathrm{Q}\,(t_2) \geq \Delta = 0.05$$

$$\frac{\mathrm{Q}(t_2)}{\mathrm{Q}_{\mathrm{line}}(t_2)} \leq 0.89$$

4) Determine the equilibrium time by subtracting the time when the earliest measured discharge occurred after the beginning of the rainfall from t_2.

In Ben-Zvi's method, it is suggested that t_c corresponds to the last measured discharge whose common logarithm is below the equilibrium discharge line at least 0.05 logarithmic cycles. However, it is more reasonable that "at most" is considered instead of "at least". In this study, in order to solve this problem, interpolation between the measured discharges is used to find the t_c corresponding to the discharge which is exactly 89 percent of the equilibrium discharge.

5.1.2 Modified Ben-Zvi Method

In Ben-Zvi's Method, t_c is the time required for the flow to reach a percentage, i.e. 89%, of the equilibrium discharge from the best-fit line. In the Modified Ben-Zvi method, the maximum discharge is used instead of the best-fit line of the equilibrium discharge. The time of

concentration herein is defined as the time required for the flow to reach a percentage, i.e. 89%, of the maximum discharge. Interpolation between the measured discharges is also used to find the t_c corresponding to the discharge which is exactly 89% of the maximum discharge.

5.1.3 Izzard's Method

Izzard (1946) suggested the equilibrium time, t_e, was defined as the time when the mathematical curve for $\frac{q}{q_e}$ reached 0.97, where q_e is the discharge at equilibrium. The time of concentration herein is defined as the time required for the flow to reach a percentage, i.e. 97%, of the maximum discharge instead of the equilibrium discharge. Interpolation between the measured discharges is also used to find the t_c corresponding to the discharge which is exactly 97 % of the maximum discharge.

$$\frac{\mathrm{Q}}{\mathrm{Q_p}} \geq 0.97 \tag{5.7}$$

5.2 Computation of the Time of Concentration

Henderson and Wooding (1964) derived an equation for the time of concentration of the overland flow assuming a kinematic-wave process. By using the method of characteristics, Singh (1996) derived analytical solutions for an overland plane subjected to stationary rainstorms and they are identical to the equation of Henderson and Wooding (1964). Based on the kinematic-wave theory, Wong (2001) derived an equation for the time of concentration of the channel flow.

The time of concentration of a watershed comprising overland planes and drainage channels is the summation of the time of concentration of the overland flows and the time of concentration of channel flow (Overton and Meadows, 1976). Yen (1982) argued that these two flow components are two separate and sequential systems, and should be considered separately. Kibler and Aron (1983) showed that this distributed approach produced better results.

The stationary rainstorm experiments in Phases 2 and 3 were conducted in a V-shaped (open book) watershed in the WES, which included a longitudinal channel of 40 ft and two lateral overland planes with a size of 20 ft × 40 ft. The surface runoff consists of two parts: the overland flow and the channel flow. Therefore, in this section, the time of concentration for the rainstorms in a V-shaped watershed is calculated with the equations proposed by Henderson and Wooding (1964) and Wong (2001).

The time of concentration for the V-shaped (open book) experimental watershed can be computed by the following equations:

$$t_c = T_{co} + T_{cc} \tag{5.8}$$

where T_{co} is the time of concentration of the overland flow, i.e. (Henderson and Wooding, 1964)

$$T_{co} = \left(\frac{n_o L_o}{\sqrt{S_o} {i_e}^{2/3}} \right)^{3/5} \tag{5.9}$$

where S_o is the slope of the overland plane, n_o is roughness coefficient of the overland plane, L_o is the length of the overland plane; and i_e is the effective rainfall intensity, which equals the rainfall intensity for the WES experiments. T_{cc} is the time of concentration of the channel flow, i.e. (Wong, 2001)

$$T_{cc} = \left(\frac{2^{2/3} n_c L_c (1 + S_o^2)^{1/3}}{\sqrt{S_c} S_o^{1/3} (2 i_e L_o)^{1/3}} \right)^{3/4} \tag{5.10}$$

where S_c is the channel slope, L_c is the channel length, and n_c is roughness coefficient of the channel. Wong's (2001) equation was derived based on the kinematic-wave theory. It is applicable to a prismatic channel with negligible backwater effect, which is subject to a uniform lateral inflow and a constant upstream inflow. Equation 5.10 is obtained when the general formula derived by Wong (2001) is applied to the V-shaped test basin, which has a triangular channel and two identical overland planes, and is subject to a rainfall of uniform intensity.

The exact rainfall intensity of the stationary rainstorms for the WES is unknown, and the nominal value of the rainfall intensity cannot be used in the computation of the time of concentration. For rainstorms that reached a plateau discharge, intensity was computed as peak discharge divided by the area.

$$i_e = \frac{Q_p}{A} \tag{5.11}$$

In Phase 2, the observed hydrographs of 29 experimental rainstorms (including 42 experiments) done in the basin with a size of 40 ft by 40 ft had plateaus in discharge. In Phase 3, the observed hydrographs of 27 experimental rainstorms done in the basin with a size of 40 ft by 40 ft reached equilibrium discharge.

The fixed value of 0.014 of the Manning's roughness coefficient, n, was used in the equations to calculate the time of concentration for rainstorms in experimental Phases 2 and 3. Xiong and Melching (2005) calibrated and determined the value of Manning's roughness coefficient n as 0.014 in the simulation of experimental data in Phase 2 by using a kinematic-wave routing

model. As noted in Section 1.2.2, Xiong and Melching (2005) fount that a kinematic-wave model yielded good results for stationary storms in Phase 2. Thus, it is felt that Wong's (2001) equation that was derived from the kinematic-wave assumption should be valid for comparison with experimental t_c data obtained from the WES. It should also be noted that the roughness coefficient is not only determined by the material of the watershed surface, but also is affected by the other factors especially the rainfall intensity (Wenzel, 1970; Shen and Li, 1973).

5.3 Applying Three Methods for Estimating t_c from the Lab Data and Comparing with Wong's Equation

5.3.1 Experimental Data

Only the 61 uniform stationary rainstorms in Phases 2 and 3 were considered for the determination of the time of concentration. Since the WES watershed is relatively small, compared to real world watersheds, only the experimental data from the maximal area (40 ft × 40 ft) of the watershed were considered in this dissertation. Furthermore, the observed hydrographs characterized by plateaus in discharge were selected for analysis. The plateau hydrographs indicated that the rainfall duration exceeded the time of concentration on the watershed. The other hydrographs which did not reach a plateau in discharge cannot be used since the time of concentration cannot be obtained from the non-plateau hydrographs.

The geometric characteristics of the watersheds and the properties of the stationary storms (dimensions of the watershed, longitudinal and lateral slopes, intensity, storm duration, etc.) for the 61 experimental runs are listed in Table 5.1. The specific experimental condition for an individual run is listed in Tables 5.2 and 5.3.

Table 5.1 Experimental Conditions of 61 Stationary Rainstorms in Phases 2 and 3

	Surface	$L \times W$ (ft × ft)	$S_c\% + S_o\%$	$I_{nominal}$ (in./hr)	T_d
Phase 2	Aluminum	40 × 40	0.5+1, 1+0.5/1/3/5, 2+1, 3+1	6, 8, 10, 15	120, 180, 240
Phase 3	Aluminum	40 × 40	1+1/3/5, 2/3+1	6, 8, 10, 15	120, 180, 240

Table 5.2 Comparison of the Time of Concentration for Stationary Storms in Phase 2

	Phase 2 Test #	S_c	S_o	T (s)	I_{nom} (in./hr)	I_{com} (in./hr)	T_e (s)	t_c_1[1]	t_c_2[2]	t_c_3[3]	err_1	err_2	err_3
1	834	1%	1%	180	15	11.4656	88.28	82.09	93.81	121.76	7.54%	-5.90%	-27.50%
2	789	1%	1%	180	15	11.4245	93.44	85.93	106.70	146.28	8.73%	-12.43%	-36.13%
3	787a	1%	1%	120	15	11.2971	93.78	84.77	94.97	122.86	10.64%	-1.25%	-23.67%
4	787b	1%	1%	120	15	10.8737	94.96	88.90	89.98	96.77	6.82%	5.54%	-1.87%
5	792a	1%	1%	240	10	8.2042	104.19	101.23	110.46	153.18	2.92%	-5.67%	-31.98%
6	792b	1%	1%	240	10	8.1321	104.49	96.29	106.76	132.83	8.51%	-2.12%	-21.34%
7	793a	1%	1%	240	8	6.8045	110.83	105.55	107.48	137.91	5.00%	3.11%	-19.64%
8	793b	1%	1%	240	8	6.8515	110.83	103.79	109.70	143.09	6.78%	1.03%	-22.55%
9	799a	1%	1%	240	6	4.5390	121.37	118.66	125.14	162.25	2.28%	-3.02%	-25.20%
10	799b	1%	1%	240	6	4.7183	125.15	120.92	136.72	151.95	3.50%	-8.46%	-17.63%
11	609	1%	1%	180	15	10.9523	78.25	86.76	76.75	106.12	-9.81%	1.96%	-26.26%
12	611	1%	1%	240	10	7.9998	86.74	79.12	86.33	112.63	9.62%	0.48%	-22.99%
13	612	1%	1%	240	10	8.4877	85.07	81.10	85.66	127.19	4.89%	-0.69%	-33.12%
14	613	1%	1%	120	10	7.5962	88.23	71.67	78.77	80.54	23.11%	12.00%	9.54%
15	623	1%	1%	120	8	6.6439	92.21	77.67	81.46	105.05	18.72%	13.20%	-12.22%
16	629	1%	1%	240	8	6.7522	91.72	82.84	90.33	150.38	10.71%	1.54%	-39.01%
17	632	1%	1%	120	6	4.4693	105.13	85.42	89.45	104.02	23.07%	17.53%	1.06%
18	634	1%	1%	240	6	4.3127	106.38	97.83	106.08	143.03	8.74%	0.28%	-25.62%
19	803	1%	1%	120	15	10.7590	78.71	55.79	66.25	90.82	41.09%	18.81%	-13.34%

[1] The time of concentration determined by Ben-Zvi's method. The difference of the result of Ben-Zvi's method compared to Wong's time of concentration equation computation is denoted as err_1.

[2] The time of concentration determined by the modified Ben-Zvi method. The difference of the result of the modified Ben-Zvi's method compared to Wong's time of concentration equation computation is denoted as err_2.

[3] The time of concentration determined by Izzard's method. The difference of the result of Izzard's method compared to Wong's time of concentration equation computation is denoted as err_3.

	Phase 2 Test #	S_c	S_o	T (s)	I_{nom} (in./hr)	I_{com} (in./hr)	T_e (s)	$t_c\_1^1$	$t_c\_2^2$	$t_c\_3^3$	err_1	err_2	err_3
20	603a	1%	1%	180	15	11.1364	77.83	70.13	81.30	137.33	10.98%	-4.28%	-43.33%
21	603b	1%	1%	180	15	11.3565	77.33	66.28	82.54	143.13	16.67%	-6.31%	-45.97%
22	603c	1%	1%	180	15	11.2423	77.59	64.14	81.60	140.77	20.96%	-4.92%	-44.88%
23	806	1%	3%	180	15	11.0114	57.73	63.54	77.76	104.18	-9.14%	-25.75%	-44.59%
24	807	1%	3%	180	15	11.3370	57.19	66.28	76.09	166.14	-13.72%	-24.84%	-65.58%
25	814	1%	3%	240	10	8.4162	63.01	74.96	81.23	134.30	-15.93%	-22.42%	-53.08%
26	816	1%	3%	240	6	4.4199	77.84	70.24	72.90	105.22	10.82%	6.78%	-26.02%
27	815a	1%	3%	240	8	7.0386	66.80	73.38	78.70	127.83	-8.96%	-15.12%	-47.74%
28	815b	1%	3%	240	8	7.2779	66.08	63.68	90.06	202.68	3.76%	-26.63%	-67.40%
29	815c	1%	3%	240	8	7.2101	66.28	76.64	88.87	126.86	-13.51%	-25.42%	-47.75%
30	817	1%	5%	120	15	10.8913	50.36	49.71	62.96	110.28	1.32%	-20.01%	-54.33%
31	820	1%	5%	180	15	11.1216	50.02	57.37	109.01	125.45	-12.81%	-54.11%	-60.13%
32	832	1%	5%	240	8	6.8669	58.51	69.43	76.96	149.90	-15.73%	-23.97%	-60.96%
33	819a	1%	5%	180	15	10.9436	50.28	58.75	79.04	113.75	-14.40%	-36.38%	-55.80%
34	819b	1%	5%	180	15	10.8842	50.37	55.65	58.64	112.36	-9.48%	-14.10%	-55.17%
35	831a	1%	5%	240	10	8.4405	54.71	68.86	89.66	220.64	-20.56%	-38.98%	-75.21%
36	831b	1%	5%	240	10	8.1508	55.33	75.15	85.49	103.23	-26.37%	-35.27%	-46.40%
37	833b	1%	5%	240	6	4.4547	67.43	64.67	70.90	77.13	4.27%	-4.90%	-12.58%
38	843a	2%	1%	180	15	10.5189	70.48	69.40	78.25	114.42	1.56%	-9.94%	-38.40%
39	843b	2%	1%	180	15	10.8805	69.68	64.84	74.45	135.76	7.46%	-6.40%	-48.67%
40	841a	3%	1%	180	15	11.6729	63.97	62.15	83.48	155.33	2.92%	-23.37%	-58.82%
41	841b	3%	1%	180	15	11.6972	63.93	63.12	66.79	140.89	1.27%	-4.29%	-54.63%

Table 5.3 Comparison of the Time of Concentration for Stationary Storms in Phase 3

	Box_3 Test #	S_c	S_o	T (s)	I_{nom} (in./hr)	I_{com} (in./hr)	Te_computed (s)	tp_1	tp_2	tp_3	err_1	err_2	err_3
1	1109	1%	1%	240	6	4.3424	106.14	143.44	165.41	208.41	-26.00%	-35.83%	-49.07%
2	1199	1%	1%	240	6	4.2255	129.84	129.57	199.61	263.19	0.21%	-34.95%	-50.67%
3	1217	1%	3%	240	6	4.0819	79.91	120.77	133.52	159.98	-33.83%	-40.15%	-50.05%
4	1229	1%	5%	240	6	4.2684	68.38	104.08	115.31	144.20	-34.30%	-40.70%	-52.58%
5	1107	1%	1%	240	8	6.8872	91.12	117.19	133.62	160.24	-22.24%	-31.81%	-43.14%
6	1196	1%	1%	240	8	6.9323	110.15	125.43	190.18	231.77	-12.18%	-42.08%	-52.48%
7	1214	1%	3%	240	8	6.5683	68.33	107.47	113.80	142.05	-36.42%	-39.95%	-51.89%
8	1227	1%	5%	240	8	6.7846	58.74	95.72	112.85	168.83	-38.63%	-47.95%	-65.21%
9	1007	1%	1%	240	10	6.9944	91.12	107.60	124.94	198.20	-15.32%	-27.07%	-54.03%
10	1190	1%	1%	240	10	7.8454	105.74	124.33	162.28	216.53	-14.96%	-34.84%	-51.17%
11	1194	1%	1%	240	10	8.2283	104.09	128.51	164.21	228.35	-19.00%	-36.62%	-54.42%
12	1213	1%	3%	240	10	7.9493	64.20	100.42	108.04	133.27	-36.07%	-40.58%	-51.83%
13	1225	1%	5%	240	10	8.0733	55.50	85.99	103.49	185.01	-35.45%	-46.37%	-70.00%
14	1106	1%	1%	180	15	10.7363	78.76	96.19	118.49	139.87	-18.12%	-33.53%	-43.69%
15	1212	1%	3%	180	15	10.7711	58.15	80.42	109.78	140.71	-27.69%	-47.03%	-58.68%
16	1221	1%	5%	180	15	10.6669	50.70	73.24	93.14	140.94	-30.77%	-45.57%	-64.03%
17	1223	1%	5%	120	15	10.4274	51.08	80.81	87.59	100.85	-36.79%	-41.68%	-49.36%
18	1230	1%	1%	180	15	10.7544	90.09	96.92	115.96	139.57	-7.05%	-22.31%	-35.45%
19	1233	2%	1%	180	15	10.8772	69.69	84.77	115.73	135.01	-17.80%	-39.79%	-48.38%
20	1236	3%	1%	180	15	10.8767	65.54	91.42	111.95	129.02	-28.32%	-41.46%	-49.20%

5.3.2 Determination of the Best-Fit Straight Line

In Ben-Zvi's method, determination of a straight line for the best fit to a group of discharge data points within a percentage of the maximum or equilibrium discharge is a key step. Ben-Zvi (1970) determined the straight trend line of the measured discharge data from 5th (or 4th) to 8th minute of the 8 min rainfall duration. It seems that Ben-Zvi decided to take the data points between $T/2$ and T of the rainfall duration to construct the best-fit straight line. However, the reason for this criterion of choosing the discharge data points to construct the best fit straight line was not clearly discussed in Ben-Zvi's (1970) dissertation. The possible reasoning for the criterion is discussed in the following paragraphs.

The upper limit of the time range of the data points for the straight line fit is the end point of the rainfall. Theoretically, the equilibrium period should last until the end point of the rainfall. Therefore, it is reasonable to choose the end point of the rainfall. The lower limit of the time range is at the halfway point of the rainfall duration. The reason for this was not clearly discussed in Ben-Zvi's (1970) dissertation. However, this approach worked pretty well for the rainstorms of duration of 240 s as the hydrograph has already reached the equilibrium discharge after the time of the halfway point of the rainfall. But this approach didn't work very well for the rainstorms of duration of 120 s and 180 s, especially 120 s.

The question is whether the data points between $T/2$ and T are good enough to represent the equilibrium state for all of the plateau discharge data points. On the one hand, it is possible that the hydrographs didn't reach or were not even close to the equilibrium discharge at the time of the halfway point of the rainfall duration. It is evident that the discharge data points far from the

equilibrium discharge should not be considered in linear regression of equilibrium discharge or they will distort the result to some degree. On the other hand, it is also possible that some of the plateau discharge data points occur before half of the rainfall duration or after the rainfall duration, and neither is used to construct the straight line. It is obvious that all discharge data points near equilibrium should be considered as the equilibrium discharge and used in determination of the time of concentration.

Therefore, for all the WES tests having rainfall durations of 120, 180, and 240 s in experimental Phases 2 and 3, the discharge data points were taken to construct a straight line from the time period between $T/2$ and T of the rainfall duration. The resulting best fit straight line is named as best-fit line 1. A second straight line is constructed from more or less discharge data points when the first best-fit straight line is considered inappropriate. This procedure was done through visual inspection of the observed hydrographs on a case by case basis as described in the following subsection.

5.3.3 Applying Three Methods

Tests 603abc, 623, 799b, and 816 from experimental Phase 2 are taken as examples for application of the three methods previously discussed for the laboratory data and are compared to the result from Wong's equation. The characteristics of these experimental storms are listed in Table 5.4.

Table 5.4 Characteristics of the Selected WES Rainstorm Experiments

Box_2 Test #	S_c	S_o	T (s)	$I_{nominal}$ (in./hr)	$I_{computed}$ (in./hr)
603abc	1%	1%	180	15	11.1364
623	1%	1%	120	8	6.6439
799b	1%	0.5%	240	6	4.7183
816	1%	3%	240	6	4.4199

In the following tables, Ben-Zvi's method is denoted as Ben-Zvi, the modified Ben-Zvi's method denoted as Modified BZ, and Izzard's method is denoted as Izzard. Difference is expressed as

$$difference = \frac{T_e - t_p}{t_p} \times 100\% \tag{5.12}$$

where T_e is computed from Wong's (2001) equation, and t_p is the time of concentration determined by the selected method.

For Test 623, since the rainfall duration is 120 s, the best-fit straight line is determined for the hydrograph measured from the 1st through 2nd minute of the rainfall duration. For Tests 799b and 816, since the rainfall duration is 240 s, the best-fit straight line is determined for the hydrograph measured from the 2nd through 4th minute of the rainfall duration. For Test 603abc, since the rainfall duration is 180 s, the best-fit straight line is determined for the hydrograph measured from the 90th through 180th second of the rainfall duration.

The first best-fit line for Test 623 is shown in Figure 5.2. It is clear that this best-fit straight line includes several non-equilibrium flows and also misses several equilibrium flows, and is not a good representation of the equilibrium condition. Thus, a second best-fit line constructed from different data points was used in Ben-Zvi's method, as shown in Figure 5.3. The results for Test 623 are listed in Tables 5.5 and 5.6. It can be seen that, the results from the Ben-Zvi's method

improved for the second best-fit line, but the results remain far from good. A similar process was also done with other experiments with 120 s durations.

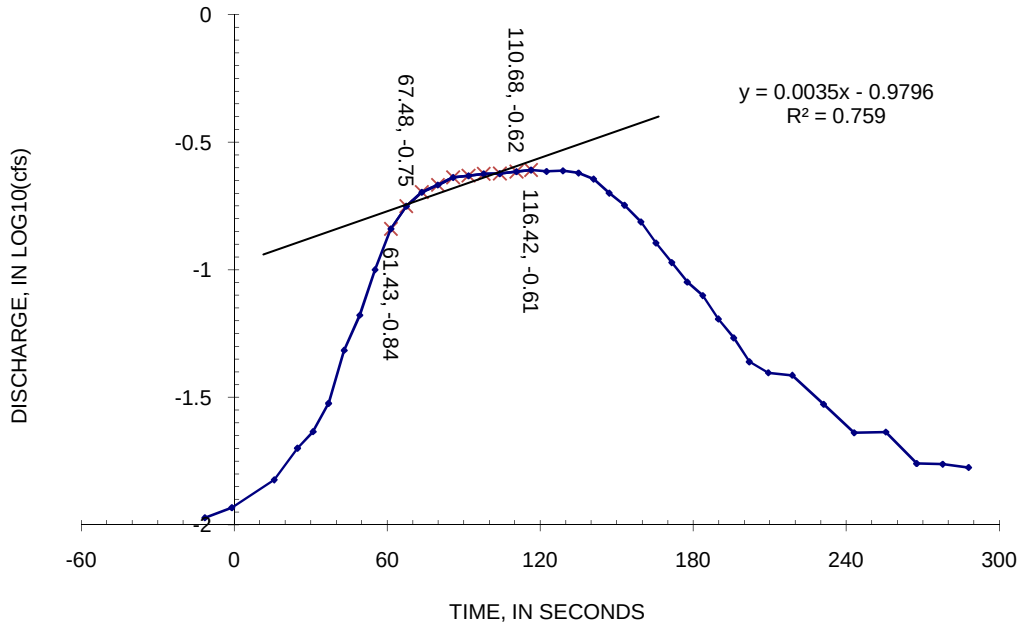

Figure 5.2 Best-Fit Line 1 for Determination of Time of Concentration for Test 623

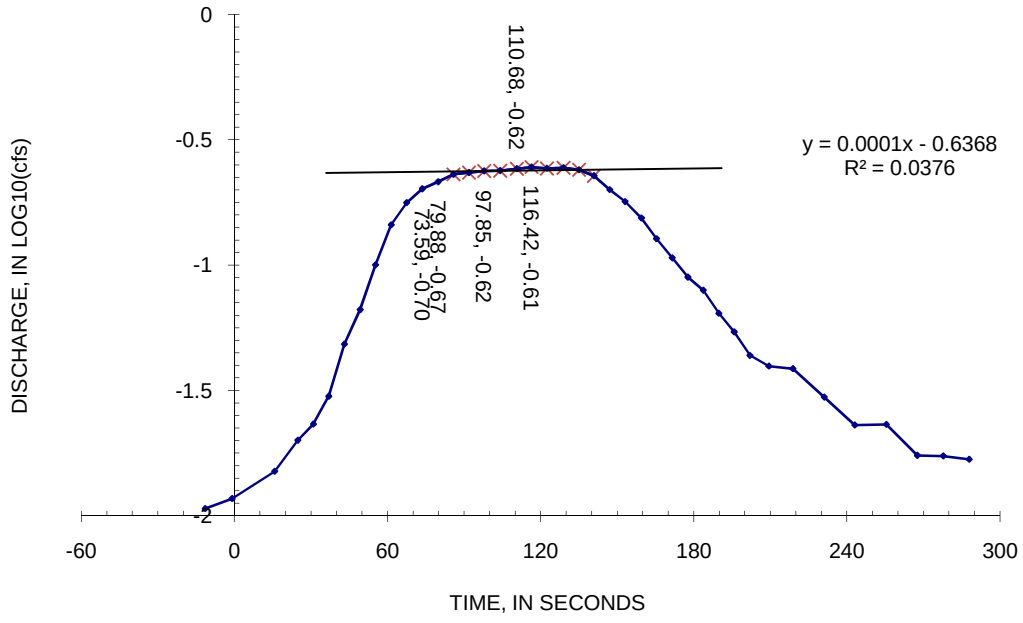

Figure 5.3 Best-Fit Line 2 for Determination of Time of Concentration for Test 623

Table 5.5 Comparison of the Time of Concentration Determined by Different Methods for Test 623

Test	Methods	T_e (s)	t_p (s)	Difference
623	Ben-Zvi	92.21	63.60	44.98%
	Modified BZ	92.21	81.46	13.20%
	Izzard	92.21	105.05	-12.22%

Table 5.6 Results from the Ben-Zvi's Method Using Best-Fit Line 2 for Test 623

Test	Methods	T_e (s)	t_p (s)	Difference
623	Ben-Zvi	92.21	77.67	18.72%

The first best-fit line applied to Test 816 is shown in Figure 5.4. It is constructed from a data series marked as ×, while four additional data points marked as plus at both ends of the data series are included to construct the second best-fit line. The results for Test 816 are listed in Tables 5.7 and 5.8. It can be seen that, the results from Ben-Zvi's method are almost the same, and equally good for the first and second best-fit lines. It is evident that the first best-fit straight line is still a good representation of the equilibrium condition, although it does not consider several equilibrium flows. The reason is that Test 816 produced a near perfect equilibrium state in its long rainfall duration of 240 s. Similar quality equilibrium states for other experiments were obtained with 240 s duration storms.

The second best-fit line for Test 799b is shown in Figure 5.5. The results for Test 799b are listed in Table 5.9. A second best-fit line was constructed when two erratic data points were excluded.

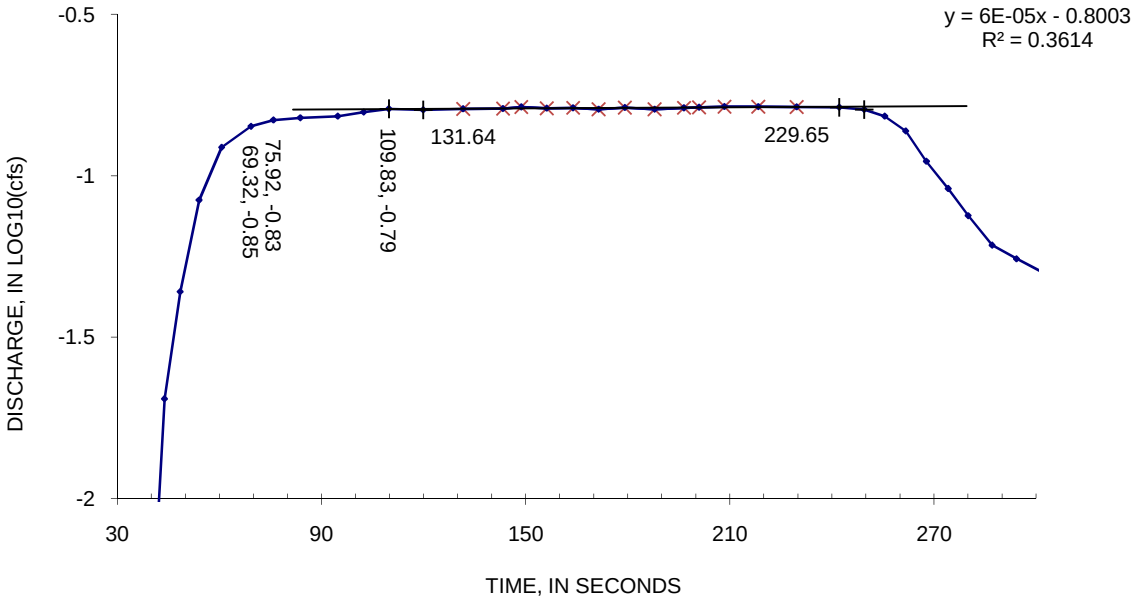

Figure 5.4 Best-Fit Line for Determination of Time of Concentration for Test 816

Table 5.7 Comparison of the Time of Concentration Determined by Different Methods for Test 816

Test	Methods	T_e (s)	t_p (s)	Difference
816	Ben-Zvi	77.84	69.61	11.83%
	Modified BZ	77.84	72.90	6.78%
	Izzard	77.84	105.22	-26.02%

Table 5.8 Results from the Ben-Zvi's Method Using Best-Fit Line 2 for Test 816

Test	Methods	T_e (s)	t_p (s)	Difference
816	Ben-Zvi	77.84	70.24	10.82%

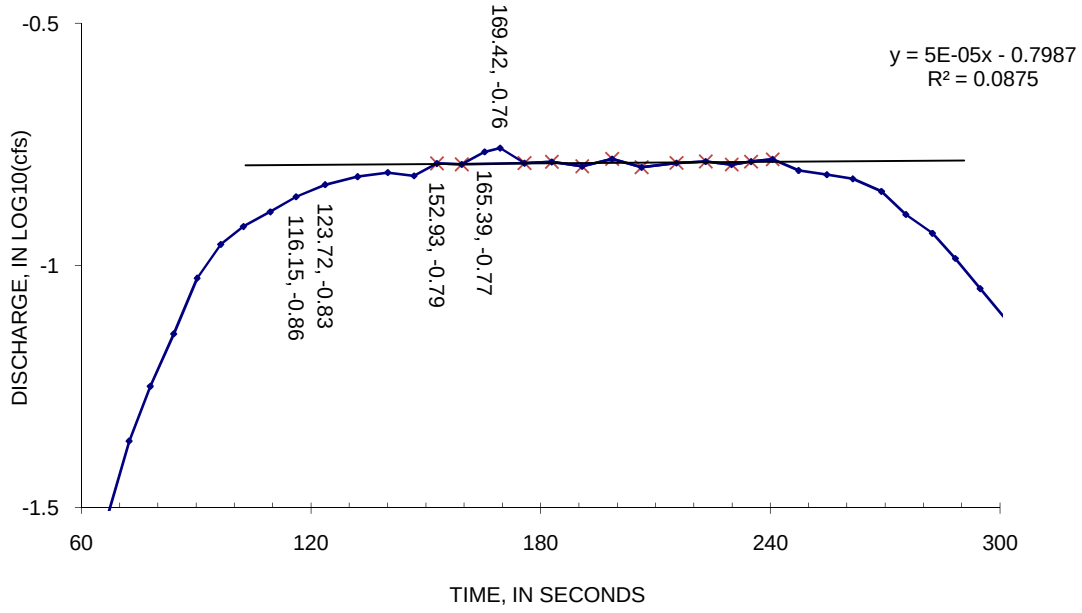

Figure 5.5 Best-Fit Line 2 for Determination of Time of Concentration for Test 799b

Table 5.9 Comparison of the Time of Concentration Determined by Different Methods for Test 799b

Test	Methods	T_e (s)	t_p (s)	Difference
799b	Ben-Zvi	125.15	120.92	3.50%
	Modified BZ	125.15	136.72	-8.46%
	Izzard	125.15	151.95	-17.63%

Tests 603a, 603b, and 603c are 3 different experiments under the same rainfall and geometric conditions, shown in Figure 5.6. The results for Test 603a, 603b, and 603c are listed in Tables 5.10, 5.11, and 5.12, respectively. There are large variations among the differences of the results for Tests 603a, b, and c using Ben-Zvi's method, although the experimental hydrographs are visually the same. However, the differences for Tests 603a, b, and c are pretty much the same when using the modified Ben-Zvi method and Izzard's method.

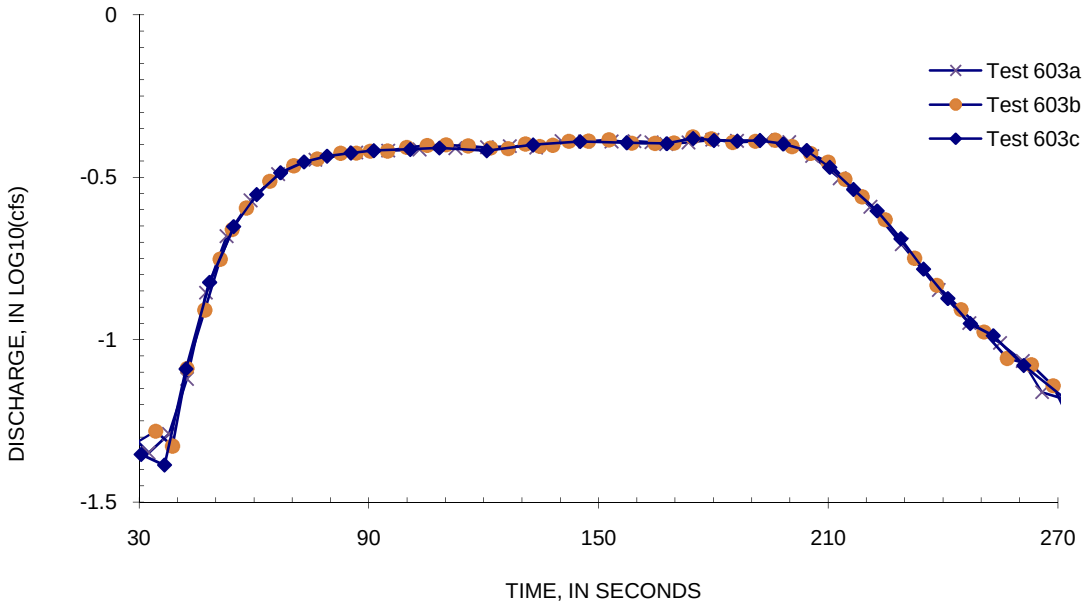

Figure 5.6 Measured Hydrographs for Tests 603a, b, and c

Table 5.10 Comparison of the Time of Concentration Determined by Different Methods for Test 603a

Test	Methods	T_e (s)	t_p (s)	Difference
603a	Ben-Zvi	77.83	70.13	10.98%
	Modified BZ	77.83	81.30	-4.28%
	Izzard	77.83	137.33	-43.33%

Table 5.11 Comparison of the Time of Concentration Determined by Different Methods for Test 603b

Test	Methods	T_e (s)	t_p (s)	Difference
603b	Ben-Zvi	77.33	66.28	16.67%
	Modified BZ	77.33	82.54	-6.31%
	Izzard	77.33	143.13	-45.97%

Table 5.12 Comparison of the Time of Concentration Determined by Different Methods for Test 603c

Test	Methods	T_e (s)	t_p (s)	Difference
603c	Ben-Zvi	77.59	64.14	20.96%
	Modified BZ	77.59	81.60	-4.92%
	Izzard	77.59	140.77	-44.88%

5.3.4 Discussion of Results

The comparison results of the time of concentration for all tests in experimental Phases 2 and 3 are listed in Tables 5.2 and 5.3.

For the 41 experiments in Phase 2, the computational results from Wong's (2001) equation vary in the range of 50 s ~ 130 s. The results of 24 experiments are between 50 s and 80 s, and 9 experiments are between 90 s and 110 s. The steep overland and channel slopes lead to the short time of concentration. The intensities don't play a big role in this case. The differences of the three methods compared to the computed time of concentration can be positive and negative. A positive value means that the computational result is greater than the experimental result, while the negative value means that the experimental result is greater than the computational result. According to Table 5.2, for Ben-Zvi's method, the differences of 29 experiments are positive; for the modified Ben-Zvi method, the differences of 12 experiments are positive; for Izzard's method, the differences of 2 experiments are positive. It can be seen that for Ben-Zvi's method and the modified Ben-Zvi method, when the time of concentration is relatively small, the difference is more likely to be positive, while the time of concentration is relatively high; the difference is more likely to be negative.

For the 41 experiments in Phase 2, the Ben-Zvi and modified Ben-Zvi methods give values closer to the computed values than Izzard's method. Izzard's method yields the largest difference from the computed values. The respective distributions of the differences of the three methods are shown in Figure 5.7. For Ben-Zvi's method, the differences are in the range of -26% to 41%, and the differences of 29 experiments are positive. The differences of 23 experiments are in the range of ±10%, and the differences of 31 experiments are in the range of ±15%. For the modified Ben-Zvi method, the differences are in the range of -54% to 18%, and the differences of 12 experiments are positive. The differences of 22 experiments are in the range of ±10%, and the differences of 26 experiments are in the range of ±15%. For Izzard's method, the differences are in the range of -75% to 10%, and the differences of 2 experiments are positive. The differences of 3 experiments are in the range of ±10%, and the differences of 5 experiments are in the range of ±15%.

For some experiments in Phase 2, the results of Ben-Zvi's Method are much better than those of the modified Ben-Zvi method, such as Tests 806, 815b, 817, 819a, 820, and 841a. However, for some experiments in Phase 2, the results of the modified Ben-Zvi method are much better than those of Ben-Zvi's Method, such as Tests 603abc. For 16 experiments in Phase 2, both methods have close and good results, with the differences in the range of ±10%, such as Tests 609, 611, 612, 634, 787b, 792ab, 793ab, 799ab, 833, 834, 843ab, and 841b. For the rest of the experiments, both methods have poor results, with the differences outside the range of ±15%, such as Tests 632, 803, 814, 831ab, and 832.

It can be seen that rainfall characteristics and watershed properties can affect the comparison results to some degree. For the experiments with $S_c = 1\%$ and $S_o = 0.5\%$, or $S_c = 0.5\%$ and $S_o = 1\%$ in Phase 2, both the Ben-Zvi and modified Ben-Zvi methods give very good results compared to the other experimental data obtained from the WES. This can be justified in that the experiments having mild overland and channel slopes, and especially with the long durations can produce much more stable plateaus during the equilibrium state in their hydrographs than were obtained for other experimental conditions. It is believed that experimental differences from the system instrumentation in such cases are minimal. The experimental hydrographs obtained are more reliable from this point of view. Therefore, the comparison of the time of concentration between the experimental data and computational results for this kind of experiment is much more likely to be trusted and accurate. Under this consideration, it is safe to say Wong's equation (5.12) can predict the time of concentration acceptably well for the simplified watershed with mild overland and channel slopes and long durations. In addition, Wong's equation tends to over-predict the time of concentration, since the differences mostly are positive. For the experiments with $S_c = 1\%$ and $S_o = 1\%$, when the rainfall durations are the longest, i.e. 240 s, the differences from both the Ben-Zvi and modified Ben-Zvi methods are smallest compared to the computational results. For the experiments with steeper channel and overland slopes, the times of concentrations are expected to be as short as 50 s, and the experimental results are sensitive to the system instrumental differences. Thus, the accuracy of the experiments is reduced.

It can be seen that it is not wise to apply Izzard's method in analyzing the experimental hydrographs. The criterion to choose the equilibrium state seems to be too strict when dealing

with the laboratory experimental data. This research indicates that it is not practicable to choose 97% as the defined percentage of the maximum as the equilibrium discharge. The experimental differences introduced by the discharge variations during the equilibrium state of the hydrographs may unduly affect the determination of the equilibrium discharge. The variations during the equilibrium state are mostly greater than 3%, and therefore, the time to reach a percentage of 97% is usually much greater than the time of concentration computed with Wong's equation, leading to the poor results obtained when comparing the Izzard's method to Wong's equation. However, the modified Ben-Zvi method seems reasonable. A percentage of 89% can be a generally agreeable percentage to evaluate the experimental data from the WES.

For 20 experiments in Phase 3, the results of the three methods are very poor. The respective distributions of the differences of the three methods are shown in Figure 5.7. For Ben-Zvi's method, the differences are in the range of -38% to 0%. The differences of 2 experiments are in the range of ±10%, and the differences of 4 experiments are in the range of ±15%. For the modified Ben-Zvi's method, the differences are in the range of -48% to -22%. No experiment has a difference in the range of ±15%. For Izzard's Method, the differences are in the range of -75% to -30%. No experiment has a difference in the range of ±15%.

The conclusions for the 41 experiments in Phase 2 cannot be drawn for the 20 experiments in Phase 3. The main reason could be that the data of the 20 experiments in Phase 3 were not accurate enough compared to the data of the 41 experiments in Phase 2. The Phase 3 data were collected when the electronic and mechanical components in the WES had deteriorated.

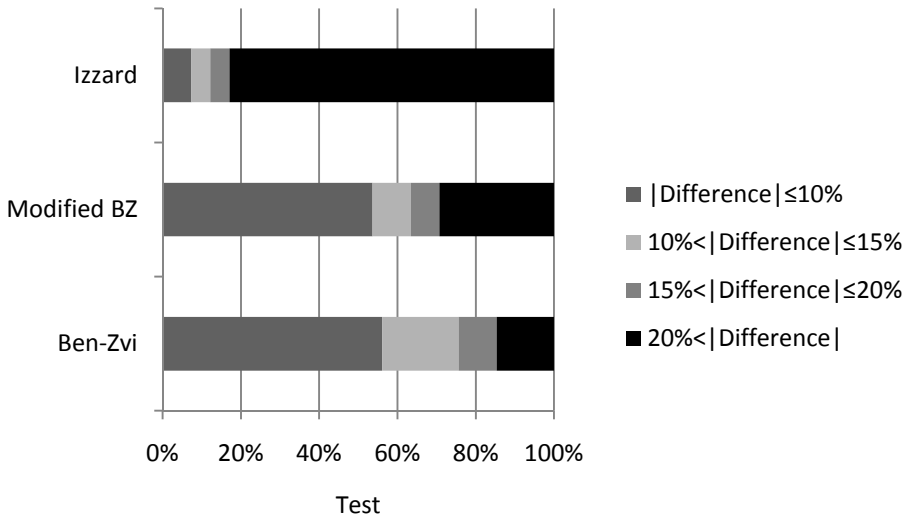

Figure 5.7 Distributions of Differences Between the of Three Different Methods and the Computed Value of the Time of Concentration for Tests in Phase 2

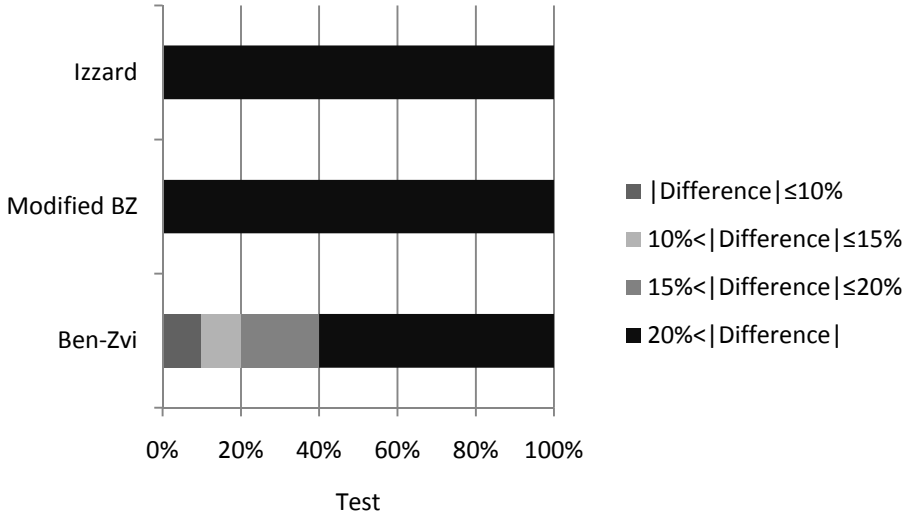

Figure 5.8 Distributions of Differences Between the of Three Different Methods and the Computed Value of the Time of Concentration for Tests in Phase 3

5.4 Effect of Rainfall Intensity on Manning's *n*

According to Wong's (2001) equation, the time of concentration, t_c, depends on the intensity of rainfall excess, i_e, the overland slope, S_o, the channel slope, S_c, and the surface roughness, n_o and n_c. In the previous section, the surface roughness of overland and channel flow is considered to be constant.

However, the rainfall intensity has been shown to have a substantial effect of flow roughness for the laminar and transitional flows in previous experimentation using the WES (Wenzel, 1970) and other experimental systems (Shen and Li, 1973). Wenzel (1970) conducted an experimental study with a laboratory flume to investigate the effect of raindrop impact on flow resistance for sheet flow. The most significant result was that for Reynolds numbers below approximately 2000, the rainfall intensity increases the resistance to flow, with a higher Darcy-Weisbach friction factor, f, values associated with higher intensities. For Reynolds numbers above approximately 2000, corresponding to the transition region between laminar and turbulent flow, the effect of rainfall intensity on the flow resistance decreases rapidly until it becomes insignificant. For Reynolds numbers below 1000, the experimental results found by (Wenzel, 1970) can be described mathematically by a straight line parallel to the theoretical $f = 24/N_R$ for laminar flow, i.e.

$$f = \frac{C}{N_R} \tag{5.13}$$

where C is a function of rainfall intensity with slope as a parameter, and N_R is Reynolds number. C increases with increasing rainfall intensity for a given slope. According to the graph plotted by Wenzel (1970), for the slope $S_0 = 0.01$ and raindrop spacing equal to 1 in., the values of C are

approximately 24, 50, 75, 85, and 95 for various rainfall intensities of 0, 1, 5, 10, and 15 in./hr, respectively, shown in Figure 5.9.

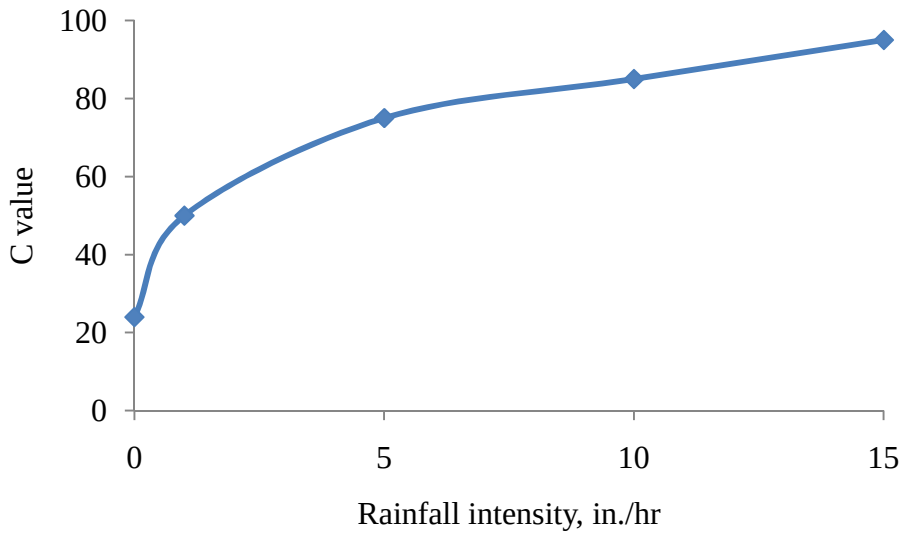

Figure 5.9 Relationship Between C Values and Rainfall Intensities

According to the Darcy-Weisbach and Manning's equations, the relation between Manning's n and the Darcy-Weisbach friction factor, f, is as follows

$$n = \frac{f^{1/2}}{8^{1/2}} \frac{R^{1/6}}{g^{1/2}} \tag{5.14}$$

It is obvious that when the friction factor f increases by 4 times due to the increasing rainfall intensities from zero to 15 in./hr, the roughness coefficient n will double, and the roughness coefficient n increases by 1.44 times when the friction factor f increases by 2.08 times due to the increasing rainfall intensities from zero to 5.8 in./hr.

5.4.1 Analysis of the Overall Manning's Roughness Coefficient Using Wong's Equation and the Experimental Data

By using Wong's equation, Manning's n values can be determined using the times of concentration obtained by the three methods from the stationary rainstorm hydrographs in experimental Phases 2 and 3. A FORTRAN program was written to calculate the Manning's n values for the 41 and 20 experiments in Phases 2 and 3, respectively. The Newton-Raphson method is applied in the algorithm to find the Manning's n values.

The calculated Manning's n values for experiments in Phases 2 and 3 are statistically analyzed via histogram analysis with EXCEL. The histograms of the calculated Manning's n corresponding to times of concentration determined with Ben-Zvi's, the modified Ben-Zvi, and Izzard's methods for experiments in Phase 2 are shown in Figures 5.16, 5.17, and 5.18, respectively. The histograms for experiments in Phase 3 are shown in Figures 5.19 to 5.21. The probability distribution of the Manning's n values can be determined and the effect of raindrops on resistance to flow can be evaluated.

For smooth metal flumes, it was reported by Franzini and Finnemore (1997) that Manning's roughness coefficient n ranges from 0.011 to 0.015. Henderson (1966) stated that Manning's roughness coefficient n for glass, plastic, and machined metal is 0.010. Posey (1949) reported that Manning's roughness coefficient n is 0.011 to 0.012 for smoothest clean wood, metal, or concrete surfaces without projections, and with straight alignment. Therefore, according to the information in the literature, the value of Manning's roughness coefficient n ranges from 0.010 to 0.015 for the smooth aluminum planes in the WES. According to the relationship between

rainfall intensity and flow resistance investigated by Wenzel (1970), the reasonable range for Manning's roughness coefficient n affected by the rainfall intensity under the experimental condition in Phases 2 and 3 is between 0.010 and 0.030.

According to Table 5.13 and Figure 5.10, the histogram shows that the highest number of the experiments having the calculated Manning's n between 0.012 and 0.013 corresponding to times of concentration determined with Ben-Zvi's method, and the number of the experiments having the calculated Manning's n between 0.013 and 0.014 is the second highest. Nearly all of the 41 values of Manning's n fall in the range of 0.010 to 0.030 obtained from the literature and adjusted for possible raindrop impact effects.

Table 5.13 Frequency of Manning's *n* corresponding to the times of concentration determined with Ben-Zvi's Method for 41 experiments in Phase 2

Interval	Number of experiments	Fraction of total experiments
~ 0.010	1	0.0244
0.010 ~ 0.011	4	0.0976
0.011 ~ 0.012	2	0.0488
0.012 ~ 0.013	12	0.2927
0.013 ~ 0.014	10	0.2439
0.014 ~ 0.015	0	0.0000
0.015 ~ 0.016	0	0.0000
0.016 ~ 0.017	4	0.0976
0.017 ~ 0.018	4	0.0976
0.018 ~ 0.019	2	0.0488
0.019 ~ 0.020	1	0.0244
0.020 ~	1	0.0244

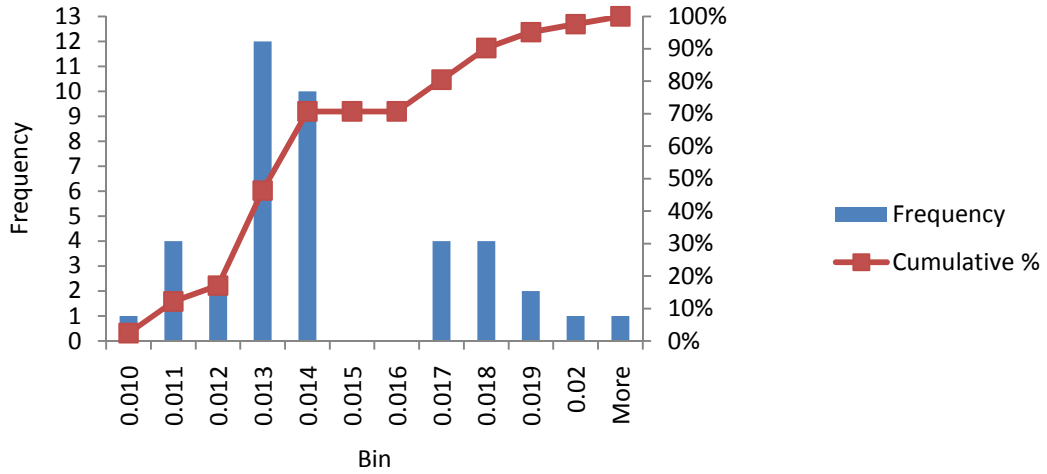

Figure 5.10 Histogram of Calculated Manning's *n* Corresponding to Times of Concentration Determined with Ben-Zvi's Method for 41 Experiments in Phase 2

According to Table 5.14 and Figure 5.11, the histogram shows that the highest number of the experiments having the calculated Manning's *n* between 0.013 and 0.014 corresponding to times of concentration determined with the modified Ben-Zvi method, and the number of the

experiments having the calculated Manning's n between 0.015 and 0.016 is the second highest. All forty one experiments have the calculated Manning's n between 0.010 and 0.030.

Table 5.14 Frequency of Manning's n corresponding to the times of concentration determined with the Modified Ben-Zvi Method for 41 experiments in Phase 2

Interval	Number of experiments	Fraction of total experiments
0.010 ~ 0.011	2	0.0488
0.011 ~ 0.012	2	0.0976
0.012 ~ 0.013	2	0.1463
0.013 ~ 0.014	7	0.3171
0.014 ~ 0.015	5	0.4390
0.015 ~ 0.016	6	0.5854
0.016 ~ 0.017	2	0.6341
0.017 ~ 0.018	3	0.7073
0.018 ~ 0.019	0	0.7073
0.019 ~ 0.020	1	0.7317
0.020 ~ 0.021	2	0.7805
0.021 ~ 0.022	4	0.8780
0.022 ~ 0.023	1	0.9024
0.023 ~ 0.024	0	0.9024
0.024 ~ 0.025	0	0.9024
0.025 ~ 0.026	0	0.9024
0.026 ~ 0.027	1	0.9268
0.027 ~ 0.028	1	0.9512
0.028 ~ 0.029	0	0.9512
0.029 ~ 0.030	1	0.9756

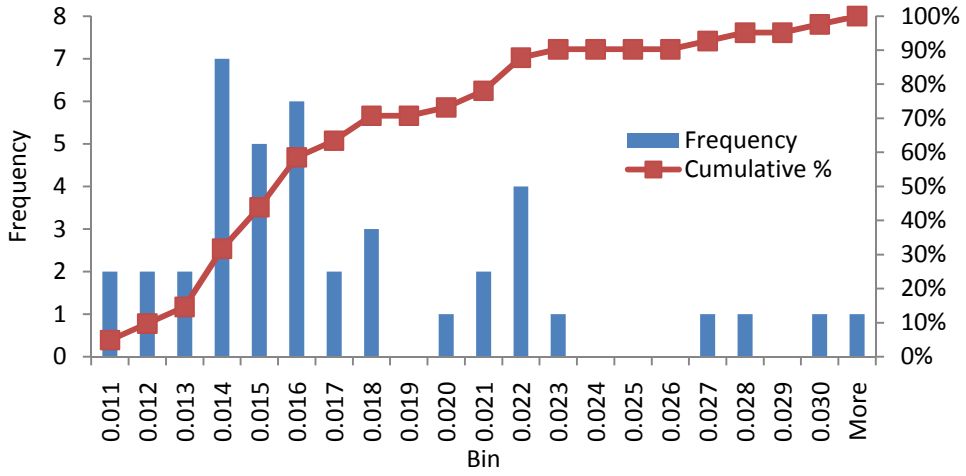

Figure 5.11 Histogram of Calculated Manning's *n* Corresponding to Times of Concentration Determined with the Modified Ben-Zvi Method for 41 Experiments in Phase

According to Table 5.15 and Figure 5.12, the histogram shows that the highest number of the experiments having the calculated Manning's n between 0.030 and 0.040 corresponding to times of concentration determined with Izzard's method, and the number of the experiments having the calculated Manning's n between 0.040 and 0.050 is the second highest. Seven experiments have the calculated Manning's n between 0.010 and 0.030.

Table 5.15 Frequency of Manning's *n* corresponding to the times of concentration determined with Izzard's Method for 41 experiments in Phase 2

Interval	Number of experiments	Fraction of total experiments
0.020 ~ 0.030	7	0.1707
0.030 ~ 0.040	14	0.5122
0.040 ~ 0.050	8	0.7073
0.050 ~ 0.060	6	0.8537
0.060 ~ 0.070	3	0.9268
0.070 ~ 0.080	1	0.9512
0.080 ~ 0.090	1	0.9756
0.090 ~	0	0.9756

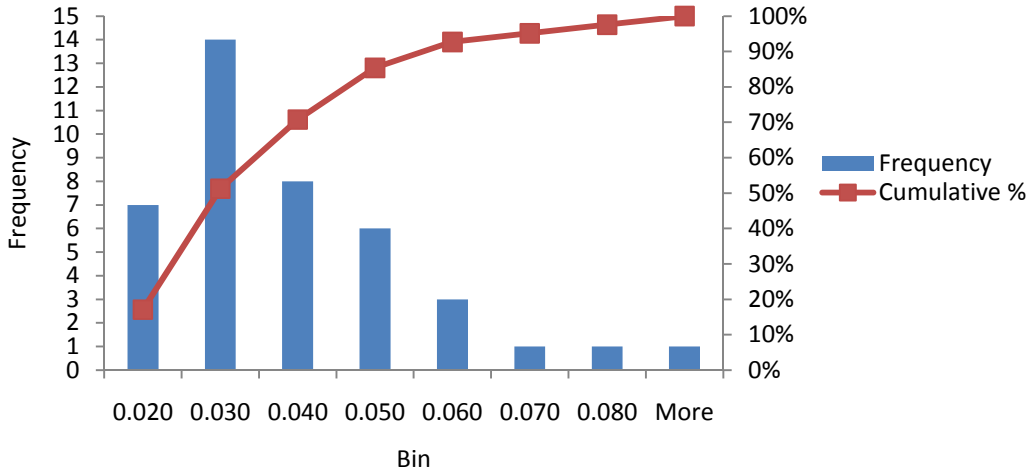

Figure 5.12 Histogram of Calculated Manning's *n* Corresponding to Times of Concentration Determined with Izzard's Method for 41 Experiments in Phase 2

According to Table 5.16 and Figure 5.13, the histogram shows the highest number of the experiments having the calculated Manning's n between 0.018 and 0.019 and between 0.027 and 0.028 corresponding to times of concentration determined with Ben-Zvi's method. According to Table 5.17 and Figure 5.14, the histogram shows the highest number of the experiments having the calculated Manning's n between 0.030 and 0.031 corresponding to times of concentration determined with the modified Ben-Zvi method. According to Table 5.18 and Figure 5.15, the histogram shows that the highest number of the experiments having the calculated Manning's n greater than 0.045 corresponding to times of concentration determined with Izzard's method.

Table 5.16 Frequency of Manning's *n* corresponding to times of concentration determined with Ben-Zvi's Method for 20 experiments in Phase 3

Interval	Number of experiments	Fraction of total experiments
0.014 ~ 0.015	1	0.0500
0.015 ~ 0.016	1	0.0500
0.016 ~ 0.017	1	0.0500
0.017 ~ 0.018	1	0.0500
0.018 ~ 0.019	3	0.1500
0.019 ~ 0.020	1	0.0500
0.020 ~ 0.021	1	0.0500
0.021 ~ 0.022	1	0.0500
0.022 ~ 0.023	1	0.0500
0.023 ~ 0.024	1	0.0500
0.024 ~ 0.025	1	0.0500
0.025 ~ 0.026	1	0.0500
0.026 ~ 0.027	2	0.1000
0.027 ~ 0.028	3	0.1500
0.028 ~ 0.029	1	0.0500

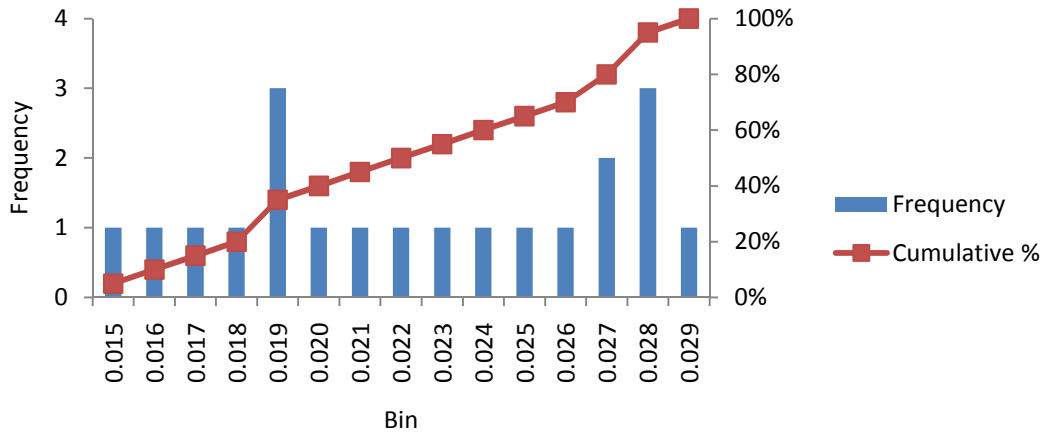

Figure 5.13 Histogram of Calculated Manning's *n* Corresponding to Times of Concentration Determined with Ben-Zvi's Method for 41 Experiments in Phase 3

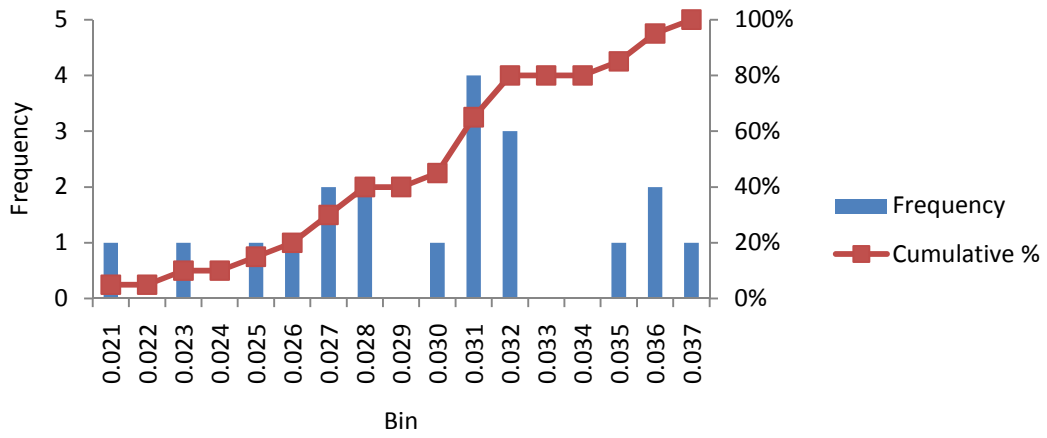

Figure 5.14 Histogram of Calculated Manning's *n* Corresponding to Times of Concentration Determined with Modified Ben-Zvi Method for 41 Experiments in Phase 3

Table 5.17 Frequency of Manning's *n* corresponding to times of concentration determined with the Modified Ben-Zvi Method for 20 experiments in Phase 3

Interval	Number of experiments	Fraction of total experiments
0.020 ~ 0.021	1	0.0500
0.021 ~ 0.022	0	0.0000
0.022 ~ 0.023	1	0.0500
0.023 ~ 0.024	0	0.0000
0.024 ~ 0.025	1	0.0500
0.025 ~ 0.026	1	0.0500
0.026 ~ 0.027	2	0.1000
0.027 ~ 0.028	2	0.1000
0.028 ~ 0.029	0	0.0000
0.029 ~ 0.030	1	0.0500
0.030 ~ 0.031	4	0.2000
0.031 ~ 0.032	3	0.1500
0.032 ~ 0.033	0	0.0000
0.033 ~ 0.034	0	0.0000
0.034 ~ 0.035	1	0.0500
0.035 ~ 0.036	2	0.1000
0.036 ~ 0.037	1	0.0500

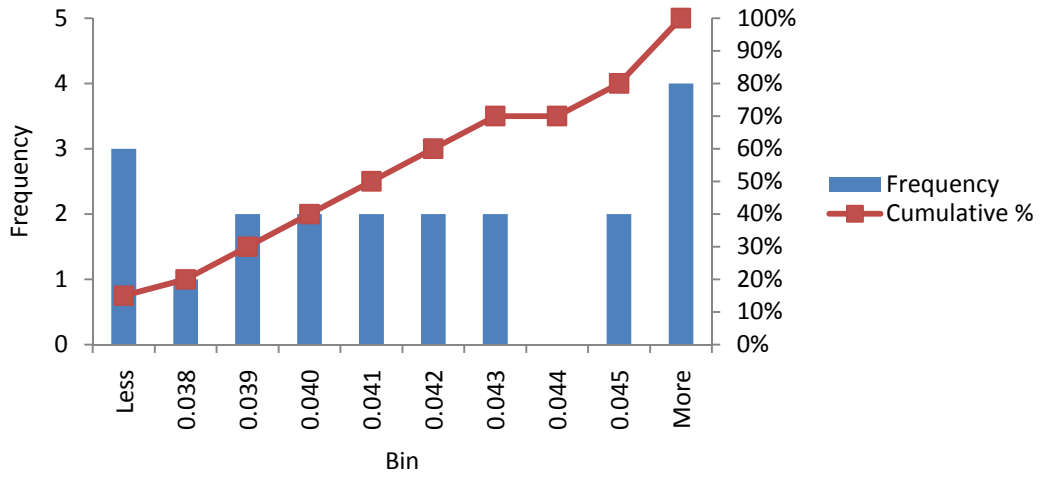

Figure 5.15 Histogram of Calculated Manning's *n* Corresponding to Times of Concentration Determined with Izzard's Method for 41 Experiments in Phase 3

Table 5.18 Frequency of Manning's *n* corresponding to times of concentration determined with Izzard's Method for 20 experiments in Phase 3

Interval	Number of experiments	Fraction of total experiments
~ 0.037	3	0.1500
0.037 ~ 0.038	1	0.0500
0.038 ~ 0.039	2	0.1000
0.039 ~ 0.040	2	0.1000
0.040 ~ 0.041	2	0.1000
0.041 ~ 0.042	2	0.1000
0.042 ~ 0.043	2	0.1000
0.043 ~ 0.044	0	0.0000
0.044 ~ 0.045	2	0.1000
0.045 ~	4	0.2000

The mean value, coefficient of variation, skewness, and kurtosis are the main descriptors of a range of possible values of a random variable to indicate the properties of the random variable. The mean value is the average value of a range of possible values of Manning's n. The coefficient of variation is an appropriate measure of the degree of dispersion relative to the central value. The skewness is a measure of the degree of the symmetry or asymmetry around its

mean value. The kurtosis is a measure of the relative peakedness or flatness compared to the normal distribution. Therefore, the mean value, coefficient of variation (COV), skewness, and kurtosis of the calculated Manning's n values for the experiments in Phases 2 and 3 are naturally of interest. These four main descriptors of the calculated Manning's n of the experiments in Phases 2 and 3 are listed in Tables 5.19 and 5.20.

Table 5.19 Four Main Descriptors of the Calculated Manning's n of the 41 Experiments in Phase 2

Phase 2	Mean value	C.O.V.	Skewness	Kurtosis
Ben-Zvi's method	0.0139	0.2055	0.832	0.539
Modified Ben-Zvi method	0.0174	0.3519	2.429	8.196
Izzard's method	0.0342	0.5523	1.8608	5.0030

Table 5.20 Four Main Descriptors of the Calculated Manning's n of the 20 Experiments in Phase 3

Phase 3	Mean value	C.O.V.	Skewness	Kurtosis
Ben-Zvi's method	0.0221	0.2052	-0.107	-1.281
Modified Ben-Zvi method	0.0294	0.1475	-0.213	-0.201
Izzard's method	0.0443	0.2911	1.728	3.319

For Manning's n of the 41 experiments in Phase 2 calculated from the times of concentration determined with Ben-Zvi's method, the mean value, coefficient of variation, skewness, and kurtosis are 0.0139, 0.2055, 0.832, and 0.539. The mean value is 0.0139, which is almost the same as the fixed value of 0.014. The coefficient of variation means that the degree of dispersion is only 20% of the mean value, which is a relatively small dispersion. The positive skewness means that the values of Manning's n above the mean value 0.0139 are more widely dispersed than the values below the mean value 0.0139, with an asymmetric tail extending toward larger values. Positive kurtosis indicates a sharper peak around the mean and fatter tails than the normal

distribution. These results mean that there is a lower probability than a normally distributed variable of values near the mean, and a higher probability than a normally distributed variable of extreme values.

According to Table 5.19, the mean value of the Manning's n calculated from the times of concentration determined with the modified Ben-Zvi method is higher than that calculated from Ben-Zvi's method. The COV for the modified Ben-Zvi method also is higher than that from Ben-Zvi's Method. The mean value and COV for Izzard's method is the highest.

For Manning's n of the 20 experiments in Phase 3 calculated from the times of concentration determined with Ben-Zvi's method, the mean value, coefficient of variation, skewness, and kurtosis are 0.0221, 0.2052, -0.107, and -1.281. The coefficient of variation indicates that the degree of dispersion is 21% of the mean value, a relatively small dispersion. The negative skewness means that the values of Manning's n less the mean value of 0.0221 are more widely dispersed than the dispersion of the values above the mean value of 0.0221, and an asymmetric tail extending toward more negative values can be observed. Negative kurtosis indicates a lower peak around the mean and thinner tails than the normal distribution. These results mean that there is a higher probability than a normally distributed variable of values near the mean, and a lower probability than a normally distributed variable of extreme values.

According to Table 5.20, the mean value of the Manning's n calculated from the times of concentration determined with the modified Ben-Zvi method is higher than that calculated from

Ben-Zvi's method, while the COV for the modified Ben-Zvi method is smaller than that calculated from Ben-Zvi's method. The mean value and COV for Izzard's method is the highest.

5.4.2 Analysis of the Relationship Between Rainfall Intensities and Calculated Manning's n

The relationships between rainfall intensities and calculated Manning's n with the three methods for the 41 experiments in Phase 2 are shown in Figures 5.9 to 5.11. The rainfall intensities in Phase 2 are in the range of 4.5 to 11.1 in./hr, and in between the typical values are 7.0 and 8.3 in./hr. According to Figure 5.9, the values of C are approximately 59, 69, 79, and 86 for various rainfall intensities of 4.5, 7.0, 8.3, 11.1 in./hr, respectively. The C values increase by 3.58 times compared to the value for the zero rainfall intensity, and the Manning's n values increase by 1.89 times.

According to Figure 5.16, Manning's n values increase by 1.05 times from 0.0134 to 0.0141. According to Figure 5.17, Manning's n values increase by 1.27 times from 0.0148 to 0.0188. According to Figure 5.18, Manning's n values increase by 1.39 times from 0.0148 to 0.0188. The calculated Manning's n values with the modified Ben-Zvi method and Izzard's method are higher than the fixed Manning's n 0.014, and the fixed value falls in the range of the calculated values with Ben-Zvi's method. For the three methods, the numbers of times of increase of calculated Manning's n values with the increasing rainfall intensities are around the value of 1.21. The degree of increase of calculated Manning's n values with modified Ben-Zvi method is smaller than the value obtained from Wenzel (1970).

The relationships between rainfall intensities and calculated Manning's n with the three methods for the 20 experiments in Phase 3 are shown in Figures 5.12 to 5.14. The rainfall intensities in Phase 3 are in the range of 4.2 to 10.7 in./hr, and in between the typical values are 6.8 and 8.0 in./hr. According to **Error! Reference source not found.Error! Reference source not found.**, the values of C are approximately 57, 63, 78, and 85 for various rainfall intensities of 4.2, 6.8, 8.0, 10.7 in./hr, respectively. The C values increase by 3.52 times compared to the value for the zero rainfall intensity, and the Manning's n values increase by 1.88 times. According to Figure 5.19, Manning's n values increase by 0.96 times from 0.0226 to 0.0217. According to Figure 5.20, Manning's n values increase by 1.04 times from 0.0288 to 0.0299. According to Figure 5.21, Manning's n values increase by 1.00 times from 0.0443 to 0.0443. The calculated Manning's n values with the three methods are higher than the fixed Manning's n 0.014. For the three methods, the numbers of times of increase of calculated Manning's n values with the increasing rainfall intensities are around 1.00, less than the value of 1.89. It means that the flow resistance estimated by Manning's n doesn't vary with the rainfall intensity. Therefore, the correlation between the rainfall intensity and flow resistance found by Wenzel (1970) isn't verified here.

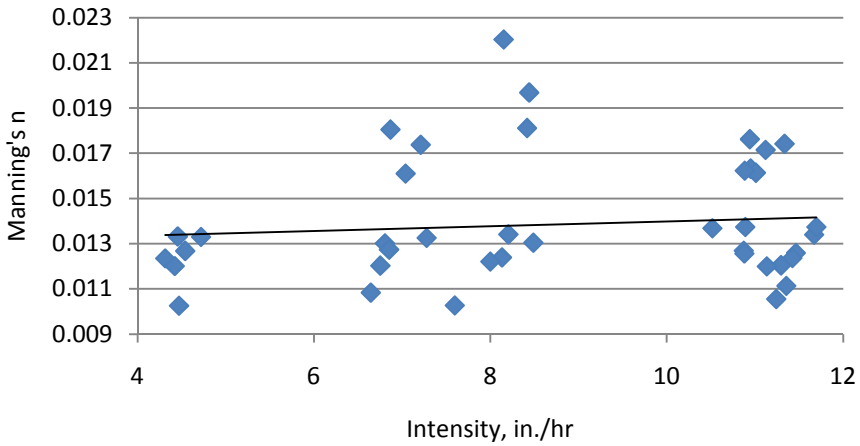

Figure 5.16 Relationship Between Rainfall Intensities and Calculated Manning's *n* for Ben-Zvi's Method for 41 Experiments in Phase 2

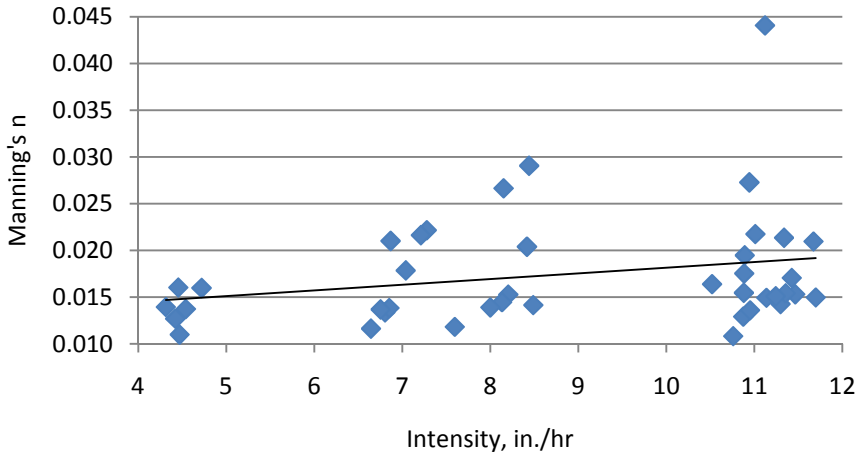

Figure 5.17 Relationship Between Rainfall Intensities and Calculated Manning's *n* for the Modified Ben-Zvi Method for 41 Experiments in Phase 2

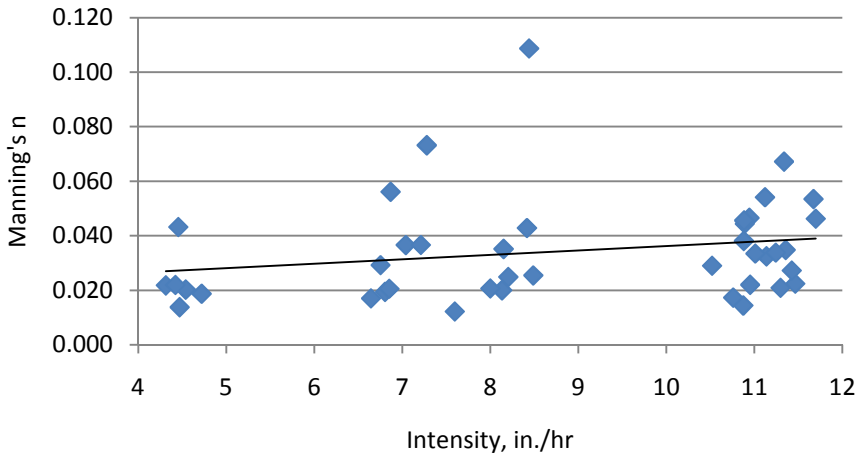

Figure 5.18 Relationship Between Rainfall Intensities and Calculated Manning's *n* for Izzard's Method for 41 Experiments in Phase 2

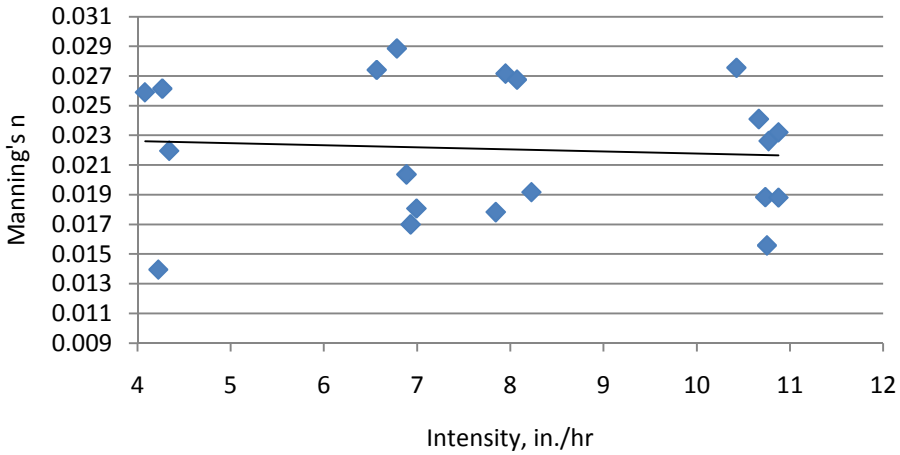

Figure 5.19 Relationship Between Rainfall Intensities and Calculated Manning's *n* for Ben-Zvi's Method for 20 Experiments in Phase 3

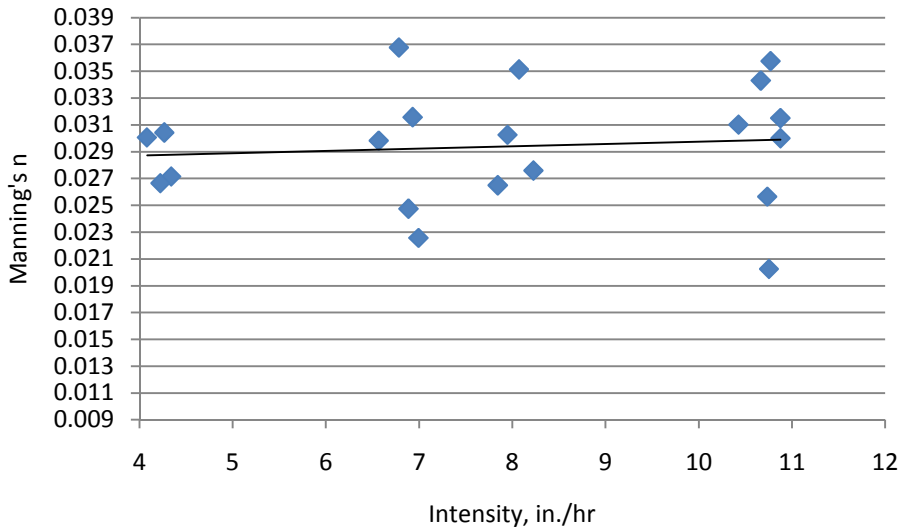

Figure 5.20 Relationship Between Rainfall Intensities and Calculated Manning's *n* for the Modified Ben-Zvi Method for 20 Experiments in Phase 3

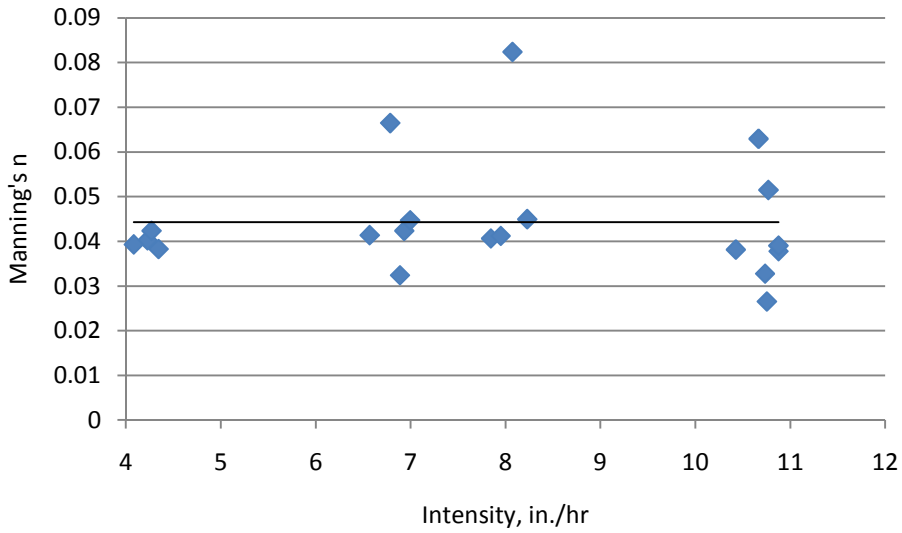

Figure 5.21 Relationship Between Rainfall Intensities and Calculated Manning's *n* for Izzard's Method for 20 Experiments in Phase 3

5.5 Conclusion on Measured t_p and Wong's Equation

Ben-Zvi's method, the modified Ben-Zvi method, and Izzard's method yield different values of times of concentration from the experimental hydrographs. Ben-Zvi's method utilizes a set of data points in the hydrograph, and the modified Ben-Zvi's method and Izzard's method only use a single data point, i.e. the peak flow point. Ben-Zvi's method and Wong's equation have reasonable agreement in the estimated time of concentration for Phase 2. Wong's equation, Ben-Zvi's method, and the modified Ben-Zvi method yield reasonable agreement in the time of concentration for the hydrographs from the experiments having mild overland and channel slopes, and especially with the long durations. Izzard's method is not suitable for obtaining the time of concentration from the experimental hydrographs. The criterion of 97 percent of the peak discharge is too strict for choosing the equilibrium state from the experimental data. The criterion of 89 percent in the modified Ben-Zvi method is acceptable to evaluate the experimental data from the WES.

The fixed value of 0.014 of Manning's n used in the models is reasonable considering the effect of rainfall intensity on the roughness. The effect of raindrop impact on Manning's n is not strongly demonstrated by the analysis. The relationship between the rainfall intensities and the flow resistance proposed by Wenzel (1970) cannot be verified.

CHAPTER 6 CONCLUSIONS

Based on the results of this dissertation, the following conclusions can be drawn:

- Downstream moving storms with storm length less than watershed length ($L_s/L_c < 1$) do not magnify the peak discharges as much as indicated by the kinematic-wave model. The kinematic-wave model overstates the increase in the peak flows resulting from downstream moving storms with $L_s/L_c < 1$. Downstream moving storms with $L_s/L_c < 1$ increase the peak discharges to a limited extent compared to stationary storms. The plot between the dimensionless peak discharge and the dimensionless storm velocity clearly shows the discrepancy between the simulation results of the kinematic-wave model and the experimental data of the downstream moving storms with various rainfall intensities obtained from the Watershed Experimentation System (WES).

- For downstream moving storms with $L_s/L_c < 1$, the maximum peak discharge occurs when the dimensionless storm velocity is approximately 0.1 ~ 0.2, which is much smaller compared to the value, i.e., 0.5 ~ 0.6 obtained from the kinematic-wave model results. For downstream moving storms with $L_s/L_c < 1$, the equilibrium discharge cannot be attained, and the maximum peak discharge is portion of the equilibrium discharge. This conclusion is demonstrated by the experimental data of the downstream moving storms with various rainfall intensities obtained from the WES.

- For downstream moving storms with $L_s/L_c \geq 1$, the equilibrium discharge can be attained, and the maximum peak discharge is equal to the equilibrium discharge. However, the range of the velocities of the moving storms attaining the equilibrium discharge for the WES experiments is quite narrower than the simulated results of the kinematic-wave model.

- The kinematic-wave model cannot deal with the backwater effects in the V-shaped watershed in the WES. The channel in the V-shaped watershed does not have enough capacity to deliver the incoming high overland flows to the outlet for the downstream moving storms where the overland flows are magnified in the downstream direction by the storm movement. However, the kinematic-wave model simulates the upstream moving and stationary storms pretty well because they do not magnify overland flows in the downstream direction.

- In impervious urban watersheds, the interacting backwater effects among the channel reaches and incoming lateral flows play a significant role in the process of flood propagation. Hence, the kinematic-wave model tends to overestimate the peak flow in the real world. From the point view of regulatory agencies, the overestimation of the peak flow using the kinematic-wave model is considered an acceptable safety factor in the hydrologic design.

-

- The previous studies that indicated downstream storm movement magnified peak discharges questioned the assumption of stationary storms made in standard hydrologic design. However, the findings from the WES data indicate that the magnification of peak discharge relative to the peak discharge from stationary storms resulting from downstream moving storms is not significant. Further, if the channel capacity in the simple experimental watershed in the WES was inadequate to deliver the increased lateral inflows to the watershed outlet, it is reasonable to assume that the capacity of real streams to transport increased lateral inflows due to downstream storm movement would be similarly limited. Thus, the assumption of stationary storms made in standard hydrologic design seems reasonable and adequate on the basis of the experiments and computations evaluated in this dissertation.

- The dynamic-wave model can incorporate the backwater effects in the V-shaped watershed in the WES. The dynamic-wave model preserves the effects of backwater from downstream by retaining the pressure term which relates the upstream depth to the downstream depth. Hence, the dynamic-wave model simulates the downstream moving storms pretty well, and equally well as for the upstream moving storms.

- Ben-Zvi's method, the modified Ben-Zvi method, and Izzard's method yield different values of the time of concentration from the experimental hydrographs. Ben-Zvi's method utilizes a set of data points in the hydrograph, and the modified Ben-Zvi's method and Izzard's method only use a single data point, i.e. the peak flow point.

- Ben-Zvi's method and Wong's equation have reasonable agreement in the estimated time of concentration. Wong's equation, Ben-Zvi's method, and the modified Ben-Zvi method yield reasonable agreement in the time of concentration for the hydrographs from the experiments having mild overland and channel slopes, and especially with the long durations. Izzard's method cannot reliably be applied to obtain the time of concentration from the experimental hydrographs. The criterion of 97 percent of the peak discharge is too strict for determining the equilibrium state from the experimental data. The modified Ben-Zvi's method with the criterion of 89 percent of the peak discharge can be reasonably applied to evaluate the experimental data from the WES.

- The fixed value of 0.014 for Manning's n used in the kinematic-wave model is reasonable considering the effect of rainfall intensity on the flow resistance. The effects of raindrop impact on the roughness in the laboratory experiments on the WES is similar to that in real watersheds, since both have similar raindrop sizes, terminal velocities and sheet flows. The effect of raindrop impact on Manning's n is not strongly demonstrated by the analysis. The relationship between the rainfall intensities and the flow resistance proposed by Wenzel (1970) cannot be verified.

- Limitations of experimental data relative to the real world include the much smaller roughness coefficient of the basin surface, a small and simple geometric watershed without any infiltration, and very short rainfall duration.

CHAPTER 7 RECOMMENDATIONS FOR FUTURE RESEARCH

Recommendations for future research include:

1) The dynamic-wave model with a fixed Manning's roughness coefficient can be studied in comparison with the experimental data and the kinematic-wave model.
2) In addition to the dynamic-wave and kinematic-wave models, the noninertia model also can be studied in comparison with the experimental data and the kinematic-wave and dynamic-wave models.
3) The backwater effect can be investigated when looking at the calculated values for each term in the dynamic-wave equation during the hydrograph calculation process.
4) Overland flow can be modeled two-dimensionally and the backwater effects also can be studied two-dimensionally.
5) The raindrop effect on the roughness can be studied in detail when looking at the Reynolds number during the flow process of the experiments.

REFERENCES

Amorocho, J. and Orlob G. T., 1961. Nonlinear analysis of hydrologic systems, University of California, Davis, *Water Resources Center Contribution*, **40**, 74-77.

Austin, P.M. and Houze, R.A., 1972. Analysis of the structure of precipitation patterns in New England. Journal of Applied Meteorology, **11**, 926-935.

Ben-Zvi, A., 1970. *On the Relationship Between Rainfall and Surface Runoff on Laboratory Watersheds*. Ph.D. Dissertation, Department of Civil Engineering, University of Illinois at Urbana-Chanmpaign.

Beran, M., 1999. Hydrograph prediction - How much skill? *Hydrology and Earth System Sciences*, **3**(2), 305-307.

Black, P.E., 1972. Hydrograph responses to geomorphic model watershed characteristics and precipitation variables. *Journal of Hydrology*, **17**, 309-329.

Chen, C.L., and Chow V.T., 1968. Hydrodynamics of Mathematically Simulated Surface Runoff. Civil Engineering Studies, Hydraulic Engineering Series No. 18, Department of Civil Engineering, Univeristy of Illinois at Urbana-Champaign.

Chow, V.T., ed., 1964. *Handbook of Applied Hydrology*, McGraw-Hill Book Company, New York.

Chow, V.T. and Yen, B.C., 1973. *Hydrodynamics of Watershed Flow*. Final Progress Report, National Science Foundation Grant GK-11292, Department of Civil Engineering, University of Illinois at Urbana-Champaign, 120 p.

Chow, V.T. and Yen, B.C., 1974. *A Laboratory Watershed Experimentation System*. Hydraulic Engineering Series Report No. 27, Department of Civil Engineering, University of Illinois at Urbana-Chanmpaign, 196 p.

Chow, V.T., and Ben-Zvi, A., 1973. Hydrodynamic modeling of two-dimensional watershed flow. *Journal of the Hydraulics Division*, ASCE, **99**(HY11), 2023-2040

Chow, V.T., Maidment D.R., and Mays L.W., 1988. *Applied Hydrology*. McGraw-Hill: New York.

Cunge, J., Holly, F.M., and Verwey, A., 1980. *Practical Aspects of Computational River Hydraulics*, Pitman, London.

Eagleson, P.S., 1970. *Dynamic Hydrology*, McGraw-Hill Book Co., New York.

Flegate, D.G. and Read, D. G., 1975. Correlation analysis of the cellular structure of storms observed by raingauges. Journal of Hydrology, **24**(3-4), 191-200.

Foroud, N., Broughton, R.S., and Austin, G.L., 1984. The effects of a moving rainstoms on direct runoff properties. *Water Resources Bulletin*, **20**, 87-91.

Franzini, J.B. and Finnemore, E.J., 1997. *Fluid Mechanics with Engineering Applications*, 9th ed. McGraw-Hill Book Company, New York.

Fread, D.L., 1978. NWS operational dynamic wave model. *Proceedings, ASCE's 26th Annual Hydraulics Divisions Conference on Verification of Mathematical and Physical Models*, College Park, Maryland, 45-46.

Fread, D.L., 1980. *Capabilities of NWS model to forecast flash floods caused by dam failures*. *Proceedings, 2nd Conference on Flash floods*, Amercian Meterorlogical Society, Altanta, Geogia, 171-178.

Fread, D.L., 1984. Flood routing. in *Hydrological Forecasting*, Anderson, M.G. and Burt, T.P., eds., Wiley, New York.

Hall, M.J., 2001. How well does your model fit the data? *Journal of Hydroinformatics*, **3**(1), 49-55.

Harbaugh, T.E., 1966. *Time Distribution of Runoff from Watershed*. Ph.D. Thesis, Department of Civil Engineering, University of Illinois at Urbana-Champaign.

Henderson, F. M. & Wooding, R. A. (1964) Overland flow and groundwater flow from a steady rainfall of finite duration. Journal of Geophysical Research. **69**(8), 1531-1540.

Henderson, F.M., 1966. Open Channel Flow. Machmillan Publishing Co., Inc. and Collier Macmillan Publishers.

Hindi, W. N. A. and Kelway, P. S., 1977. Determination of storm velocities as an aid to the quality control of recording rainguage data. *Journal of Hydrology*, **32**, 115-137.

Hobbs, P. V. and Locatelli, J. D.,1978. Rainbands, precipitation cores and generating cells in a cyclonic storm. Journal of the Atmospheric Sciences, **35**, 230-241.

Hsie, C.H. and Chow, V.T, 1974. *The Evaluation of a Hydrodynamic Watershed Model (IHW Model IV).* Hydraulic Engineering Series No. 28. University of Illinois at Urbana-Champaign.

Isaacson, E., Stoker, J.J., and Troesch, A., 1954. *Numerical Solution of Flood Prediction and River Regulation Problems*. Report II, IMM-NYU-235. Institute of Mathematical Sciences, New York University, New York.

Izzard, C.F., 1946. Hydraulics of runoff from developed surfaces, *Proceedings of the Highway Research Board*, **26**, 129-146.

James, L.D. and Burges, S.J. 1982. Selection, calibration, and testing of hydrologic model. In *Hydrologic Modeling of Small Watersheds*, Haan, C.T., Johnson, H.P., and Brakensiek, D.L., eds., American Society of Agriculture Engineers, St. Joseph, Mich., 437-472.

Julien, P. Y., Moglen, G. E., and Sunada, G. U., 1988. *CASC Users Manual – A Finite Element Model for Spatially Varied Overland Flow Simulation*, Report No. CER 87-88 GEO7, Center for Geosciences, Colorado State University, Fort Collins, 529 p.

Kareliotis, S.J., and Chow V.T., 1971. Computer Solution of a Hydrodynamic Model (IHW Model II). Civil Engineering Studies, Hydraulic Engineering Series No. 25, Department of Civil Engineering, Univeristy of Illinois at Urbana-Champaign.

Kibler, D.F. and Aron, G. (1983). Evaluation of Tc methods for urban watersheds. Frontiers in Hydraulic Engineering: Proceedings of Cambridge Conference, Massachusetts, H.T. Shen (Ed.). ASCE, New York, 553-558.

Krause, P., Boyle, D.P., and Base, F., 2005. Comparison of different efficiency criteria for hydrological model assessment. *Advances in Geosciences*, **5**, 89-97.

Lee, K.T. and Huang, J.K., 2007. Effect of moving storms on attainment of equilibrium dishcarge, *Hydrological Processes*,**21**(24), 3357-3366.

Li, R.M., Simons, D.B., and Stevens, M.A. 1975. Nonlinear kinematic wave approximation for water routing. *Water Resource Research*, **11**, 245-252.

Lighthill, M.J., and Whithman, G.B., 1955. On kinematic waves, 1, Flood movement in long rivers. *Proceedings of Royal Society London, Series A*, **229**, 281-316.

Maksimov, V.T., 1964. Computing runoff produced by a heavy rainstorm with a moving center, *Soviet Hydrology: Selected Papers*, English translation, **5**, 510-513.

Marcus, N., 1968. *A Laboratory and Analytical Study of Surface Runoff Under Moving Rainstorms*. Ph.D. Dissertation, Department of Civil Engineering, University of Illinois at Urbana-Chanmpaign.

McFarland, M.J., 2008. Precipitation: Remote Sensing Measurement, Trimble S.B., Stewart B.A., Howell T.A., ed., Encyclopedia of Water Science, 2nd edition.

Nash, J.E. and Sutcliffe, J.V., 1970. River flow forecasting through conceptual models. Part 1- A discussion of principles. *Journal of Hydrology*, **10**, 282-290.

Niemczynowicz, J. and Dahlblom, P., 1984. Dynamic properties of Rainfall in Lund, *Nordic Hydrology*, **15**, 9-24.

Niemczynowicz, J., 1984a. Investigation of the influence of rainfall movement on runoff hydrograph, Part I—Simulation of conceptual catchment, *Nordic Hydrology*, **15**, 57-70.

Niemczynowicz, J., 1984b. Investigation of the influence of rainfall movement on runoff hydrograph, Part II—Simulation on real catchments in the City of Lund, *Nordic Hydrology*, **15**, 71-84.

Niemczynowicz, J., 1988. The rainfall movement – A valuable complement to short-term rainfall data. *Journal of Hydrology*, **104**, 311-326.

Ogden, F.L. and Julien, P.Y., 1993. Runoff sensitivity to temporal and spatial rainfall variability at runoff plane and small basin scales, *Water Resources Research*, **29**(8), 2589-2597.

Ogden, F.L., Richardson, J.R., and Julien, P.Y., 1995. Similarity in catchment response, 2, Moving rainstorms, *Water Resources Research*, **31**(6), 1543-1547.

Overton, D.E., and Meadows, M.E., 1976. Stormwater Modeling, Academic Press, New York.

Posey, C.J., 1949. Gradually varied channel flow. In *Engineering Hydraulics, Proceedings of the Fourth Hydraulic Conference Iowa Institute of Hydraulic Research*. Rouse, H., ed., 589-622. John Wiley & Sons, Inc. and Chapman & Hall, Limited.

Rasmer, C.E., 1927. Runoff from small agricultural areas, *Journal of Agriculture Ressource*, **34**(9), 797-823.

Richardson, J.R. and Julien, P.Y., 1989. One-dimensional modeling of moving rainstorms, in Catchment Runoff and Rational Formula, Yen, B.C., ed., Water Resources Publications, Littleton, CO, 155-167.

Shearman, R. J., 1977. *The speed and direction of movement of storm rainfall patterns*. Meteorological Office. Bracknel, Berkshire, UK, Report UDC 551.515.43.

Shen, H. W. and R. M. Li. 1973. Rainfall effect on sheet flow over smooth surface. *Journal of the Hydraulics Division Proceddings*, ASCE, **99**(HY5), 1367-1386.

Shen, Y.Y., Yen, B.C., and Chow, V.T., 1974. *Experimental Investigation of Watershed Surface Runoff*. Hydraulic Engineering Series Report No. 29, Department of Civil Engineering, University of Illinois at Urbana-Champaign, 197 p.

Singh, V.P., 1996. *Kinematic Wave Modeling in Water Resources: Surface-Water Hydrology*, John Wiley & Sons, Inc.

Singh, V.P., 1997a. Effect of spatial and temporal variability in rainfall and watershed characteristics on stream flow hydrograph. *Hydrological Processes*, **11**, 1649-1669.

Singh, V.P., 1997b. *Kinematic Wave Modeling in Water Resources: Environmental Modeling*, John Wiley & Sons, Inc.

Singh, V.P., 1998. Effect of the direction of storm movement on planar flow. *Hydrological Processes*, **12**, 147-170.

Singh, V.P., 2002a. Effect of the duration and direction of storm movement on infiltrating planar flow with full areal coverage. *Hydrological Processes*, **16**, 1479-1511.

Singh, V.P., 2002b. Effect of the duration and direction of storm movement on planar flow with full and partial areal coverage. *Hydrological Processes*, **16**, 3437-3466.

Stephenson, D., 1984. Kinematic study of effects of storm dynamics on runoff hydrographs. *Water SA*, **10**, 189-196.

Stoker, J.J., 1953. Numerical solution of flood prediction and river regulation problems: 1. Derivation of basic theory and formulation of numerical methods of attack. *Report IMM-NYU-200*. Institute of Mathematical Sciences, New York University, New York.

Surkan, A.J., 1974. Simulation of storm velocity effects on flow from distributed channel network. *Water Resources Research*, **10**, 1149-1160.

Tabios, G.Q., Obyesekera, J.T.B., and Shen, H.S., 1988. The influence of storm movement on streamflow hydrograph through space-time rainfall generation and hydraulic routing. Unpublished Paper. Colorado State University, Fort Collins, Colorado.

Townson, J.M. and Ong, H.S., 1974. A laboratory study of runoff caused by line storm moving over a conceptual catchment. Water Services, USA.

Watts, L.G. and Calver, A., 1991. Effects of spatially-distributed rainfall on runoff for a conceptual catchment. *Nordic Hydrology*, **22**, 1-14.

Wenzel, H. G., 1970. The Effect of Raindrop Impact and Surface Roughness on Sheet Flow. Research Report No. 34, Water Resources Center, University of Illinois at Urbana-Champaign.

Wong, T.S.W., 2001. Formulas for time of travel in channel with upstream inflow. Journal of Hydrologic Engineering, ASCE **6**(3): 416-422.

Xiong, Y.Y. and Melching, C.S., 2005. Comparison of kinematic-wave and nonlinear reservoir routing of urban watershed runoff. *Journal of Hydrologic Engineering*, **10**(1), 39-49.

Yen, B.C. and Chow, V.T., 1968. A Study of Surface Runoff due to Moving Rainstorms. Hydrologic Engineering Series No. 17, Department of Civil Engineering, University of Illinois, at Urbana-Champaign.

Yen, B.C. and Chow, V.T., 1969. A laboratory study of surface runoff due to moving rainstorms. *Water Resources Research*, **5**(5), 989-1006.

Yen, B.C., 1982. Some measures for evaluation and comparison of simulated models. Urban Stormwater Hydraulics and Hydrology. Proceedings of 2nd International Conference on Urban Storm Drainage, Urbana, Illinois, Yen, B.C., ed.. Water Resources Publications, Littleton, CO, 341-349.